UPPSALA
UNIVERSITET

Digital Comprehensive Summaries of Uppsala Dissertations from the Faculty of Science and Technology 1863

Fat-IBC

A New Paradigm for Intra-body Communication

NOOR BADARIAH ASAN

ACTA
UNIVERSITATIS
UPSALIENSIS
UPPSALA
2019

ISSN 1651-6214
ISBN 978-91-513-0770-1
urn:nbn:se:uu:diva-393444

Dissertation presented at Uppsala University to be publicly examined in Häggsalen, Ångströmlaboratoriet, Lägerhyddsvägen 1, Uppsala, Wednesday, 27 November 2019 at 09:15 for the degree of Doctor of Philosophy. The examination will be conducted in English. Faculty examiner: Dr. Ali Khaleghi (Norwegian University of Science and Technology).

Abstract
Asan, N. B. 2019. Fat-IBC. A New Paradigm for Intra-body Communication. *Digital Comprehensive Summaries of Uppsala Dissertations from the Faculty of Science and Technology* 1863. 116 pp. Uppsala: Acta Universitatis Upsaliensis. ISBN 978-91-513-0770-1.

In the last two decades, a significant development in the field of medical technology occurred worldwide. This development is characterized by the materialization of various body implants and worn devices, that is devices attached to the body. These devices assist doctors and paramedical staff in effectively monitoring the patient's health and helping increase patients' average life expectancy. Furthermore, the various implants inside the human body serve different purposes according to the humans' needs. As this situation became more prominent, the development of protocols and of reliable transmission media is becomes essential to improve the efficiency of inter-device communications. Positive prospects of the use of human tissue for intra-body communication were proven in recent studies. Fat tissues, for example, which also work as energy banks for human beings, can be potentially used in intra-body communications as transmission media. In this thesis, the fat (adipose) tissue's function as an intra-body communication channel was investigated. Therefore, various simulations and experimentations were performed in order to characterize the reliability of the fat tissue in terms of communication, considering, for example, the effect that the variability in the thickness of adipose and muscular tissues could have on the communication performance, and the possible effect that the variability in the transmitted signal power could have on the data packet reception. Fat tissue displays superior performance in comparison to muscle tissue in the context of a low loss communication channel. For example, at 2.45 GHz, the path losses of ~0.7 dB/cm and ~1.9 dB/cm were observed for phantom and ex-vivo measurements, respectively. At a higher frequency of 5.8 GHz, the ex-vivo path loss was around 1.4 dB/cm. It was concluded from the results that the adipose tissue could function as a reliable medium supporting intra-body communication even under low power transmitted signals. Moreover, although the presence of thick blood vessels could degrade the signal strength, the results show that communication is possible even under the presence of perturbant tissues. Overall, the results of this thesis would provide a foundation in this area and assist researchers in developing innovative and solutions for intra-body communication.

Keywords: Fat-Intrabody Communication, Fat Tissue, Microwave, Propagation, Data Packet Reception, Ex-vivo, Phantom, Communication, Reliability, Implants

Noor Badariah Asan, Department of Engineering Sciences, Solid State Electronics, Box 534, Uppsala University, SE-75121 Uppsala, Sweden.

ISSN 1651-6214
ISBN 978-91-513-0770-1
urn:nbn:se:uu:diva-393444 (http://urn.kb.se/resolve?urn=urn:nbn:se:uu:diva-393444)

Dedicated to
my love, Zulkifli Shariff,
my lovely angel, Nur Alia Safiyya,
my little hero, Alexander Dzulqarnayn,
and my beloved parents, Asan Abdullah & Minah Sidek.

List of papers

The thesis is based on the following papers, which are referred to in the text by their Roman numerals.

I. **Noor Badariah Asan**, Daniel Noreland, Emadeldeen Hassan, Syaiful Redzwan Mohd Shah, Anders Rydberg, Taco J. Blokhuis, Per-Ola Carlsson, Thiemo Voigt, and Robin Augustine. 2017. "Intra-body Microwave Communication through Adipose Tissue," *Healthcare Technology Letters*, 4(4), pp. 115–121. Doi: 10.1049/htl.2016.0104

   Part of this work was presented at *Medicinteknikdagarna (MTD)* by Swedish Society for Medical Engineering in Örebro, Sweden, 2016.

II. **Noor Badariah Asan**, Emadeldeen Hassan, Jacob Velander, Syaiful Redzwan Mohd Shah, Daniel Noreland, Taco J. Blokhuis, Eddie Wadbro, Martin Berggren, Thiemo Voigt, and Robin Augustine. 2018. "Characterization of the Fat Channel for Intra-Body Communication at R-Band Frequencies," *Sensors*, 18(9): 2752.
   Doi: https://doi.org/10.3390/s18092752

III. **Noor Badariah Asan**, Emadeldeen Hassan, Mauricio D. Perez, Laya Joseph, Martin Berggren, Thiemo Voigt, and Robin Augustine. 2019. "Fat-Intra Body Communication at 5.8 GHz Including Impacts of Dynamic Body Movements" (manuscript).

IV. **Noor Badariah Asan**, Jacob Velander, Syaiful Redzwan Mohd Shah, Emadeldeen Hassan, Daniel Noreland, Taco J. Blokhuis, Thiemo Voigt, and Robin Augustine. "Reliability of the Fat Tissue Channel for Intra-Body Microwave Communication," *in 2017 IEEE Conference on Antenna Measurements & Applications (CAMA)*, Tsukuba, Japan. 2017, pp. 310–313. Doi: 10.1109/CAMA.2017.8273435

V. **Noor Badariah Asan**, Jacob Velander, Syaiful Redzwan Mohd Shah, Mauricio D. Perez, Emadeldeen Hassan, Taco J. Blokhuis, Thiemo Voigt, and Robin Augustine."Effect of Thickness Inhomogeneity in Fat Tissue on In-Body Microwave Propagation," *in 2018 IEEE International Microwave Biomedical Conference (IMBioC)*, Philadelphia, PA, USA. 2018, pp. 136–138. Doi: 10.1109/IMBIOC.2018.8428872

Part of this work was presented at Swedish Microwave Days, AntennEMB Symposium at Lund, Sweden, 2018.

VI. **Noor Badariah Asan**, Emadeldeen Hassan, Mauricio D. Perez, Syaiful Redzwan Mohd Shah, Jacob Velander, Taco J. Blokhuis, Thiemo Voigt, and Robin Augustine. 2019. "Assessment of Blood Vessel Effect on Fat-Intrabody Communication Using Numerical and Ex-Vivo Models at 2.45 GHz," *in IEEE Access*, vol. 7, pp. 89886–89900. Doi: 10.1109/ACCESS.2019.2926646

Part of this work was presented at *2018 IEEE Conference on Antenna Measurements & Applications (CAMA)* in Västerås, Sweden, 2018.

VII. **Noor Badariah Asan**, Carlos P. Penichet, Syaiful Redzwan Mohd Shah, Daniel Noreland, Emadeldeen Hassan, Anders Rydberg, Taco J. Blokhuis, Thiemo Voigt, and Robin Augustine. 2017. "Data Packet Transmission through Fat Tissue for Wireless IntraBody Networks," *in IEEE Journal of Electromagnetics, RF and Microwaves in Medicine and Biology*, 1(2), pp. 43–51. Doi: 10.1109/JERM.2017.2766561

Part of this work was presented at *2017 First IEEE MTT-S International Microwave Bio Conference (IMBIOC)* in Gothenburg, Sweden 2017.

Reprints were made with permission from the publishers.

Author's contributions

I. Major part of planning, experimental work, data analysis, and writing with input from co-authors.

II. Major part of planning, experimental work, data analysis, and writing with input from co-authors.

III. Major part of planning, experimental work, data analysis, and writing with input from co-authors.

IV. Major part of planning, experimental work, data analysis, and writing with input from co-authors.

V. Major part of planning, experimental work, data analysis, and writing with input from co-authors.

VI. Major part of planning, experimental work, data analysis, and writing with input from co-authors.

VII. Major part of planning, experimental work, data analysis, and writing with input from co-authors.

List of papers not included in the thesis

The author has been involved in the following publications that are not part of this thesis, either due to contents overlapping that of appended papers, or due to contents not related to the thesis.

VIII. **Noor Badariah Asan**, Robin Augustine, and Thiemo Voigt, "In-Body Internet of Things Networks Using Adipose Tissue," *IEEE Internet of Things (IoT) Newsletter*, May 14, 2019.
Retrieved from URL: https://iot.ieee.org/newsletter/may-2019/in-body-internet-of-things-networks-using-adipose-tissue.

IX. **Noor Badariah Asan**, Emadeldeen Hassan, Syaiful Redzwan Mohd Shah, Jacob Velander, Thiemo Voigt, and Robin Augustine, "Impact of Blood Vessels on Data Packet Transmission Through the Fat Channel," *2018 IEEE International RF and Microwave Conference (RFM)*, Penang, Malaysia 2018, 17–19 Dec 2018.

X. **Noor Badariah Asan**, Emadeldeen Hassan, Syaiful Redzwan Mohd Shah, Jacob Velander, Mauricio D. Perez, Thiemo Voigt, Taco J. Blokhuis, and Robin Augustine, "Effects of Blood Vessels on Fat Channel Microwave Communication", *2018 IEEE Conference on Antenna Measurements & Applications (CAMA)*, Västerås, Sweden, September 3–6, 2018, pp. 1–4. Doi: 10.1109/CAMA.2018.8530527

XI. **Noor Badariah Asan**, Mauricio D. Perez, Jacob Velander, and Robin Augustine, "Effect of the Fat Thickness Variation on In-Body Microwave Propagation", *Swedish Microwave Days, AntennEMB Symposium*, Lund, Sweden, May 24–25, 2018.

XII. **Noor Badariah Asan**, Daniel Noreland, Syaiful Redzwan Mohd Shah, Emadeldeen Hassan, Anders Rydberg, Thiemo Voigt, and Robin Augustine, "Human Fat Tissue: A Microwave Communication Channel," *2017 First IEEE MTT-S International Microwave Bio Conference (IMBIOC)*, Gothenburg, 2017, pp. 1–4. Doi: 10.1109/IMBIOC.2017.7965801

XIII. Thiemo Voigt, Robin Augustine, **Noor Badariah Asan**, Mauricio D. Perez, Anders Ahlén, André Teixeira, Sam Hylamia, Christian Rohner, Wenqing Yan, Anna Nilsson, and Maria Mani, "Short Talk: LifeSec

– Don't Hack my Body," *4th IEEE European Symposium on Security and Privacy & Cybersecurity and Privacy (CySeP)*, Stockholm, Sweden, 10–14 June, 2019.

XIV. Thiemo Voigt, Robin Augustine, **Noor Badariah Asan**, Mauricio D. Perez, Anders Ahlén, André Teixeira, Sam Hylamia, Christian Rohner, Wenqing Yan, Anna Nilsson, and Maria Mani, "Poster: Tumor Sensing Privacy in In-Body Networks," *4th IEEE European Symposium on Security and Privacy & Cybersecurity and Privacy (CySeP)*, Stockholm, Sweden, 10–14 June, 2019.

XV. Syaiful Redzwan Mohd Shah, Jacob Velander, Parul Mathur, Mauricio D. Perez, **Noor Badariah Asan**, Dhanesh G. Kurup, Taco J. Blokhuis, and Robin Augustine, "Split-Ring Resonator Sensor Penetration Depth Assessment Using In Vivo Microwave Reflectivity and Ultrasound Measurements for Lower Extremity Trauma Rehabilitation," *Sensors*, vol. 18, no. 2, pp. 636, Feb. 2018. Doi: https://doi.org/10.3390/s18020636

XVI. Syaiful Redzwan Mohd Shah, **Noor Badariah Asan**, Jacob Velander, Doojin Lee, Mauricio D. Perez, Marco Raaben, Taco J. Blokhuis, and Robin Augustine, "Frequency domain analysis of hip fracture using microwave Split-Ring Resonator sensor on phantom model," *2016 IEEE Asia-Pacific Conference on Applied Electromagnetics (APACE)*, Langkawi, 2016, pp. 244–247. Doi: 10.1109/APACE.2016.7916434

XVII. Syaiful Redzwan Mohd Shah, Jacob Velander, Mauricio D. Perez, **Noor Badariah Asan**, Daniel Nowinski, Anders Lewén, Per Enblad, Robin Augustine, and Mina Rajabi, "Initial In-Vitro Trial for Intra-Cranial Pressure Monitoring Using Subdermal Proximity-Coupled Split-Ring Resonator," *2018 IEEE International Microwave Biomedical Conference (IMBioC)*, Philadelphia, PA, 2018, pp. 73–75. Doi: 10.1109/IMBIOC.2018.8428854

XVIII. Syaiful Redzwan Mohd Shah, Jacob Velander, Mauricio D. Perez, **Noor Badariah Asan**, Robin Augustine, Parul Mathur, Dhanesh G. Kurup, and Taco J. Blokhuis, "Penetration Depth Evaluation of Split-Ring Resonator Sensor Using In-Vivo Microwave Reflectivity and Ultrasound Measurements", *12th European Conference on Antennas and Propagation (EuCAP 2018)*, London, UK, 2018. Doi: 10.1049/cp.2018.0500

XIX. Syaiful Redzwan Mohd Shah, Jacob Velander, **Noor Badariah Asan**, Mauricio D. Perez, and Robin Augustine, "Assessment of Signal Transmission Using Microwave Sensors for Health Monitoring Applica-

tions," *2018 IEEE International RF and Microwave Conference (RFM)*, Penang, Malaysia 2018, 17–19 Dec 2018.

XX. Jacob Velander, Syaiful Redzwan Mohd Shah, Mauricio D. Perez, **Noor Badariah Asan**, Robin Augustine, and Taco J. Blokhuis, "Multi-Functional Phantom Model to Validate Microwave Sensors for Health Monitoring Applications", *12th European Conference on Antennas and Propagation (EuCAP 2018)*, London, UK, 2018, pp. 1–5.
Doi: 10.1049/cp.2018.0504

XXI. Jacob Velander, Syaiful Redzwan Mohd Shah, Mauricio D. Perez, **Noor Badariah Asan**, Daniel Nowinski, Anders Lewén, Per Enblad, and Robin Augustine, "A Four-Layer Phantom for Testing In-Vitro Microwave-Based Sensing Approach in Intra-Cranial Pressure Monitoring," *2018 IEEE International Microwave Biomedical Conference (IMBioC)*, Philadelphia, PA, 2018, pp. 49–51.
Doi: 10.1109/IMBIOC.2018.8428861

XXII. Mauricio D. Perez, George Thomas, Syaiful Redzwan Mohd Shah, Jacob Velander, **Noor Badariah Asan**, Robin Augustine, Parul Mathur, Mohammad Nasir, Daniel Nowinski, and Dhanesh G. Kurup, "Preliminary Study on Microwave Sensor for Bone Healing Follow-up after Cranial Surgery in Newborns", *12th European Conference on Antennas and Propagation (EuCAP 2018)*, London, UK, 2018.
Doi: 10.1049/cp.2018.1250

XXIII. Mauricio D. Perez, Syaiful Redzwan Mohd Shah, Jacob Velander, Marco Raaben, **Noor Badariah Asan**, Taco J. Blokhuis, and Robin Augustine, "Microwave sensors for new approach in monitoring hip fracture healing," *2017 11th European Conference on Antennas and Propagation (EUCAP)*, Paris, 2017, pp. 1838–1842.
Doi: 10.23919/EuCAP.2017.7928698

XXIV. Mauricio D. Perez, Viktor Mattsson, Syaiful Redzwan Mohd Shah, Jacob Velander, **Noor Badariah Asan**, Parul Mathur, Mohammad Nasir, Daniel Nowinski, Dhanesh G. Kurup, and Robin Augustine, "New Approach for Clinical Data Analysis of Microwave Sensor Based Bone Healing Monitoring System in Craniosynostosis Treated Pediatric Patients," *2018 IEEE Conference on Antenna Measurements & Applications (CAMA)*, Västerås, Sweden, September 3-6, 2018, pp. 1–4.
Doi: 10.1109/CAMA.2018.8530485

Contents

Abbreviations

3D	Three-dimensional
BAN	Body-Area Network
BAT	Brown Adipose Tissue
BCC	Body-Coupled Communications
BER	Bit Error Rate
bps	bit per second
BPSK	Binary Phase Shift Keying
CST	Computer Simulation Technology
CVD	Cardiovascular Diseases
DI	Deionized
E-field	Electric Field
EM	Electromagnetic
FSDT	Frequency-Selective Digital Transmission
i-BANs	Intra-body Area Networks
IBC	Intra Body Communication
ICD	implantable Cardioverter/Defibrillators
igWAT	inguinal White Adipose Tissue
ISM	Industrial, Scientific and Medical
kbps	kilo bit per second
MICS	Medical Implant Communications Service
MUT	Material Under Test
NFC	Near Field Communication
PANs	Personal Area Networks
PEC	Perfect Electric Conductor
PML	Perfectly Matched Layers
PRR	Packet Reception Rate
PT	Perturbant Tissue
RF	Radio Frequency
RF-NB	Narrow-band
RF-UWB	Ultra-wide-band
RFID	Radio Frequency Identification
RSS	Received Signal Strength
RX	Receiver
SAR	Specific Absorption Rate
SDR	Software Defined Radio
SMA	SubMiniature Version A
TE	Transverse Electric
TEM	Transverse Electromagnetic

Continued on next page

TM	Transverse Magnetic
TOPA	Topology-Optimized Planar Antenna
TX	Transmitter
USRP	Universal Software Radio Peripheral
VNA	Vector Network Analyzer
vWAT	Visceral White Adipose Tissue
WAT	White Adipose Tissue
WBAN	Wireless Body-Area Network
WHO	World Health Organization
WMTS	Wireless Medical Telemetry Service
WSN	Wireless Sensor Network

Thesis outline

This thesis is based on seven papers and divided into seven chapters.

Chapter 1 gives the motivations of this research and outlines an overview of existing intra-body communication methods. At the end of this chapter, comprehensive introduction to the main subject of this thesis, Fat-IntraBody Communication (Fat-IBC) are given.

Chapter 2 presents the anatomical multilayer tissue model, followed by numerical modeling and analytical channel modeling. The chapter continues with the characterization of tissues and materials and follows with a comparison of the dielectric properties of tissue-equivalent phantoms, ex-vivo animal tissues, and literature-reported human tissues. A dedicated measurement setup for ex-vivo and a phantom verification of the simulation results are also given in this chapter. Details of the probes' prototypes and the probe-to-probe results are presented (**Papers I–III**).

Chapter 3 discusses the design considerations of Fat-IBC with the special focus on the signal path loss at 2.0 GHz (**Paper I**), 2.4–2.45 GHz (**Paper II**), and 5.8 GHz (**Paper III**).

Chapter 4 summarizes the results and analyses performed from the experimental works that have been conducted from various parameters such as perturbants in the channel (**Paper IV**), fat thickness inhomogeneity (**Paper V**), and the effect of blood-vessels orientation, placement and numbers of vessels on communication link (**Paper VI**). We further investigated the effect of the body movement on communication (**Paper III**). These are used to determine the factors affecting signal transmission in the Fat-IBC.

Chapter 5 discusses the issue of data packet transmission through fat tissue supporting wireless connectivity of intra-body devices. The numerical modeling, experimental setup, and results are discussed (**Paper VII**). The possibility of using Fat-IBC as a sensing system is presented in **Paper IV**.

Chapter 6 provides a comprehensive summary of results and analysis from the studies conducted in **Papers I**, **II**, **III**, **IV**, **V**, **VI**, and **VII**.

Chapter 7 presents the conclusions of the thesis and potential avenues for future research.

1. Introduction

Throughout history, humans have developed certain mechanisms that promote the accumulation of fat during periods of feast to survive during the upcoming periods of famine and cold. However, what was once an asset has become a liability in our current society and, in particular, as recalled by Galgani et al. (2005) [1] "the obesogenic environment" because too much fat accumulation may lead to obesity. As per statistical reports [2], fat contents varies with age. In males, the mean percentage body fat ranges increases from 22.9 % at age 16–19 years to 30.9 % at age 60–79 years. These figures are significantly different to those ones in females, as the mean percentage body fat ranges from 32.0 % at age 8–11 years to 42.4 % at age 60–79 years [3]. Therefore, essential fats in females (10–13 %) are approximately 2 to 3 folds more than for males (3–5 %).

Essentially, a healthy male body comprises 15 % of fat, while a female body comprises around 23 % of fat. For this reason, with 25 % of fat content in a male body, he would be considered obese. As for females, they would be considered obese when their bodies possess more than 32 % of fat content. Obesity is linked with a number of diseases, such as metabolic disorders [4], cardiometabolic diseases [5], liver and kidney disorder [6], [7], chronic inflammation [8], and cardiovascular diseases (CVD) [9]. According to the World Health Organization (WHO), deaths related to cardiovascular diseases are the most frequent. Approximately, 17.9 million people died from CVD in 2016 [10]. However, most CVDs could be prevented through healthy diets, exercise, and weight control, as per WHO's recommendation.

With this prospect in mind, the regular monitoring of human vital signs is crucial for early and accurate diagnosis of patients' medical condition and immediate commencement of proper treatment for them. For instance, patients with Type-1 diabetes would be assisted with closed-loop insulin delivery systems which would autonomously measure glucose levels and administer insulin based on glucose levels using the implanted glucose sensor and insulin pump devices [11].

In response to the above situations, the health care market has become a four trillion-dollar industry worldwide. It has been predicted that this figure will double within ten years. Apart from the unparalleled growth in the human population, nearly every country is faced with population aging [12]. The increasing environmental pollution occurs due to industrialization and urbanization, leading to new pollution-related diseases [13]. Furthermore, there has been a rapid increase in technology spending due to various factors, including the intensively competitive healthcare market, strong pressure to prevent

medical errors, and the need to comply with regulations among others. Medical implantable devices are gaining more popularity these days due to their role as life-saving devices. Medical implantable devices are getting more popular these days because of the role as a life-saving device in addition to the sophistication and comfort that recent research and improved manufacturing processes have managed to bring in them [14], [15]. A wide range of medical implants is available with various functions. Pacemakers and defibrillators are used to monitor and treat cardiac conditions, and neuro-stimulators are used for deep brain stimulation to observe various brain-related illnesses, such as epilepsy, and Parkinson's disease. Drug delivery systems are used in the form of infusion pumps, while a range of biosensors is used to obtain and process various bio-signals [16].

The human body consists of a fascinating communication network. Human organs provide metabolic functions to the body. As per previous discussion, early detection of diseases is important for immediate treatment. When a disease is detected earlier, would it enable the implantation of certain artificial devices at various locations in the human body which could ease the detection of anomalies through the communication between them? A disability could occur after an accident or other medical cases due to the dysfunctionality of one or more natural body communication links, but what if those links could be recovered? Although the efficient delivery of drugs to a certain body part is a challenging task, what if it could be improved, leading to the prevention of damaged cells in cancer treatment? What if the real-time statistics of human vitals function could be identified? What if our intra-body communication network can communicate with the on-body and off-body devices as well? The answers and solutions to these questions would shape the future. Additionally, the answers to these questions would assist in managing the diseases and disorders mentioned above. This thesis aims to provide the foundation of the use of the human adipose (fat) tissue as a medium for communications within the body. This new intra-body communication paradigm would provide answers to these questions in the future.

In this thesis, the use of human body tissues for intra-body communication (IBC) was investigated. It was proven in studies of humans that poor lifestyle, eating habits, and pollution could bring adverse effects on the human body. Due to the significant increase in several diseases, such as hypertension, diabetes, and CVD, frequent monitoring of them is essential. Furthermore, early detection of diseases, such as cancer, would increase the average life expectancy. Therefore, new techniques and methods which could facilitate early disease detection are important. Moreover, if human body tissues could be utilized to guide the signals with vital and control information more efficiently, implanted devices would not only be able to communicate in a better manner with the outer world but also with other implanted devices.

By in-cooperating human tissues for IBC, the materialization gap in this technology can be fulfilled and new horizons in this field can be opened. An

important literary contribution in this matter was by Wegmüller (2007) [17], where the human body was categorized as a transmission medium that could transmit electrical currents and develop the electrical models of the human tissue. Additionally, individual-specific variations of the transmission characteristics were investigated in a clinical trial.

1.1 Intra-body communication

The first work in the field of intra-body communication was performed by Zimmerman (1996) [18]. The idea of Personal Area Networks (PANs) was contributed to illustrate that electronic devices that were attached near a human body could form a network and exchange data through capacitive coupling. The state-of-the-art method in electronic devices with highly power-efficient characteristics and the advancements in the field of wireless communication have expanded new horizons in human body area networks (BANs). In human body-area communication, multiple devices are worn or placed inside or within the vicinity of the human body. These devices could form a wireless link or a small-scale wireless network to share data and enable new services. Notably, IBC may also contribute to endless opportunities in the field of healthcare services by connecting various on/in-body devices to form the BAN of personal health information. For instance, patients with diabetes could use an automatic insulin pump which autonomously measures glucose levels and administers insulin upon high levels of glucose. A sensor, which may be developed in the future, may reduce the occurrences of heart attack or stroke, decreasing the burden from hospitals by avoiding frequent patient visits [19].

One of the possible scenarios of the communication between the sensor and the external world is shown in Figure 1.1. A system consisting of a wireless power receiver, rechargeable battery unit, and wireless communication system was implanted inside the human body [20]. The implant performed its intended task and transmitted human vitals to the mobile phone through Bluetooth. A wireless charging mechanism was also provided to avoid surgeries for replacing batteries.

There are two primary methods for signals to be coupled into the body for IBC, namely capacitive coupling and galvanic coupling. Other, less popular approaches also exist, such as inductive coupling, ultrasound, and classical RF coupling in the form of narrow-band (RF-NB) and ultra-wide-band communication (RF-UWB). The next section provides further details on these approaches.

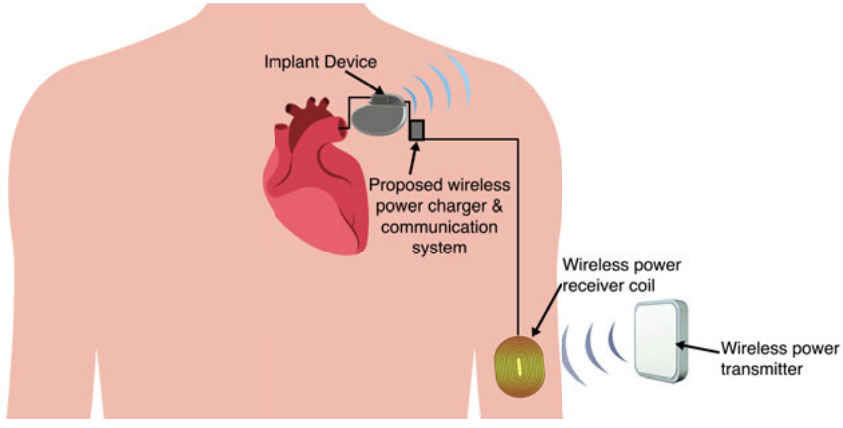

Figure 1.1. *Implantable medical device communicates with the external world.*

1.1.1 Capacitive coupling

In capacitive coupling, a signal is applied to a transceiver electrode, and an electric field is build up [21]. This approach mainly aims to maximize the coupling between the transceiver and the human body, thus reducing the interference because of ambient noise. Furthermore, signal electrodes are used for transmission and reception. The signal from the transmitter creates an electric potential, followed by the connection between the ground electrode and the earth ground. Directed by the dielectric characteristics of the human body tissues, the major part of the electric current travels between the two transmitter electrodes, while a minor part travels towards the two receiver electrodes. This small current leads to a potential difference which is detected in various ways by the receiver electrodes. As the capacitive coupling requires a return path through the parasitic earth ground, external interference could disrupt the IBC.

The maximum data rate, which was achieved through a capacitive coupling, was 60 Mbps multi-level coded frequency-selective digital transmission (FSDT) for body channel communication [22]. As for the frequencies above 60 kHz, capacitive coupling displayed a more superior performance compared to galvanic coupling. Figure 1.2(a) illustrates the channel model of capacitive coupling for IBC.

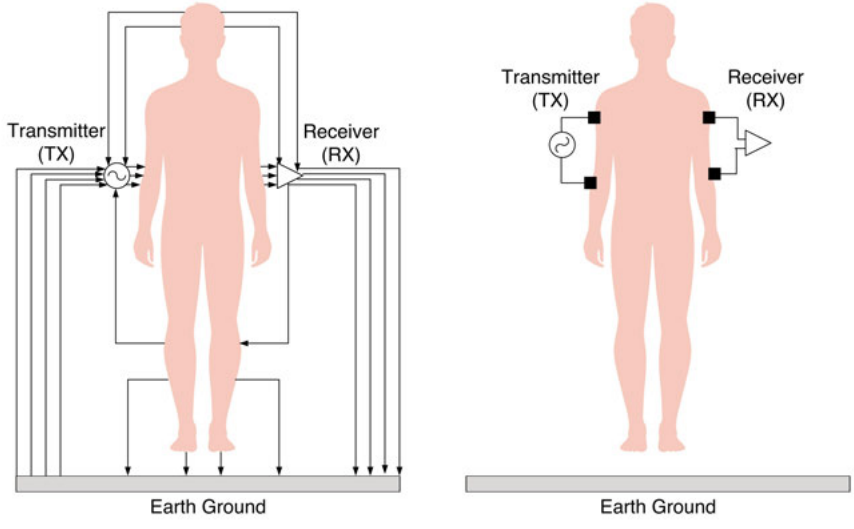

(a) *Capacitive coupling.* **(b)** *Galvanic coupling.*

Figure 1.2. *Channel model for intra-body communication:* ***(a)*** *capacitive coupling* ***(b)*** *galvanic coupling.*

1.1.2 Galvanic coupling

In galvanic coupling, a signal is controlled by the applied current flow, while the human body could be considered as the waveguide [23]. In comparison to capacitive coupling, the propagation of the current in galvanic coupling through the body does not involve any return path, as shown in Figure 1.2(b). Therefore, this method is less susceptible to noise. Furthermore, besides the small energy absorption in the tissue, the galvanic coupling-based tissue communication is effective for frequencies below 1 MHz. However, at low frequencies, the signal propagation would heat up the tissues. Without a proper administration of the heating process, the tissue may be damaged [24]. Another drawback of this technique is that the bandwidth is lower compared to capacitive coupling, which leads to a lower data rate.

1.1.3 Inductive coupling

In inductive coupling, the electromagnetic coupling is used to provide a communication link to implanted devices, by placing the external coil close to the patient that couples to a coil implanted below the skin surface. The implant is powered by the coupled magnetic field. The best power transfer is achieved in inductive coupling when it is used in large transmitting and receiving coils. Therefore, this method could be used effectively if space is not a constraint [25]–[27]. For example, Hannan et al. [28] states that "based on current liter-

ature, we believe that the inductive coupling link is the suitable method to be used to power the battery-less devices". However, in the case of IBC, a compact size of implants is required. However, this technique is not capable of supporting a high data rate and initiating a communication session from inside of the body [29]. Therefore, it is not suitable for IBC.

1.1.4 RF coupling

RF based IBC is one of the alternative techniques that can increase the bandwidth and enable two-way data communication. Popularly known as Wireless Medical Telemetry Service (WMTS) and Medical Implant Communications Service (MICS), RF-NB functions on a band dedicated to medical applications. The details of the bands reserved for these applications are illustrated in Table 1.1 [30].

Table 1.1. *RF-NB Band. Copyright ©2019, IEEE [30].*

Band	Frequency range	Application(s)
WMTS	608–614 (MHz) 1395–1400 (MHz) 1429–1432 (MHz)	Remote patient monitoring
MICS / MedRadio	401–406 (MHz) 2.36–2.4 (GHz)	On-body and embedded sensor communication
RF-Ultra wideband	3.1–10.6 (GHz)	Intra-body communication
Milimeter wave	>30 (GHz)	Device to device communication

1.2 Fat-intrabody communication

The transmission of data out of many parts of the body is a challenging process [31]. Utilizing fat tissues as a communication channel in order to establish communication between implanted devices separated by some distance is called fat intra-body communication, Fat-IBC. However, low-frequency propagation (kHz range) is not an ideal choice for IBC as it results in lower bandwidth and higher path loss. Microwave frequencies are highly attenuated by skin and muscle tissues due to the higher dielectric coefficient of skin and muscles [32]–[34]. It could be seen IBC works well for R-band (1.70 to 2.60 GHz) communication in previous work [35].

The pioneer work for Fat-IBC was done by the thesis author in a previous research article [36], where various aspects of Fat-intrabody communication were explored [37],[38]. Essentially, fat functions as a good communication channel for frequencies around 2.0 GHz [36]. The loss is smaller than for other tissues and the bandwidth is higher which means that functionalities such as cardiac pacemakers, implantable cardioverter/defibrillators (ICD), and neuroprosthetics can be supported. It is worth mentioning that Fat-IBC research is

in its early state and some applications with the present-day tools available cannot be realized today due to number of reasons which includes lack of bandwidth inside the body.

Figure 1.3 shows a human body with multiple implants such as artificial kidney, heart sensor, and liver sensor. Wireless communication is the most ideal method for communication between these sensors to take place. Besides this method, fat tissue could be used as a microwave communication between them. In the cases where the sensors are separated by a large distance, the signal strength may be attenuated as it propagates through the fat tissue. In order to enhance the signal strength, a repeater node may be used as an amplifier stage. All the body vitals are collected by the aggregator node that transfers information to the outside of the human body.

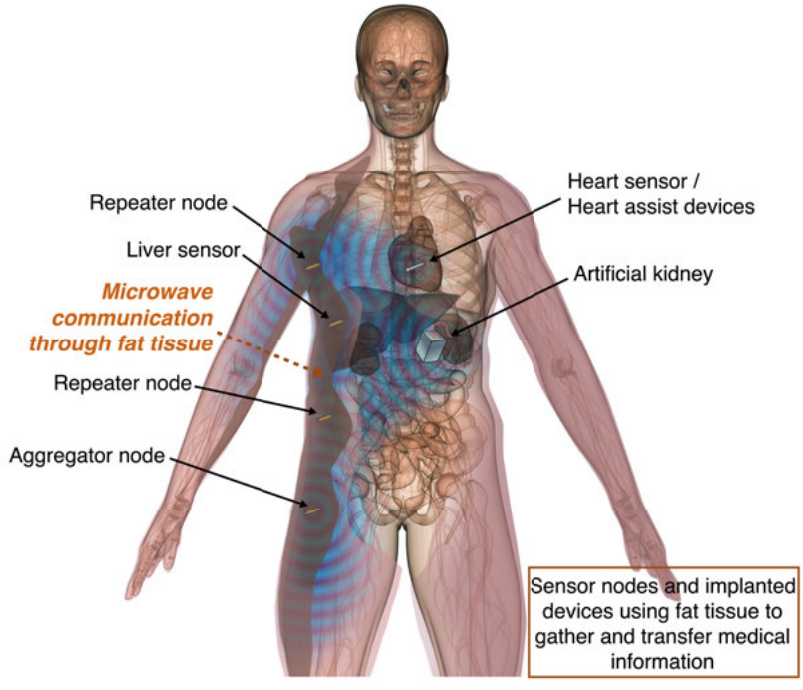

Figure 1.3. *Conceptual rendering of fat intra-body microwave communication (Fat-IBC) network.* ***Paper VII****. Reprinted, with permission, from [39]. Copyright ©2017, IEEE.*

The goal of this thesis is to provide the foundation of the use of the human adipose (fat) tissue as a medium for communications within the body. In this thesis, the channel for Fat-IBC is modeled numerically and analytically. This thesis could contribute to the construction of an end to end network by a quantitative path loss for the Fat-IBC obtained based on a numerical and experimental approach. In the next chapter of the thesis discusses the relia-

bility of the behavior of the fat channel in the presence of perturbants, inhomogeneity, and blood vessels. Finally, the fat tissues were used in this study as the medium of microwave communication to transfer and receive a packet. This process involved real data or health information and determined the data packet reception.

2. Fat-IBC channel modeling

In this chapter, the channel for Fat-IBC is modeled numerically and analytically. The dielectric properties measurement technique is presented and also the experimental setup, including the topology-optimized waveguide-based probe designs toward the channel modeling of fat-intrabody microwave communication are presented in **Papers I–III** and are summarized in this chapter as follows:

- **Section 2.1**: The anatomy of a multi-layered tissue model, which consists of skin, fat, and muscle is presented. Subsequently, numerical simulation models and analytical modeling for parallel plate waveguide are shown. In **Paper I**, the method to characterize fat or adipose tissue and muscle tissue for intra-body communication at 2.0 GHz is presented. The characterization is extended to the Industrial, Scientific and Medical (ISM) band frequencies at 2.4 GHz and 5.8 GHz, respectively. The skin and muscle communication are compared to Fat-IBC. The parallel plate waveguide hypothesis is discussed in **Paper II**, and the analytical channel modeling based on the parallel plate waveguide is explained.
- **Section 2.2**: The measurement techniques and instruments used for measuring the dielectric properties are discussed. The dielectric properties of the tissue-equivalent phantom, the ex-vivo porcine tissue, and other materials are presented and compared.
- **Section 2.3**: This section details the three main components of the measurements setup for the Fat-IBC system. A thorough discussion is made on the three different prototypes of the topology-optimized waveguide-based probe used in **Papers I–III** and their elements.

2.1 Fat-IBC characterization

2.1.1 Anatomy of multi-layer tissue model

The human body is a complex structure comprising different tissues, organs, and bone structures of varying geometries. The human body parts such as arms, legs, and torso basically consist of three types of tissues; namely skin, fat, and muscle which were approximated to simplify the geometrical and physical properties of an anatomical model.

The work in **Papers I–VII** is based on the simplified three-layered (i.e., skin-fat-muscle) tissue model. Due to several reasons, the bone layers were excluded in numerical and experimental studies. For example, to establish a network between sensors, the implanted devices used for the delivery of drugs such as insulin are commonly located in the soft human tissue [40]. Besides, in some areas, the bone is located as the inner layer in the human body. The laterally transmitted signals are attenuated by the muscles and they hardly reach the bone. Figure 2.1 shows the extraction method of the three-layered tissue model. It is obvious that fat tissue is widespread around the model and generally surrounds all the major organs in the human body[1].

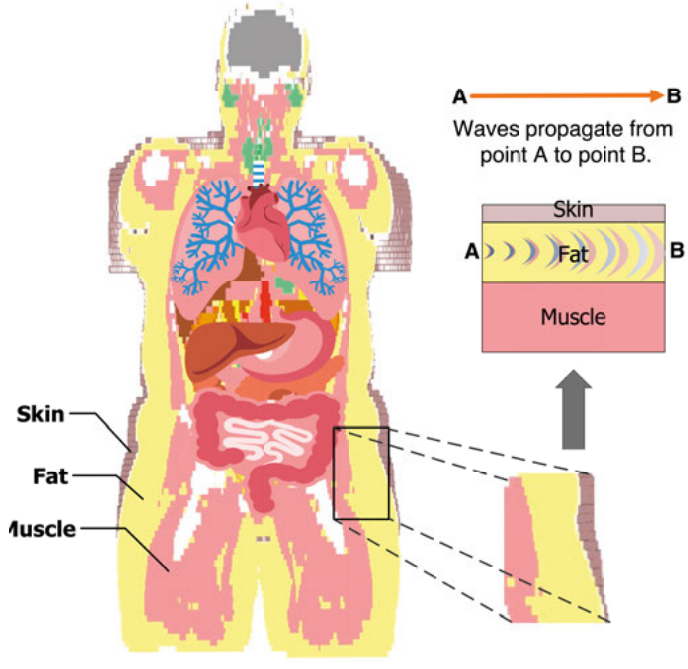

Figure 2.1. *The model shows that the vital organs are surrounded by adipose tissue. The smaller picture of the 3 types of tissues outlines how the intra-body microwave is transmitted through the fat tissue.* ***Paper II****. Reprinted, with permission, from [35] Copyright ©2018, MDPI.*

[1]Coronal plane of the Emma voxel human model from the CST software

Human body fat can be classified into three types, namely white fat, brown fat, and brite fat. White adipose tissue (WAT) is the major adipose part in adults and is the prime storage location of energy. When energy is needed, fatty acids are released from WAT by lipolysis [41]. WAT is extensively dispersed all over the body, separate/specific depots can be illustrious: visceral white adipose tissue (vWAT) primarily covers internal organs, whereas inguinal white adipose tissue (igWAT) is present under the skin. Brown adipose tissue (BAT) is a distinct class of adipose organ which is present in all mammals including humans, however, pig is an exception [42]. The prime role of BAT is to perform non-shivering thermogenesis action by burning lipids and glucose, resulting in heat production. Unlike WAT, BAT are located only in the supraclavicular, neck, and perirenal regions of the human body [43]. The role of brite fat is to reserve brown adipose tissue that can be induced by cold acquaintance to release energy [44]. To establish a communication channel through a tissue, one has to rely on the geometrical integrity of the channel. Since WAT provides a stable tissue layer, when compared to other types of tissues, it is selected as a potential candidate for communication.

Characteristics of fat tissue have been widely studied in the literature [45]–[47]. The relative permittivity and electric conductivity of the tissue depend on a number of factors, namely the frequency, moisture level, temperature, fluid, and mineral contents. It is important to understand the behavior of the tissues and how to measure dielectric properties of the tissues in order to transmit and receive electromagnetic radiations in the biological tissues. Generally, animal bodies are studied in order to develop and implement new technologies. Porcine tissues have great resemblance with the human tissues due to metabolic similarities, and the results obtained from porcine tissues can be more or less mapped to human tissues [48]. A detailed investigation has been conducted by Karacolak et al. (2012) [49] to measure dielectric properties of porcine skin, and its similar to human skin.

The relative permittivity and conductivity of human muscle and fat tissue given by Werber et al. (2006) [50] is tabulated in Table 2.1. From Table 2.1, at higher frequency, it can be seen that the relative permittivity decreases as the frequency increases while the conductivity increases. The observations which can be made are: for higher frequencies, the relative permittivity goes down slowly, while the conductivity increases gradually with higher frequencies. Furthermore, muscles have a high water content, whereas the water contents in fat is lower. Based on the values in Table 2.1, it is worth investigating the viability of muscle and fat tissue for the purpose of the communication channel.

Table 2.1. *Relative permittivity and conductivity of human fat and muscle tissue. Copyright ©2006, IEEE [50].*

Parameter /	Relative permittivity		Conductivity (S/m)	
Frequency (Hz)	Fat	Muscle	Fat	Muscle
100	4.57×10^5	9.33×10^6	2.08×10^{-2}	2.27×10^{-1}
100 k	92.9	8.9×10^3	2.44×10^{-2}	3.62×10^{-1}
400 M	5.58	57.1	4.11×10^{-2}	7.69×10^{-1}
1 G	4.6	42.8	5.85×10^{-1}	10.6

2.1.2 Numerical modeling

The 3D EM simulation commercial package CST Microwave Studio (CST Studio Suite - Dassault Systémes, France) from CST[2] software is used for the preliminary study. The main interest in designing and developing a numerical model is to assess the dependence of the attenuation factor on different tissue layer properties such as variation in the tissue thicknesses, and the distance between the transmitter and receiver.

The transmission channel of the biological tissues was characterized by designing two models, which comprise of the skin, fat (adipose), and muscle layers (arranged from top to bottom). To examine the effect of human anatomy on signal propagation, two separate models were designed with the same length and width of 50 mm (W) $\times$ 100 mm (L) as shown in Figure 2.2. To prove that the fat tissue is a better communication channel compared to the muscle tissue, the results of using the fat tissue as a communication channel were compared against the results obtained when using the muscle tissue. Figure 2.2(a) shows the waveguide port excitation in the fat tissue, and Figure 2.2(b) shows the waveguide port excitation in the muscle tissue. In the third dimension, the thickness for the fat (T_{F}) and muscle (T_{M}) tissues are varied from 5 mm to 45 mm with 5 mm steps. The skin thickness, T_{S} were fixed at 2 mm based on the average thickness of the skin [51], [52]. The distance L was selected according to the distance between major vital organs, for example, kidney-liver, kidney-pancreas, and heart-liver, and also from the previous experimental models used in other published studies [53]–[55].

A transmitting probe (TX) is used to launch a horizontal electromagnetic signal towards the opposite side of the tissue to the receiving probe (RX), which detects the signal. As a proof of concept, the built-in waveguide ports in the CST package were used to simulate the electromagnetic probes (TX and RX) with a radiation boundary condition surrounding the models to simulate non-reflecting environments. For the numerical studies, the human tissue[3] in the frequency range of 1–10 GHz was used.

In **Paper I**, the signal transmission in fat and muscle layers was investigated. From the results, it is observed that the signal transmission improves

[2]Computer Simulation Technology: https://www.cst.com

[3]Bio-tissue materials from CST software

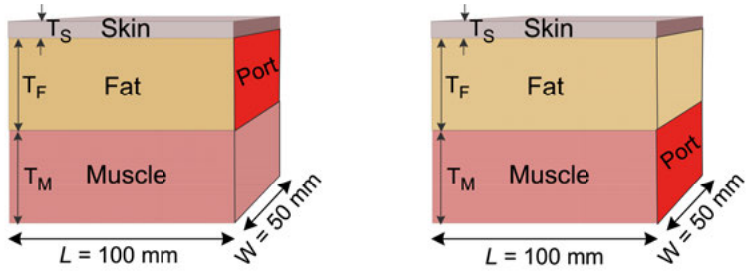

(a) *Transmission in the fat tissue.* **(b)** *Transmission in the muscle tissue.*

Figure 2.2. *The preliminary model to study the impact of the thickness variation in fat and muscle layers on the transmitted and reflected signals.*

as the thickness of the fat layer increases until 25 mm and does not change much when the thickness is increased further. In muscle, the signal transmission was found to be inefficient due to high dielectric losses in the layer. The comparative study was extended further to compare the performance of signal transmission between the fat and muscle tissues at a frequency of 5.8 GHz. Figure 2.3 shows the comparison of the signal transmission through the fat and muscle tissues. It can be seen that the signal transmission through the fat tissue is higher compared to the muscle tissue, which is expected due to the difference in dielectric constants. The attenuation in the muscle tissue is more than twice compared to the one in the fat tissue. For example, when the fat thickness is 25 mm, and the muscle thickness is 30 mm, the signal attenuation is –30 dB, –35 dB, and –36 dB at 2.0 GHz, 2.4 GHz, and 5.8 GHz, respectively. The signal attenuates considerably in the muscle, by –94 dB, –101 dB, and –107 dB, respectively.

To observe the channel characteristics, in **Paper VII**, measurements on three cases were performed, where the details are summarized in Table 2.2. According to **Paper VII**, results for Case 1 show that by varying the thickness from 10 mm to 35 mm, S_{21} increases until the thickness reaches 25 mm and then becomes approximately constant. Results also suggest that varying the thickness of muscle has a negligible effect on S_{11} and S_{21}. Results for Case 2 suggest that by varying the thickness of fat or muscle tissue, no significant changes are observed for S_{11} and S_{21}. When comparing the results of Case 1 with Case 2, it could be concluded that fat tissue is a better channel, which gives approximately 10 dB better signal strength than the muscle tissue. For Case 3, measurement results suggest that the amplitude of S_{21} roughly decreases by 2 dB per 20 mm for the case of phantom and 4 dB per 20 mm for the case of ex-vivo. Furthermore, the transmission loss is higher for the muscle tissue than for the fat tissue. Thus, fat tissue is more suitable as a channel for intra-body communication as compared to the muscle tissue.

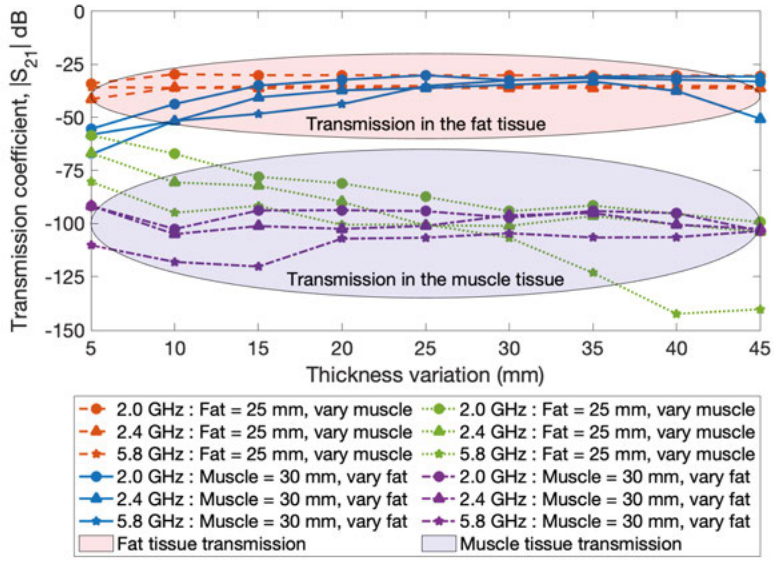

Figure 2.3. *The impact on the transmission coefficient, S_{21}, due to varying fat and muscle layer thicknesses.*

Table 2.2. *Cases to conduct experiments.*

Cases	Experiment 1		Experiment 2	
	Tissue	Thickness	Tissue	Thickness
Case 1: Waveguide aligned with fat layer	Skin Fat Muscle	Fixed at 2 mm 10–35 mm Fixed at 30 mm	Skin Fat Muscle	Fixed at 2 mm Fixed at 25 mm 20–45 mm
Case 2: Waveguide aligned with muscle layer	Skin Fat Muscle	Fixed at 2 mm 10–35 mm Fixed at 30 mm	Skin Fat Muscle	Fixed at 2 mm Fixed at 25 mm 20–45 mm
Case 3: Signal transmission distance	Probe alignment in the fat layer. Channel length varies from 20 to 100 mm with a step of 20 mm.		Probe alignment in the muscle layer.	

From this finding, it is indicative that the fat tissue is capable of becoming the transmission medium for in-body communication or labeled as Fat-intrabody communication (Fat-IBC). When fat tissue is sandwiched with the skin and the muscle tissues, a structure similar to a parallel plate waveguide is formed. In general, a parallel plate waveguide is formed by having two conductors on both sides of a dielectric material. The high contrast in dielectric properties between fat on one hand and skin and muscle, on the other hand, allows the signal to be confined within the fat layer.

In this research, it also strived to improve the performance of the Fat-IBC technique by increasing the signal transmission. The theoretical limitations of open-ended rectangular waveguides were superseded by mean of topology optimized probes that give a better matching along a wider range of frequencies. These probes were used as both transmitter and receiver in the studies. With the help of numerical and experimental characterization, deeper understanding and improvement of the performance of the Fat-IBC technique, were obtained.

2.1.3 Analytical channel modeling

Since the parallel plate waveguide is formed by two conducting plates, it can support transverse electric (TE), transverse magnetic (TM), and also transverse electromagnetic (TEM) modes.

By using an analytical channel model for a parallel plate waveguide, the propagation was studied in the z-direction keeping both plates infinite in the x-direction. Therefore, a simple parallel plate waveguide structure shown in Figure 2.4 is considered, where d is the distance separating the two perfect electric conductor (PEC) plates.

Figure 2.4. Parallel plate waveguide structure.

The boundary conditions are classified as to whether E_z or H_z exists accordingly as below:

TEM : $E_z = 0$, $H_z = 0$
TE : $E_z = 0$, $H_z \neq 0$
TM : $E_z \neq 0$, $H_z = 0$

According to Pozar [56], the transverse field components in TM modes can be computed as:

$$H_x = \frac{j\omega\varepsilon}{k_c} A_n \cos\frac{n\pi y}{d} e^{-j\beta z} \tag{2.1a}$$

$$E_y = \frac{-j\beta}{k_c} A_n \cos\frac{n\pi y}{d} e^{-j\beta z} \tag{2.1b}$$

$$E_x = H_z = 0 \tag{2.1c}$$

For TM mode, when $n = 0$ and $\beta = k = \omega\sqrt{\mu\varepsilon}$, and $E_z = 0$, the E_y and H_x fields are constant at any x-y plane. TEM mode has no cutoff frequency;

therefore in this condition, the TM_0 mode is identical to the transverse electromagnetic (TEM) mode. For $n > 0$, it corresponds to a different TM mode (i.e., TM_1, TM_2, TM_3, etc.) and each mode has its own propagation constant and field expression.

Next, the transverse field components for TE modes are:

$$E_x = \frac{j\omega\mu}{k_c} B_n \sin\frac{n\pi y}{d} e^{-j\beta z} \tag{2.2a}$$

$$H_y = \frac{j\beta}{k_c} B_n \sin\frac{n\pi y}{d} e^{-j\beta z} \tag{2.2b}$$

$$E_y = H_x = 0 \tag{2.2c}$$

For TE mode, when $n = 0$, then $E_x = H_y = 0$ there is no TE_0 mode. The propagation constant, β and the cutoff frequency, f_c are the same as TM_n mode.

The propagation constant of the TM_n mode and the TE_n mode are given as:

$$\beta = \sqrt{k^2 - \left(\frac{n\pi}{d}\right)^2} \tag{2.3}$$

The cutoff frequency of the TM_n and TE_n mode is defined to be at the onset of propagation.

$$f_c = \frac{n}{2d\sqrt{\mu\varepsilon}} \tag{2.4}$$

where:

f_c = rectangular waveguide cut-off frequency in Hz
d = distance between the plates
n = mode propagation number (e.g., 1, 2, 3)

It should be emphasized that the concept of Fat-IBC is not equivalent to a parallel waveguide since the skin and muscle characteristics are lossy, which will not give perfect conductor boundary conditions.

2.2 Dielectric properties of tissue and materials

The dielectric properties of any material provide an insight into the feasibility of using that material for potential applications. In the work of this thesis, the dielectric properties of each material and tissues that are used during the laboratory experimentation were measured to confirm that these values are similar to the real human tissue values. It is also important to understand the properties of the dielectric materials, especially the permittivity and loss tangent at the operating conditions. That will be explained in the next section. According to Keysight Technologies application note [57], there are six measurement techniques for the dielectric constant and the loss tangent of a material. The methods include Coaxial Probe, Transmission Line, Free Space, Resonant Cavity, Parallel Plate, and Inductance measurement. In order to select the most appropriate measurement technique, different factors such as the frequency range, accuracy, material form (i.e., liquid, powder, semi-solid, solid, or sheet), and the convenience to handle the measurement must be taken into consideration. Upon deliberation, the coaxial probe measurement technique was selected as it is an ideal method to measure homogeneous and semi-solid material.

2.2.1 Dielectric properties theory

The permittivity of dielectric material, denoted by ε, has a real and an imaginary part,

$$\varepsilon = \varepsilon' - j\varepsilon'' \tag{2.5}$$

where the real part $\varepsilon' = \varepsilon_r \varepsilon_0$ relates the material dielectric constant ε_r to the free space permittivity $\varepsilon_0 \approx 8.854 \times 10^{-12}$ F/m. The dielectric constant refers to the efficiency of dielectric material in storing the electric energy, whereas the imaginary part ε'' indicates loss of electrical energy [58]. The imaginary part ε'' is labeled as the loss factor. The loss factor includes the effects of dielectric loss [59]. It is common to combine the material dielectric and ohmic losses to define the so-called loss tangent.

$$\tan\delta = \frac{\omega\varepsilon'' + \sigma}{\omega\varepsilon'} \tag{2.6}$$

where σ is the material electric conductivity. The numerator of (2.6) is known as the real part of the displacement current, and the denominator is its imaginary part [56]. Moreover, in some occasions the numerator terms is called the material effective conductivity $\sigma_{\text{effective}} = \omega\varepsilon'' + \sigma$. Figure 2.5 shows a representation of the loss tangent as a vector diagram.

For loss-free materials, the loss tangent is zero. The loss tangent increases as the dielectric or ohmic losses increase. Therefore, the loss tangent is typically used to indicate the energy dissipation in the material.

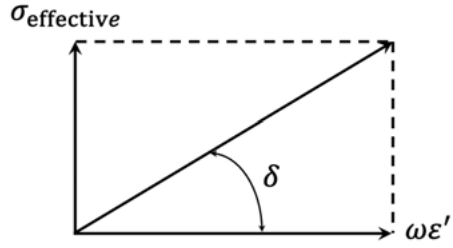

Figure 2.5. The loss tangent defined by the vector diagram.

Table 2.3. *Comparison of dielectric properties between the skin, fat, and muscle tissue [60].*

Frequency (GHz)	Tissue	Relative Permittivity, ε_r'	Conductivity, (S/m)	Loss Tangent, $\tan\delta$
2.4	Skin	42.92	1.56	0.27
	Fat	5.29	0.10	0.15
	Muscle	52.79	1.71	0.24
5.8	Skin	38.62	4.3	0.34
	Fat	4.95	0.29	0.18
	Muscle	48.48	4.96	0.32

In communication systems, a material with a large dielectric loss has a high degree of dielectric absorption and thus higher attenuation. Hence, this represents a limitation in the transmission of long-range signals. From the perspective of Fat-IBC, the fat tissue has lower dielectric loss than the skin and muscle tissue. Table 2.3 presents the dielectric properties of the skin, fat, and muscle tissue [60]. It can be seen that the permittivities of the skin and muscle are about 8–10 times higher, which makes the wave propagate slower and have more cycles to attenuate itself in a given physical length. Therefore, fat tissue can be considered to be an effective low-loss communication medium.

2.2.2 Coaxial probe measurement technique

In this study, the open-ended coaxial dielectric probe techniques was applied to evaluate the lossy material sample over different ranges of frequencies. The open-ended coaxial probe consists of a flat cut-off section of the transmission line. The reflection coefficient (S_{11}) of an open-ended coaxial line is dependent on the dielectric properties of the material under test (MUT) that is attached to it [57] making the method suitable for this study. Furthermore, it can be used on liquid, solid, or semi-solid samples.

For the measurement of the dielectric properties for a tissue-equivalent phantom and ex-vivo tissue samples, the slim form probe in the Agilent 85070E (now Keysight N1501A) Dielectric Probe Kit was used. A proper calibration procedure is necessary to produce reliable dielectric properties measurements. In general, for coaxial probe measurements, a three-load standard calibration procedure for one-port error correction is applied. There are three common standards used for coaxial probe calibration, including open, short, and water. During the calibration process, the normal three standard calibrations as mentioned above, would be performed at the end of the probe based on the guidance of the 85070E Dielectric Probe Kit software. For this study, a conducting elastomer-based standard was used for short calibration. As for load calibration, any liquid with known dielectric properties can be used, and the deionized (DI) water was chosen for this purpose. The calibration was performed at the reference plane of the probe, and the probe was connected via a cable with a 2.4 mm to 3.5 mm adapter to the Vector Network Analyzer (VNA) or FieldFox Handheld RF and Microwave Analyzer.

For the measurement of a solid MUT, the probe was brought into contact with the flat surface of the material. The measured reflected signal is a function of the fringing electromagnetic (EM) fields interacting with the MUT at the open-ended aperture of the probe. Based on the reflected signal, the software is able to calculate and display the complex permittivity in different formats, including dielectric constant, dielectric loss factor, loss tangent, or Cole-Cole plots. According to the datasheet of the 85070E Dielectric Probe Kit, the measured value typically has an uncertainty of 10 %. In order to reduce any additional systematic error, five repeated dielectric measurements were taken to ensure that the standard deviation of these repetitions was much smaller than the typical instrument uncertainty. Figure 2.6 shows the example of N9918A FieldFox Handheld Microwave Analyzer operating as a VNA and the dielectric probe kit setup.

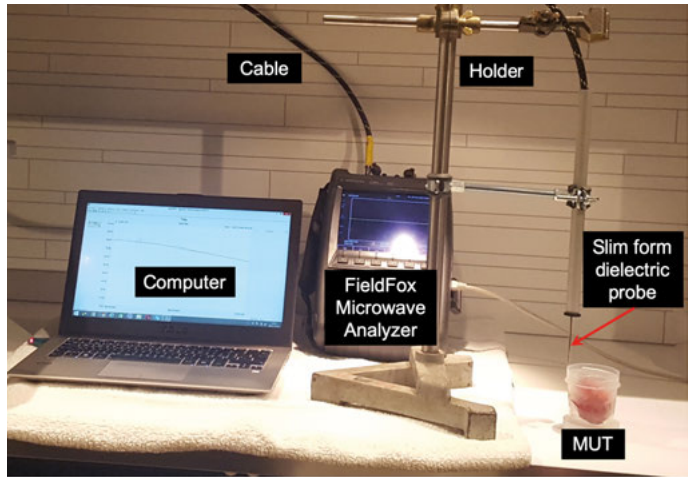

Figure 2.6. *N9918A FieldFox Handheld Microwave Analyzer and 85070E Dielectric Probe Kit setup.*

2.2.3 Dielectric properties of tissues and materials

To improve the performance of Fat-IBC, various types of tissue-equivalent phantom and ex-vivo porcine tissue were used in this study and reported in **Papers I–VII**. Figures 2.7–2.9 show the comparison between the dielectric properties for tissue-emulating phantom materials, ex-vivo porcine tissues, and human tissues as a function of frequency. Agar-based compounds were used to fabricate phantom materials to emulate the typical response of the human skin and muscle tissues to microwave signals. Similarly, rubber- and oil-based materials were used to fabricated phantom materials emulating fat tissue. These skin, muscle, and fat phantom materials were used to create fat channel models for laboratory studies. Samples of skin, fat, and muscle tissues were separated from a fresh part of a porcine belly. The fat and muscle tissues were also minced. The skin slab samples and the minced fat and muscle samples together with very-low-permittivity 3D printed molds were used to create fat channel models for laboratory studies as well.

As can be seen in Figures 2.7–2.9, in the frequency of interest, the dielectric properties are almost constant for fat tissue, while for the skin and muscle slightly linear. This is because the skin and the muscle are frequency dependent in the dielectric constant and conductivity.

In order to have a more realistic scenario to study the Fat-IBC approach in laboratory, it is crucial to characterize the different types of materials including tissue-equivalent phantoms and ex-vivo tissues that can emulate the human fat tissue as well as the skin and muscle tissues in a better manner. Figure 2.8 shows the comparison of the real part of the permittivity (ε_r') and loss factor (ε_r'') for different materials, which emulate the microwave properties of the fat tissue. In **Paper I**, a synthetic rubber material was used to develop the rectangular waveguide probes, and an adhesive putty was used to mimic the fat tissue channel. The frequency used in the paper was 2.0 GHz. In **Paper II** and **III**, a vulcanized rubber material was used to fill the fat-equivalent in the rectangular waveguide probes operated at R-band (1.7–2.6 GHz) frequencies and F-band (4.9–7.05 GHz) frequencies. The vulcanized rubber was chosen over the synthetic rubber because its properties are similar to the human tissue, and its robust and solid nature makes it easily machined into different geometrical shapes. The vulcanized rubber and oil-based phantom materials have both been used as phantom materials for a fat channel model.

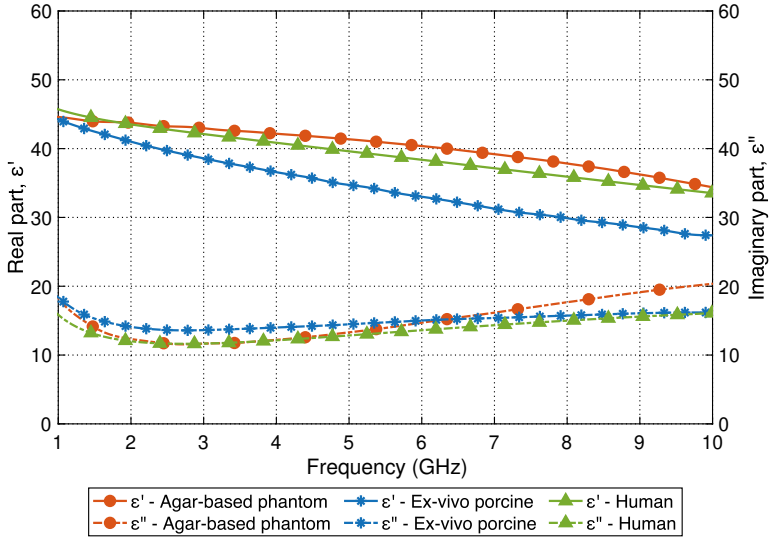

Figure 2.7. *Dielectric properties of different materials of the skin tissue for 1–10 GHz frequency range.*

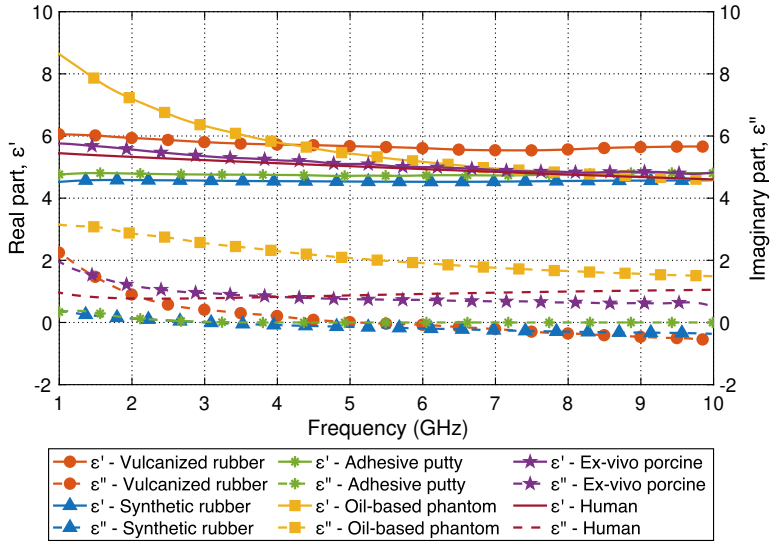

Figure 2.8. *Dielectric properties of different materials of the fat tissue for 1–10 GHz frequency range.*

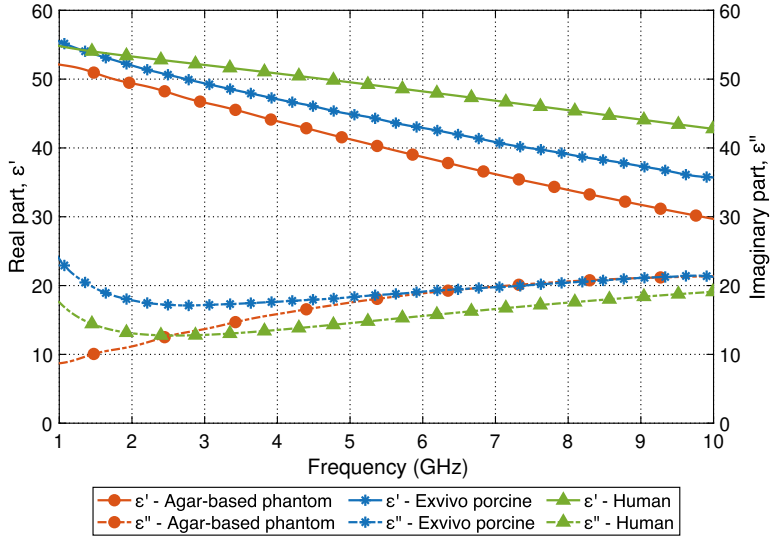

Figure 2.9. *Dielectric properties of different materials of the muscle tissue for 1–10 GHz frequency range.*

The real part of the relative permittivity (dielectric constant) and loss tangent for different materials of the skin, fat, and muscle tissues that are relevant for medical implants are listed in Tables 2.4–2.6. The data is given for the frequencies of 2.4 GHz and 5.8 GHz, which constitutes two ISM frequency

bands. The human tissue data were extracted from Gabriel et al. [58]. It is important to highlight that the fat tissue has significantly lower permittivity and conductivity than skin and muscle tissues.

Table 2.5 shows that the loss tangent of the oil-based phantom is slightly higher than the actual tissue. This may result in substantial variation in the transmission signal results when compared to the human and the ex-vivo tissue. Despite that, the oil-based phantom allows the phantom to be more flexible. Future experimental studies should take the dynamics associated with human movements into consideration. Flexible and elastic phantom materials will enable the incorporation of dynamics in the future. The measured dielectric dispersion profiles for the considered materials and/or tissues were used in our numerical fat channel models as a primary approach to validate the measurement results.

Table 2.4. *Relative permittivity (real part) and loss tangent for different materials of the skin tissue at 2.4 GHz and 5.8 GHz.*

Material	Relative Permittivity, ε'_r		Loss Tangent, tan δ	
	2.4 GHz	5.8 GHz	2.4 GHz	5.8 GHz
Agar-based phantom	44 ± 4	41 ± 4	0.28 ± 0.03	0.36 ± 0.04
Ex-vivo porcine	40 ± 4	33 ± 3	0.34 ± 0.03	0.45 ± 0.04
Human tissue	38 ± 2	35 ± 2	0.28 ± 0.01	0.33 ± 0.02

Table 2.5. *Relative permittivity (real part) and loss tangent for different materials of the fat tissue at 2.4 GHz and 5.8 GHz.*

Material	Relative Permittivity, ε'_r		Loss Tangent, tan δ	
	2.4 GHz	5.8 GHz	2.4 GHz	5.8 GHz
Synthetic rubber	4.5 ± 0.5	4.5 ± 0.5	0.017 ± 0.002	0.04 ± 0.004
Adhesive putty	5.0 ± 0.5	4.7 ± 0.5	0.01 ± 0.001	0.016 ± 0.002
Vulcanized rubber	5.9 ± 0.6	5.6 ± 0.6	0.11 ± 0.01	0.01 ± 0.001
Oil-based phantom	6.8 ± 0.7	5.2 ± 0.5	0.41 ± 0.04	0.37 ± 0.04
Ex-vivo porcine	5.5 ± 0.5	5.0 ± 0.5	0.19 ± 0.02	0.15 ± 0.01
Human tissue	5.3 ± 0.3	5.0 ± 0.2	0.15 ± 0.01	0.18 ± 0.01

Table 2.6. *Relative permittivity (real part) and loss tangent for different materials of the muscle tissue at 2.4 GHz and 5.8 GHz.*

Material	Relative Permittivity, ε'_r		Loss Tangent, tan δ	
	2.4 GHz	5.8 GHz	2.4 GHz	5.8 GHz
Agar-based phantom	49 ± 5	39 ± 4	0.23 ± 0.02	0.48 ± 0.05
Ex-vivo porcine	51 ± 5	43 ± 4	0.34 ± 0.03	0.44 ± 0.04
Human tissue	53 ± 3	48 ± 2	0.24 ± 0.01	0.32 ± 0.02

2.3 Measurements setup

In this section, the measurement setups used to obtain the experimental data for the characterization of the Fat-IBC techniques (**Papers I–III**) are explained. Figure 2.10 shows the measurement setup as applied in the Fat-IBC system. Measurements were conducted to demonstrate the performance of the signal transmission through the fat tissue using the Fat-IBC technique.

The measurement setup consists of three main components:

1. A pair of rectangular waveguide-based probes as a transmitter (TX) and receiver (RX).
2. A microwave analyzer, for example, the FieldFox Handheld RF and Microwave Analyzer or Vector Network Analyzer.
3. A three-layered tissue consisting of skin, fat, and muscle as a fat channel model.

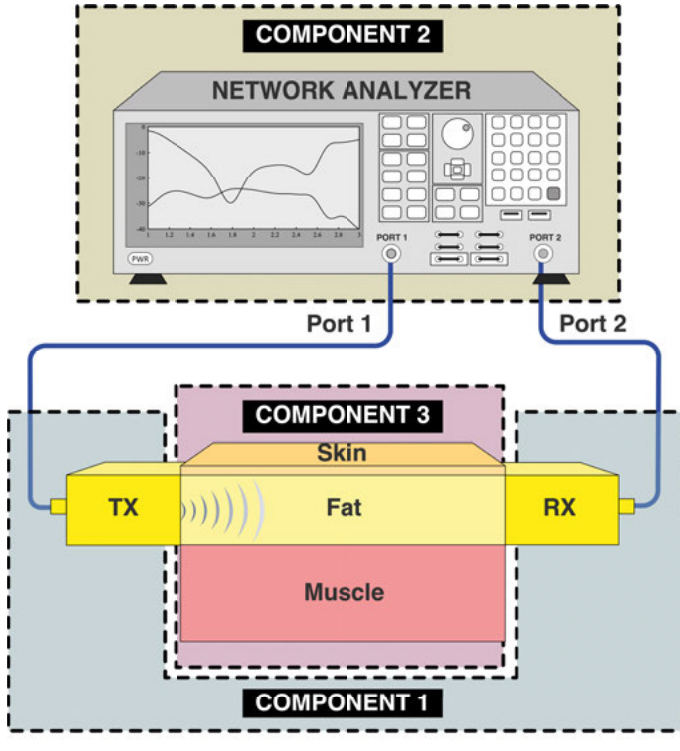

Figure 2.10. The Fat-IBC measurement setup.

The transmitter (TX) probe radiates the electromagnetic (EM) waves from Port 1 of the microwave analyzer. The signal travels through the fat tissue, which is the transmission medium before reaching the receiving probe (RX) at the other end. As the EM wave travels away from the transmitter, the strength of the signal decreases.

Papers I–III use the same experimental setup except for Component 1, the rectangular waveguide-based probes. Different probes were used to examine the performance at different frequencies, namely 2.0 GHz, 2.4 GHz, and 5.8 GHz. The probe in **Paper I** was used for determining the performance of the signal transmission at a frequency of 2.0 GHz, whereas other different probes were used to examine the performance at frequencies of 2.4 GHz and 5.8 GHz in **Papers II** and **III**, respectively. In **Papers IV–VI**, the measurement setups were similar except for changes in Component 3. Several modifications in the fat channel model were performed to examine the factors that influence the performance of Fat-IBC. In Chapter 5, the experimental setup reported in **Paper VII** was used in which the Components 1 and 2 were both different from **Papers I–VI**.

2.3.1 Topology-optimized waveguide-based probe design

To achieve our vision to demonstrate the concept in a real scenario, three types of topology-optimized waveguide-based probes were designed and developed, and each of them was optimized for a specific frequency band. The design of the probes is to determine the insertion loss in the fat-channel based on a realistic probe excitation.

The first research direction which explored the frequency 2.0 GHz was inspired by a numerical study, as explained in **Paper I**. Considering that the probe should operate in the ISM band, the necessary step was taken to make it possible for the realization of the implants. Therefore, the second research focused on investigating the use of typical ISM band at 2.4–2.45 GHz to be incorporated into the medical application by implementing the second probe at R-band frequencies (**Paper II**). In **Paper III**, another ISM band frequency of 5.8 GHz was chosen to allows a small probe size design, taking into consideration that higher frequencies are beneficial. Apart from miniaturization purposes, high frequencies allow larger bandwidth, and, therefore, higher bit rates.

The probe consists of three elements:
1. A rectangular waveguide probe filled with the fat-equivalent phantom.
2. A standard SubMiniature version A (SMA) connector.
3. A topology-optimized planar antenna (TOPA).

Figure 2.11 shows the cross-sections of the three probes to explain the elements inside the probes and their dimensions. The probes are similar to waveguide-coax transitions with Figure 2.11(a) fed on the broad side of the waveguide at a distance of $\lambda/4$ to the end side, and Figures 2.11(b) and 2.11(c) are fed like an end-launcher waveguide-coax probe. In addition, the waveguides are filled with fat-equivalent material and excited by the TOPA element, which is in yellow color in the figures to match with the fat in the transmission channel. The topology-optimized planar antenna is immersed at the center of the equivalent fat-filled (i.e., rubber compound) copper waveguide. An SMA connector is attached at the end of the waveguide probe.

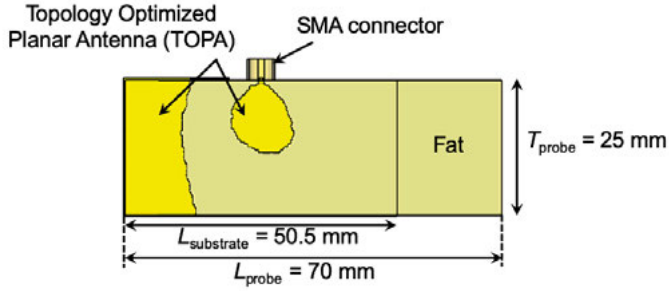

(a) *2.0 GHz waveguide probe.*

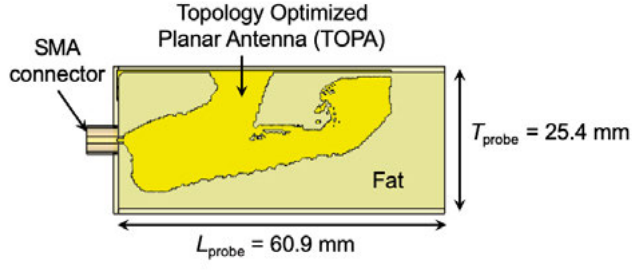

(b) *2.4 GHz waveguide probe.*

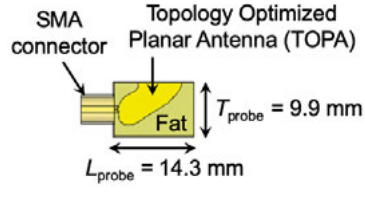

(c) *5.8 GHz waveguide probe.*

Figure 2.11. *The cross-section view of the topology-optimized planar antenna and the rectangular waveguide probes used to characterized the Fat-IBC. Yellow color in the figures is the TOPA element.*

First prototype: ***R-band probe, optimized for 2.0 GHz***

The design of the probe is chosen from the standard waveguide size. The cross-section of the waveguide-based probe was based on a standard WR430 waveguide, but scaled down by the square root of the dielectric constant of fat tissue. This is because, it helps to reduce the size for the same operating frequency. The WR430 waveguide is chosen according to the needs of the study, which are the operating frequency ranges and the inner dimensions of the waveguide aperture. To ensure the continuity of the electromagnetic waves from the probe to the fat tissue, the probe was filled with synthetic rubber with dielectric properties similar to the fat tissue. A topology-optimized planar antenna was then immersed at the center of the synthetic rubber and the whole rubber structure was covered with copper tape to form a coaxial-to-waveguide probe. To validate the performance of the fabricated probes, their scattering parameters were measured. Figure 2.12 shows the simulated and measured scattering parameters of the probe-to-probe measurement. The probe-to-probe S_{21} results are the attenuation of the waveguide probes at 0 mm channel length at certain frequency. The S_{21} results will be used as a reference for the subsequent measurements, especially when determining the signal path loss in Chapter 3. As can be seen from the results, this prototype did not perform well in the entire range of the R-band. However, it fulfilled the requirement of operating well at a frequency of 2.0 GHz. Here, the probe-to-probe S_{21} results at 2.0 GHz is –1.5 dB and –2.9 dB for simulation and measurement, respectively. With this in mind, it is also strived to work harder to improve the design of the probes to achieve better signal coupling between the two probes in the fat tissue.

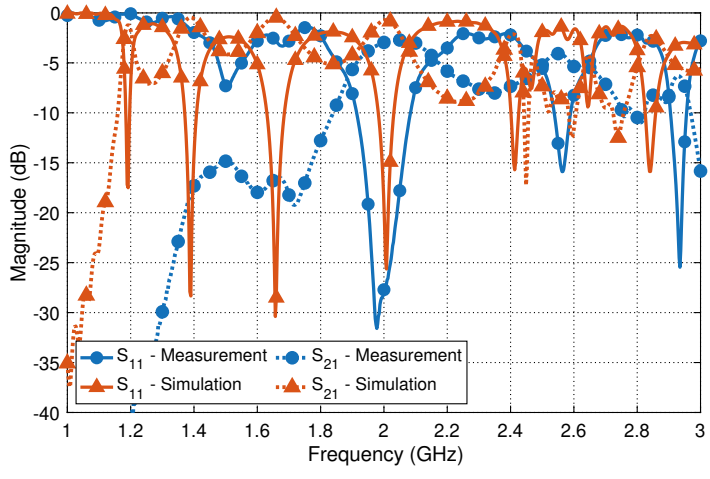

Figure 2.12. *Scattering parameters of the probe-to-probe measurements (first prototype).*

Second prototype: ***R-band probe, optimized for 2.40–2.45 GHz***

The second prototype was successfully produced and tested. A novel waveguide-based probe that performed excellently within the R-band frequencies (1.7–2.6 GHz) in the fat tissue. This second prototype was developed based on a standard WR430, but scaled down by the square root of the dielectric constant of fat tissue as well. The design of the topology-optimized planar antenna (TOPA) was improved, which is an essential element in the probe development. The synthetic rubber of the probe was substituted with vulcanized rubber. A slot was made at the center of the rubber to immerse the TOPA. During the development of this prototype, the copper plate was used to form the outer layer of the probes. Figure 2.13 shows the measured and simulated scattering parameters of probe-to-probe measurements. The results show an excellent match between the two probes, and the signal coupling recorded was almost constant in the range of R-band frequencies. The attenuation of the probe-to-probe (reference) for this prototype is essentially a constant value of 2 dB over the whole R-band frequencies and at 2.4–2.45 GHz ISM band.

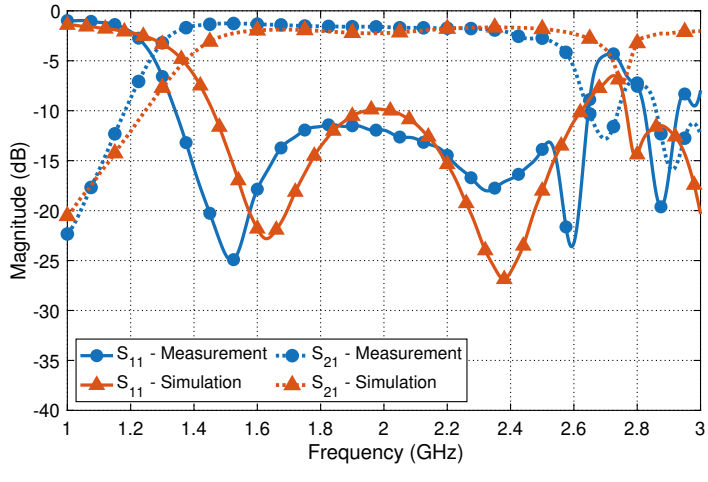

Figure 2.13. *Scattering parameters of the probe-to-probe measurements (second prototype).*

Third prototype: ***F-band probe, optimized for 5.8 GHz***

The motivation to design a third probe was to explore other ISM band frequencies and to broaden the possibility of using the Fat-IBC technique at higher frequencies. A standard WR75 waveguide was chosen in the development of the probe with a volume of $9.9 \times 19.1 \times 14.3$ mm^3. Similar to the previous probes, this probe also consisted of the topology-optimized planar antenna. It used the same fabrication method as the second prototype, where vulcanized rubber with dielectric properties that are similar to the human fat tissue was used. Figure 2.14 shows the simulated and measured scattering parameter of the third prototype. The waveguide covered the F-band frequencies of 4.9–7.05 GHz, including the 5.8 GHz ISM band. The probe-to-probe (reference) has an attenuation of 2 dB and 2.2 dB for simulated and measured results, respectively.

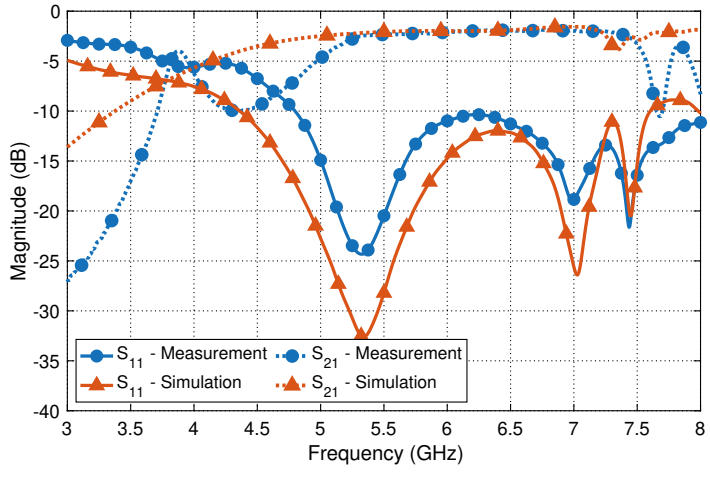

Figure 2.14. *Scattering parameters of the probe-to-probe measurements (third prototype).*

The prototypes of the waveguide-based probes are shown in Figure 2.15. In Table 2.7, the characteristics of the different prototypes of the probe are summarized. The quantitative simulation and measurement results of the path loss are discussed and analyzed in Chapter 3.

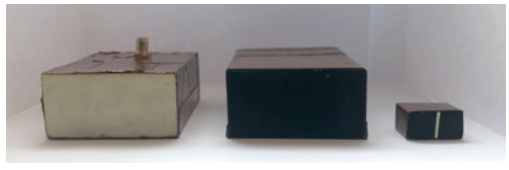

(a) *Front view.*

(b) *Top view.*

Figure 2.15. *The prototypes of the rectangular waveguide-based probes. The probes are designed for 2.0 GHz, 2.4 GHz, and 5.8 GHz (from left to right).*

Table 2.7. *Specifications of 2.0 GHz, 2.4 GHz, and 5.8 GHz probes, including those of the topology-optimized planar antenna.*

Parameters	Prototype of the probe		
	1st probe	2nd probe	3rd probe
Waveguide section, $W \times T \times L$ (mm^3)	$25 \times 50.5 \times 70$	$25.4 \times 50.7 \times 60.9$	$9.9 \times 19.1 \times 14.3$
Frequency range	1.9–2.1 GHz	1.7–2.6 GHz	4.9–7.05 GHz
Design frequency	2.0 GHz	2.4–2.45 GHz	5.8 GHz
Fat-filled permittivity	4.5 ± 0.5	5.9 ± 0.6	5.6 ± 0.6
Antenna dimension	25×50.5 mm^2	25.4×50.7 mm^2	9.90×10.35 mm^2
Type of substrate	Rogers RO3203	Rogers RO3203	Rogers TMM6
Substrate permittivity	3.02 ± 0.04	3.02 ± 0.04	6 ± 0.08
Substrate thickness	0.75 mm	0.75 mm	0.64 mm
Substrate loss tangent	0.0016	0.0016	0.0023

3. Fat-IBC signal path loss

Path loss, or path attenuation, is defined as the reduction in the power density (attenuation) of an electromagnetic wave as it propagates through a medium [61]. Notably, path loss varies across certain frequencies when the signal propagates through different media [62]. Furthermore, it is a major component in the analysis and design of the link budget of a communication system. It enables the reuse of wave frequency after certain distances in a communication network, contributing to an increase in the system's capacity and efficient use of the allocated frequency for its relevant applications. Although the channel's characteristics could be determined by modeling the path loss, the communication link would be broken when the signal is not amplified or regenerated. In this study, a quantitative path loss for the Fat-IBC was obtained based on a numerical and experimental approach.

The path loss is caused by various phenomena, such as reflection, refraction, aperture medium coupling loss, absorption, and the reflective and refractive index of the incident surface among others. In the case of Fat-IBC, there are various factors of path loss in the communication channel, namely the propagation medium (dry or moist air, skin, fat, muscle), the distance between the transmitter and the receiver, and the height and location of antennas. By modeling the path loss, new insights could be developed regarding the channel characteristics, contributing to the construction of an end to end network. In this study, numerical modeling and experimentation for Fat-IBC were performed, leading to notable results of path losses at 2.0 GHz, 2.4 GHz, and 5.8 GHz. Moreover, the characterization techniques possibly held a significance, especially in the cases where more than two frequency bands were concurrently used to propagate in the fat tissue. In mathematical terms, it could be expressed through Eq. (3.1).

$$PL_{dB} = \frac{P_{in}}{P_{out}} = -10\log_{10}|S_{21}|^2 = -|S_{21}|_{dB} \tag{3.1}$$

This chapter elaborates on parameter considerations, which are the essential components in designing Fat-IBC systems. The remaining sections of this chapter are summarized as follows:

- **Section 3.1**: In **Paper I**, the signal path loss at 2.0 GHz was investigated to characterize the Fat-IBC. The signal transmission results from the tissue-equivalent phantom and ex-vivo tissue were measured and simulated.
- **Section 3.2**: In **Paper II**, further investigation was performed on the characterization of the signal transmission and the signal path loss at 2.4 GHz, which had not been identified in **Paper I**.
- **Section 3.3**: Besides the purpose of miniaturization for implanted devices application, further characterization of the 5.8 GHz ISM band frequency was a remarkable aspect of this study. The signal path loss of the homogeneous model on the Fat-IBC are illustrated in **Paper III**.

For **Papers I–III**, the three-layered structure consisting of skin, fat, and muscle with a total length of 100 mm was used. The coupling coefficient, S_{21} was demonstrated for tissue-equivalent phantom and ex-vivo. The length of the channel was made to range from 20 mm to 100 mm with a step size of 20 mm. Furthermore, the thickness of the skin was determined as 2 mm, with a muscle thickness of 30 mm. The experiments conducted were compared with the simulations for both phantom and ex-vivo environments.

3.1 Signal path loss at 2.0 GHz

The signal path loss at 2.0 GHz was investigated to describe the Fat-IBC. The first optimized probe prototype was used for simulation and experimentation. The signal transmission results from the tissue-equivalent phantom and ex-vivo tissues were obtained through the aforementioned approaches.

As a result, there was a good correlation between S_{21} measurement and the simulation results. It could be seen that for the simulated and measured results, the path loss for the phantom was 1 dB/cm. In the case of the ex-vivo, the path loss was condensed by 2 dB/cm. Moreover, the improvement in signal transmission was noticeable with the thickness of adipose tissues. As for the adipose tissue, the ideal signal-coupling occurred at 25 mm tissue thickness or higher. Therefore, 25 mm could be considered as the optimal thickness for transmission through the adipose tissue. Additionally, the amplitude of the S_{21} was observed at –15 dB. There was no significant change observed by varying the muscle layer thickness. Overall, satisfactory results between simulation and measurements were obtained.

3.2 Signal path loss at 2.4 GHz

To observe the signal path loss at 2.4 GHz, the second optimized probe prototype was used to study the average path loss of the fat channel. After the investigation of the signal path loss behavior, it was summarized into three cases. Figure 3.1 summaries the signal path loss behavior in the three cases:

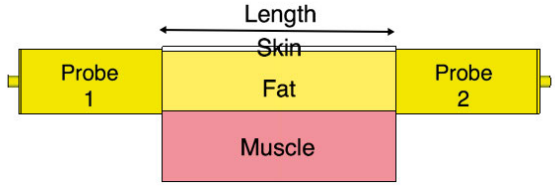

(a) *Case 1: The three-layered skin-fat-muscle waveguide section.*

(b) *Case 2: A dielectric rectangular waveguide section made of fat as a fat channel model.*

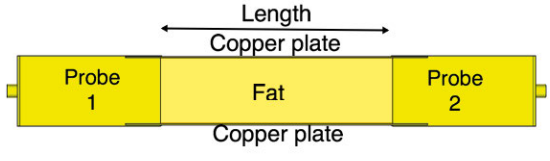

(c) *Case 3: A parallel-plate waveguide section filled with fat as a fat channel model.*

Figure 3.1. *The fat channel model cases for **(a)** generic three-layered structure, **(b)** in the absence of skin and muscle tissue, and **(c)** in the presence of parallel copper plates. **Paper II**. Reprinted, with permission, from [35]. Copyright ©2018, MDPI.*

In respect of the first case (see Figure 3.1(a)), the R-band frequencies for S_{21} were constant over the frequency range from 1.7 GHz to 2.6 GHz. These frequencies then transitioned with –3.5 dB to approximately –9 dB due to the increase in the channel length from 20 mm to 100 mm. For every 10 mm channel length, the average path loss was nearly 0.7 dB. This was followed by S_{21} results for porcine tissue. Similar to the results regarding the three-layered phantoms, a similar trend could be seen from S_{21} for the porcine tissue. To be specific, a flat response was obtained over the R-band frequencies. Furthermore, the magnitude of S_{21} amounted to –7 dB with a 20 mm channel length. Another remarkable observation of S_{21} was the decrease in its magnitude by 1.9 dB for each 10 mm increase in the channel length. Based on the comparison between the results of phantom and ex-vivo tissue, it could be concluded

that the propagation loss in the phantom and the ex-vivo environments is $\sim$0.7 dB/cm and $\sim$1.9 dB/cm respectively.

In further investigations on the first case, the skin and muscle tissues were detached from the model. The S_{21} was evaluated between the transmitting and receiving probes in the sole presence of the fat tissue (see Figure 3.1(b)). In this case, the fat tissue was similar to a dielectric waveguide [63]. Furthermore, the value of S_{21} between the two probes was reduced compared with the case of the presence of skin and muscle layers (generic structure). This reduction was due to the leakage of the transmitted signal into the free space from the boundaries of the waveguide. Nevertheless, this signal leakage from the waveguide was prevented by the skin and muscle. The S_{21} between the probes was also constant across the R-band frequencies. This was followed by a minor change in S_{21} when the length of the channel increased from 20 mm to 100 mm.

The parallel plate waveguide structure is illustrated in Figure 3.1(c). The behavior of the channel was investigated upon the absence of the skin and muscle tissues. Notably, these tissues were replaced by two parallel plates of copper. As expected, the path losses were reduced. This is because the copper did not allow the leakage of signal from the waveguide, contributing to an overall increase in the magnitude of S_{21}. Furthermore, the presence of skin and muscle tissues preserved the transmission coefficient. However, their absence would lead to decreased signal strength. Compared to the absence of the copper plate, S_{21} displayed a better response when the fat tissue was covered by the copper plate for the second time. In a nutshell, based on the comparison between the results of all aforementioned three cases, it could be concluded that the three-layered structure was better than a single layer fat channel (dielectric waveguide) in terms of a communication link. It should be noted that dielectric waveguide phenomenon is not applicable in real life as the human body naturally consists of three-layered, skin-fat-muscle tissues. The three-layered channel model functioned as a waveguide structure, where the path loss was lower than the path loss in the fat dielectric waveguide. In contrast, the waveguide structure path loss was higher than the copper plate waveguide, because of the lossy nature of the skin and muscle tissues compared to the copper.

An observation was conducted on the electric field distribution for certain cases. Through this observation, new insights could be developed into the propagation of the signal when it was launched to the channel and any phenomena occurring during the transmission. As shown in Figure 3.2(a), the electric field was observed when the two probes were located in the free space. High values could be seen from the electric field only located within the transmitting probe. Meanwhile, a mismatch was found between the probe and the free space. Based on the fat dielectric waveguide structure in Figure 3.2(b), the leakage of a significant portion of E-field was found in the free space, followed by the acquirement of a small amount of energy at the receiving probe. In respect of the third case in Figure 3.1(a) and the results shown in Figure 3.2(c), the signal was confined between the skin and the muscle, which could be seen as a wave flow through the fat channel.

(a) *The free space channel.*

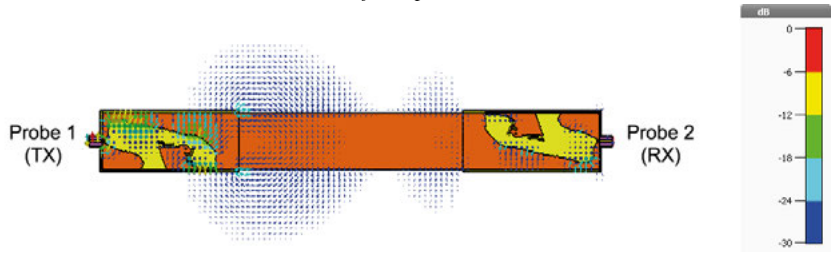

(b) *The fat layer channel.*

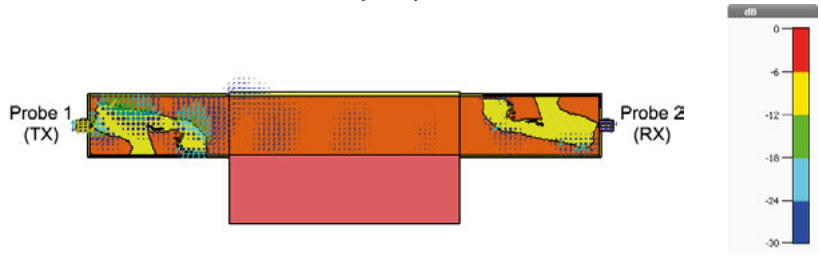

(c) *The three-layered fat channel.*

Figure 3.2. *The simulated electric field distribution of three models at 2.4 GHz.* ***Paper II****. Reprinted, with permission, from [35]. Copyright ©2018, MDPI.*

Based on the statistics shown in Figure 3.3, a minimum average path loss was present in the third case (copper plates) where the path loss was at 0.15 dB/cm for simulation and measurement. Meanwhile, the maximum average path loss was found in the second case (single layer fat channel), where the loss was at 0.65 dB/cm for simulation and 0.55 dB/cm for measurement. It was indicated from these findings that fat only channel has a significant wave leakage. Nevertheless, proper protection of the leakage signal was present in parallel plates, making it ideal for skin, fat, and muscle configuration. Overall, the above findings were in an agreement at 2.4 GHz. A remarkable correlation could also be seen from the simulated and measured results.

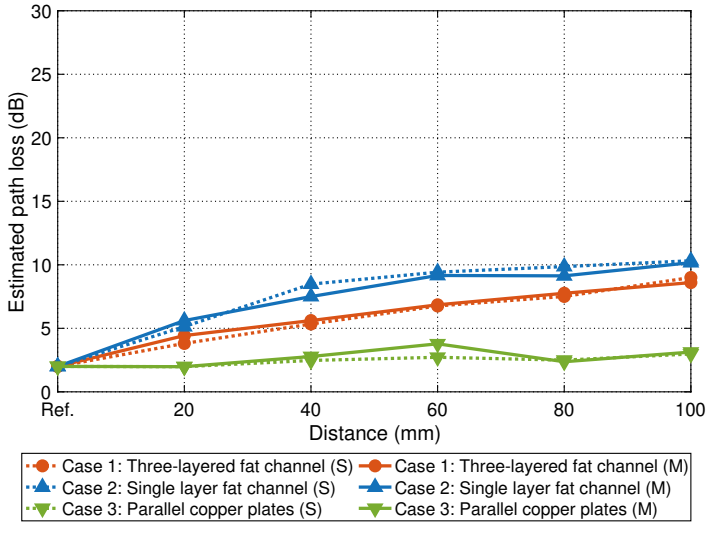

Figure 3.3. *The comparison of simulated and measured path loss summary for cases 1, 2, and 3 at 2.4 GHz.*

3.3 Signal path loss at 5.8 GHz

In this section, the simulation and experimental details are demonstrated for the observation of the signal path loss at 5.8 GHz. Therefore, the modeling of the system was conducted through several methods, which will be elaborated in the following parts of this section. The S_{21} parameters were then registered for each configuration.

The Fat-IBC system was modeled through four configurations, namely Type A, Type B, Type C, and Type D. In Type A, the three-layered structure was modeled in a way that a constant width, W of all the layers was used. Meanwhile, Figure 3.4(a) illustrates the three-layered structure for Type A configuration. As for Type B, we extended the channel width, W_{extend} to 50 mm. The thickness of skin and muscle in Type B was perceived to be similar to Type A. The Type B arrangement is shown in Figure 3.4(b). In respect of Type C configuration, the width of the channel was kept to be fixed as Type A, with an increase in the thickness of the fat. The structure of Type C is shown in Figure 3.4(c). In the case of Type D, the attributes of Type B and Type C were simultaneously incorporated by increasing the thickness and the width of the fat-channel and the formation is shown in Figure 3.4(d).

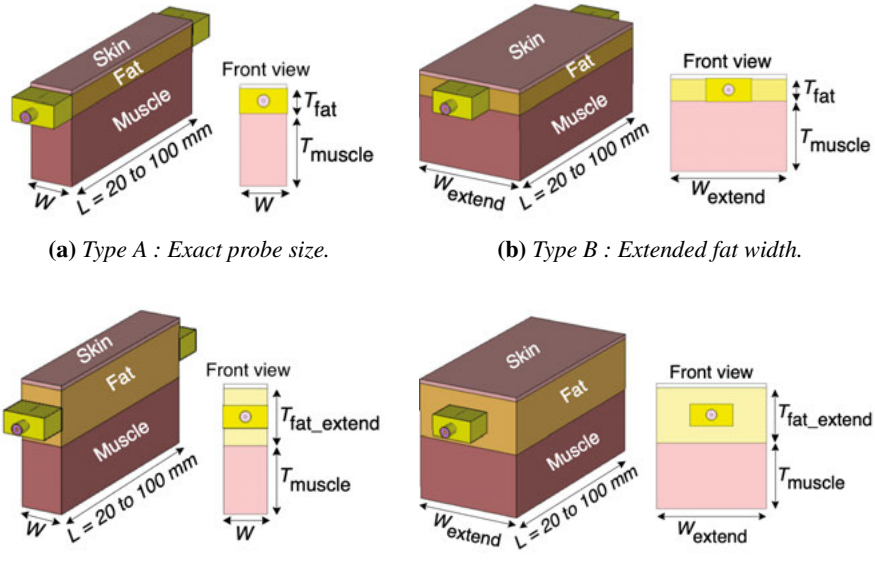

(a) *Type A : Exact probe size.* **(b)** *Type B : Extended fat width.*

(c) *Type C : Extended fat thickness.* **(d)** *Type D : Extended fat width and thickness.*

Figure 3.4. *Four types of model structures for the measurement of signal loss at 5.8 GHz.* ***Paper III****. Adapted, from [64].*

The third prototype was used to launch the electromagnetic signal in the fat tissue for the phantom (see Figure 3.5(a)) and ex-vivo (see Figure 3.5(b)) setup. In order to have a general picture, the results are presented over the frequency ranged from 3 to 8 GHz.

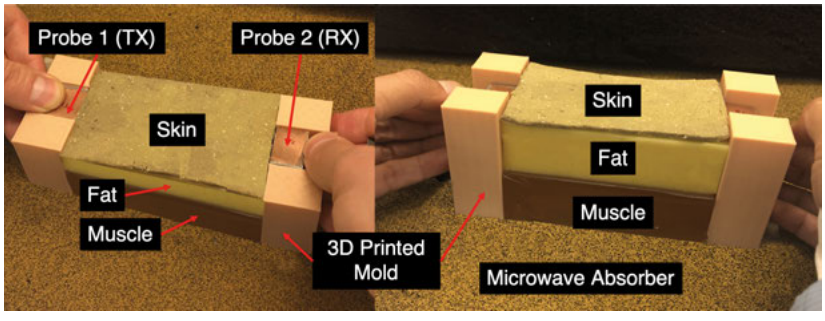

(a) *Phantom measurement.*

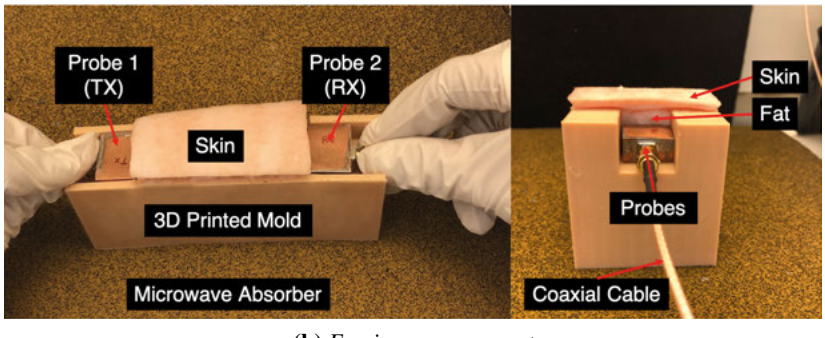

(b) *Ex-vivo measurement.*

Figure 3.5. *The configuration setup for* ***(a)*** *Phantom and* ***(b)*** *Ex-vivo environment.* ***Paper III****. Adapted, from [64].*

The transmission coefficient S_{21} was then measured and computed. This was followed by a discussion on the results of Type A to Type D configurations for ex-vivo and phantom. The simulated and measured S_{21} results for all types were compared with the ex-vivo and the phantom across various channel lengths. In measuring S_{21}, N9918A FieldFox Handheld Analyzer was used to record the transmission coefficient. Provided that this analyzer possessed a maximum dynamic range of –45 dBm for all the frequency ranges, the plotting was conducted based on its limit in terms of dynamic range. Therefore, the measurement results for the dynamic range lower than –45 dB were regarded as defective measurements and complemented by simulation results.

It could be seen from Type A S_{21} results that the simulated and experimental results were in a good agreement with each other. Through the noticeable loss in the signal strength due to the increasing channel length, an average path loss of 3 dB/cm at 5.8 GHz was observed. Provided that the loss tangent of the fat-equivalent phantom was twice the loss tangent of the ex-vivo tissue, it was

predicted that the average path loss would amount to 6 dB/cm. The S_{21} results are illustrated by taking Type B into account, specifically its configuration for the simulation and experimentation of the ex-vivo and phantom. A similar trend in this matter was also present in the results for Type A configuration. Furthermore, the average channel path loss almost amounted to 3.2 dB/cm, with a fat-equivalent phantom amounting to 5.1 dB/cm decay. In respect of Type C, the signal coupling increased by more than 10 dB at 100 mm distance compared to Type A and Type B. Through the comparison between Type C results at 60 mm channel length, an increase in the values of S_{21} could be seen compared to the values of S_{21} in Type A and Type B, which amounted to by 2.5 dB and 4.6 dB.

In the case of Type D, the fat tissue was extended around the probes for both environments, namely ex-vivo porcine tissue and tissue-equivalent phantom. Notably, Type D was a case that was almost equivalent to real-life scenarios, where the fat tissue surrounds the implant. It could be seen that the difference between Type C and D results was not significant in terms of their signal transmission. This finding emphasized that the fat thickness poses a significant influence on the signal transmission. The S_{21} simulated for a 100 mm ex-vivo channel length amounted to –25.6 dB, while the measured S_{21} amounted to –25 dB. Meanwhile, for the phantom at 60 mm channel length, the simulated S_{21} amounted to –45 dB, while the measured S_{21} amounted to –44. dB.

Overall, Type C and D displayed lower signal path loss, which was similar to Type A and B. The increased fat thickness in Type C and D did not only indicate the alteration between Type A and B, but it also recovered path loss. It could also be seen that the measurement results were in a good agreement with the simulation results. Through observation on all average distances, the path loss per centimeter for the ex-vivo porcine tissue and the tissue-equivalent phantom environment was estimated. Specifically, as for the ex-vivo configuration for Type A, both the simulated and measured path loss amounted to 3.2 dB/cm. In respect of the phantom for the same type, the simulated path loss amounted to 5.3 dB/cm, with 7.4 dB/cm measured path loss. In the case of the ex-vivo configuration for Type B, simulated and measured path loss amounted to 3.2 dB/cm and 3.4 dB/cm, respectively. Meanwhile, the simulated path loss for phantom amounted to 5.1 dB/cm, 6.3 dB/cm measured path loss. On the other hand, with respect to the ex-vivo for Type C, the simulated and measured path loss amounted to 1.5 dB/cm, while the phantom displayed 4.4 dB/cm and 4.0 dB/cm simulated and measured path losses, respectively. Lastly, in the case of the ex-vivo average path loss for Type D, the simulated path loss amounted to 1.4 dB/cm. As for the phantom for the same type, the simulated path loss of 4.6 dB/cm was recorded, with 4.7 dB/cm of measured path loss.

Table 3.1 and Table 3.2 display a summary of the simulated and measured transmission coefficient S_{21} for different methods. An emphasis was placed on the channel length for ex-vivo porcine tissue and tissue-equivalent phantom at 5.8 GHz. The values in Figure 3.6 were plotted based on the results in Table 3.1. It could also be seen from Figure 3.6 that different environments possessed diverse path loss profiles.

Table 3.1. *The S_{21} simulated and measured results for Type A–D at a varying channel length for ex-vivo equivalent tissue at 5.8 GHz.* ***Paper III****. Adapted, from [64].*

Types /	Measured (Simulated), S_{21} (dB)				
Distance	20 mm	40 mm	60 mm	80 mm	100 mm
Type A	-8.8 (-8.4)	-15.3 (-14.6)	-21.9 (-21.3)	-27.9 (-27.4)	-34.6 (-34.1)
Type B	-11.9 (-10.2)	-18.5 (-17.0)	-25.5 (-24.4)	-31.4 (-31.7)	-37.9 (-37.3)
Type C	-13.4 (-12.1)	-16.3 (-14.9)	-19.6 (-18.0)	-22.4 (-21.2)	-25.4 (-24.2)
Type D	-14.7 (-14.0)	-18.6 (-16.8)	-22.6 (-22.3)	-24.0 (-23.6)	-25.6 (-25.0)

Table 3.2. *The S_{21} simulated and measured results for Type A–D at a varying channel length for phantom equivalent tissue at 5.8 GHz.* ***Paper III****. Adapted, from [64].*

Types /	Measured (Simulated), S_{21} (dB)				
Distance	20 mm	40 mm	60 mm	80 mm	100 mm
Type A	-16.2 (-15.5)	-30.1 (-28.6)	-44.2 (-43.1)	-55.8 (-53.1)	-58.9 (-75.0)
Type B	-18.2 (-17.5)	-32.2 (-31.4)	-46.3 (-45.3)	-59.2 (-59.9)	-59.4 (-67.9)
Type C	-20.5 (-19.8)	-31.0 (-29.3)	-41.7 (-39.8)	-54.1 (-53.0)	-56.0 (-51.6)
Type D	-22.3 (-21.2)	-34.2 (-33.4)	-45.0 (-44.6)	-54.6 (-54.1)	-58.9 (-58.5)

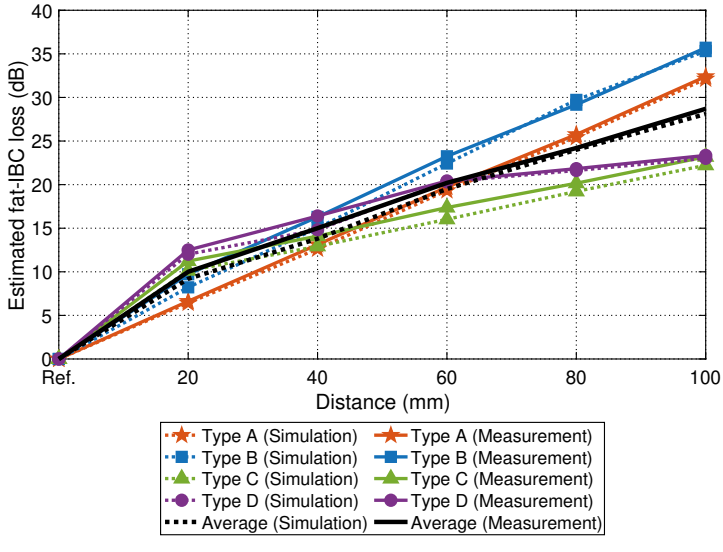

Figure 3.6. *Path loss of the ex-vivo porcine tissue at 5.8 GHz.* ***Paper III****. Adapted, from [64].*

3.4 Summary of the path loss

This section elaborates on the simulations and measurements of the signal path losses, which had been reported in **Papers I–III**. These path losses were in relation to the tissue-equivalent phantom and ex-vivo tissue. Figure 3.7 represents the channel path loss of the homogeneous three-layered skin-fat-muscle tissue layer with a dimension of 50 mm (W) $\times$ 25 mm (T) $\times$ 100 mm (L), with 2 mm skin thickness and 30 mm muscle thickness.

In the case of the phantom at 5.8 GHz, it could be seen from Figure 3.7(a) that with the increase in the distance between the transmitter and the receiver, a rapid increase in the path loss parameter occurred. To illustrate this point, the value of the path loss is 10 dB/cm channel length, while this value amounted to 60 dB for 100 mm channel length. This difference between values was due to the higher value of the loss tangent of the phantom material. Furthermore, similar results could be seen from the simulated and measured path loss at this frequency. Although a slight decrease was found at all the frequencies when the length of the channel increased, the maximum path loss was recorded at 5.8 GHz. From Figure 3.7(b), in respect of the path loss results for ex-vivo, no rapid increase was identified at any frequency. The ex-vivo properties are close to human tissues. In a nutshell, we can conclude that the frequencies 2.0 GHz, 2.4 GHz, and 5.8 GHz, are all favorable for Fat-IBC. However, it was notable that the 5.8 GHz displayed more path loss both for the phantom and the ex-vivo environments as compared to the other two frequencies.

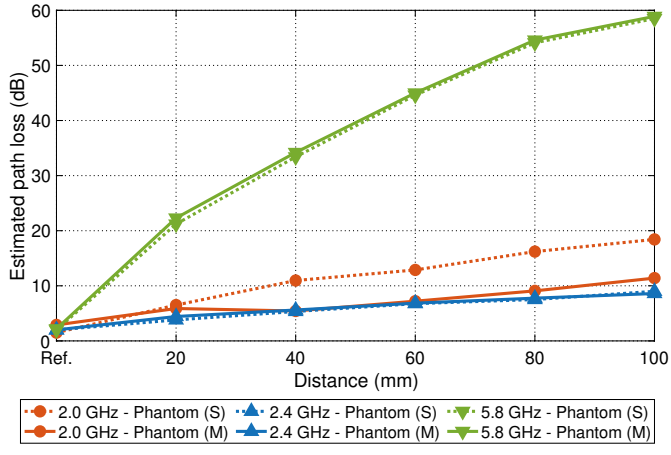

(a) *Path loss for phantom.*

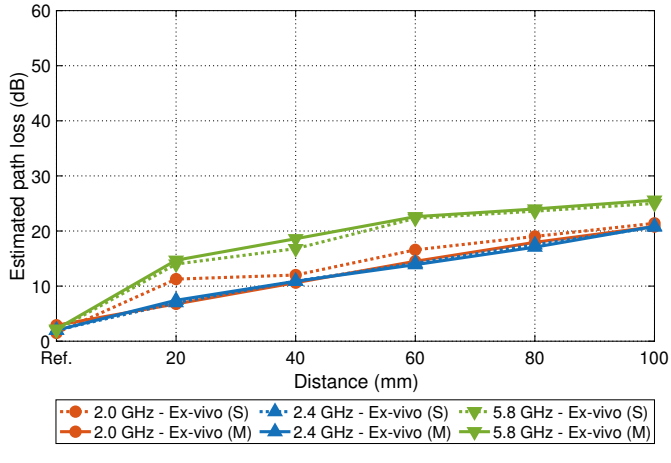

(b) *Path loss for ex-vivo.*

Figure 3.7. *The path loss of three prototypes at 2.0 GHz, 2.4 GHz, and 5.8 GHz.*

4. Factors affecting the performance of Fat-IBC

Intra-body communication (IBC) is gaining popularity due to its potential in drug delivery and the establishment of a sensor network for wearable and implanted devices. These applications are critical for monitoring patients' health and health care systems in the future. As the channels for IBC, fat tissues have been introduced as a channel and investigated further in works of research. However, the fat tissues inside the human body are not isolated entities. To illustrate, a wide range of nerve cells and blood vessels overlap the fat tissues. Therefore, it is important to consider the reliability of the behavior of the fat channel in the presence of these vessels. In this study, the effects of the increase in the number of vessels, blood vessel orientation, fat surface structure (homogeneous/non-homogeneous) on the communication system were determined. This chapter discusses these important aspects and presents the results in **Papers III**, **IV**, **V**, and **VI**.

.

- **Section 4.1**: In **Paper IV**, the impacts of the signal coupling caused by the muscle tissue perturbance placed within the fat tissue are discussed.
- **Section 4.2**: The analysis of inhomogeneity in the fat tissue thickness to assess the impact on the signal transmission for Fat-IBC are illustrated in **Paper V**.
- **Section 4.3**: In **Paper VI**, the effects on the signal transmission under the presence of the blood vessels with the modeling of three different blood vessel's orientations are elaborated.
- **Section 4.4**: The impacts on the signal coupling caused by the probe's misalignment in the fat channel are discussed in **Paper III**.

The measurement setups used to obtain the experimental data in **Papers III–VI** involved the same experimental setup shown in Section 3 of Chapter 2. In Component 3, modifications were performed in the transmission channel waveguide, specifically the fat tissue to determine the factors affecting the performance of Fat-IBC.

4.1 Assessing the reliability of fat tissue as a channel supporting intra-body microwave communication

An investigation was conducted on the reliability of the fat tissue as a channel for intra-body communication that supported the communication between various implanted devices. In achieving this study's objectives, simulations and experiments were conducted. The details of numerical/simulation modeling and experiments are illustrated in the following sections of this thesis.

4.1.1 Numerical modeling for determining the reliability of fat tissue as a communication channel

A numerical model was developed to assess the viability of fat tissue as a channel for intra-body communication in the microwave region. The first prototype was used in this study, where a 2.0 GHz frequency was set. The overall three-layered structure is shown in Figure 4.1.

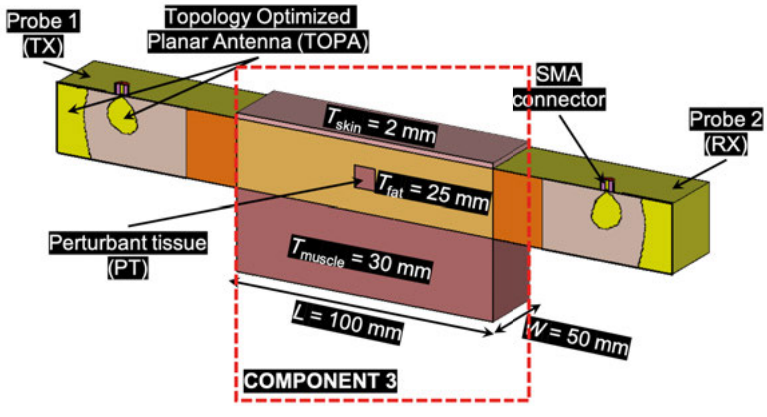

Figure 4.1. Simulation setup for three layered structure in CST.

In a typical human body, blood vessels or embedded muscles may be present in the fat tissue. Taking the effects of these blood vessels or muscles into consideration, a perturbant tissue (PT) inside the fat tissue was introduced with dimensions of 5 mm, 10 mm, 15 mm, and 20 mm. One dimension was introduced at a time. Besides the varied diameter sizes of the PT, the location of the PT inside the fat tissue was moved within 20 mm from the transmitter towards the receiver. Nevertheless, the variations allowed for monitoring the effects of perturbant with different sizes inside the fat tissue and the effect of the location of the perturbant. Moreover, electromagnetic waves at a frequency of 2.0 GHz were launched into the fat tissue channel through TOPA under various perturbant sizes and distances from the transmitter. A reference signal was also incorporated without the presence perturbants.

4.1.2 Experimental setup for determining the reliability of fat tissue as a communication channel

To verify the results from the simulation setup, an experimental evaluation on the equivalent phantom tissue was conducted, as shown in Figure 4.2. In this evaluation, the same dimensions of skin, fat, and muscle tissues as the ones in the simulation setup were used. To determine the similarity between the dielectric properties of human tissues and the phantom, repeated measurements were carried out. An average frequency of 2.0 GHz was maintained, followed by the calculation of their differences using the ratio of the phantom to the human tissue. These differences are shown in Table 4.1.

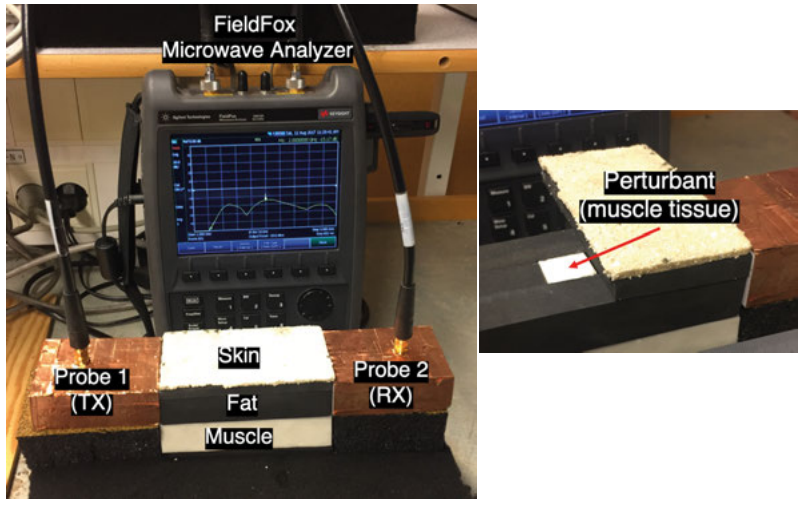

Figure 4.2. *Experimental setup of a complete setup and a magnified view of PT.* ***Paper IV****. Reprinted, with permission, from [65]. Copyright ©2017, IEEE.*

Table 4.1. *Dielectric properties of phantom in comparison with human tissues at 2.0 GHz.*

Materials	Parameters					
	Relative permittivity			Loss tangent		
	Phantom	Human	Diff.(%)	Phantom	Human	Diff. (%)
Skin	36.50	38.57	–5.37	0.22	0.30	–26.67
Fat	5.43	5.33	+1.88	0.16	0.15	+6.67
Muscle	53.86	53.29	+1.07	0.21	0.25	–16.00

4.1.3 Results and discussion on the reliability of fat tissue as a microwave communication channel

In this study, the influences of various interferences in the channel on $|S_{21}|$ were analyzed. The simulation results of the $|S_{21}|$ parameter upon the use of PT of different sizes are illustrated in Figure 4.3. It can be seen from the figure that in the comparison between small-sized PT and channel thicknesses, such as 5 mm or 10 mm, no significant variation in the amplitude was found in the S-parameter. However, when the ratio of PT with respect to the channel thickness was higher than 0.6, amplitude degradation could be observed. This degradation indicated that compared to the channel thickness, small blockages posed insignificant effects on the $|S_{21}|$ parameter. However, $|S_{21}|$ degradations occurred when PT size was comparable to the channel thickness.

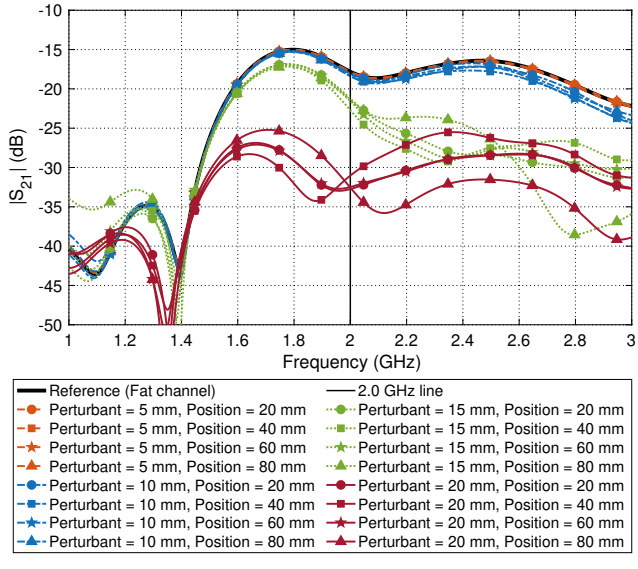

Figure 4.3. *The $|S_{21}|$ parameters simulation results for various sized PT at different locations.* ***Paper IV****. Reprinted, with permission, from [65]. Copyright ©2017, IEEE.*

A reference signal without the presence of PT was first obtained, followed by the incorporation of PT of various sizes inside the fat tissue. It was found that 10 mm PT did not affect the signal coupling irrespective of its position. In the case of 15 mm PT, a degradation of 4 dB/cm was observed in $|S_{21}|$ parameter. Furthermore, experiments that were similar to the simulation were conducted on PT of various sizes and different locations. Figure 4.4 shows the comparison between the measured and simulated when 10 mm and 15 mm size of PT was located at 40 mm distance from the transmitter in the fat tissue. Similar results as for the simulation results were observed. Based on the simulated and measured results, it was indicated that compared to the homogeneous thickness of the fat tissue, the fat tissue could be used as a reliable media for intra-body communication even when blockages of small size were present. Overall, the measurement results obtained from the investigation on the $|S_{21}|$ parameter were in an agreement with the simulation results.

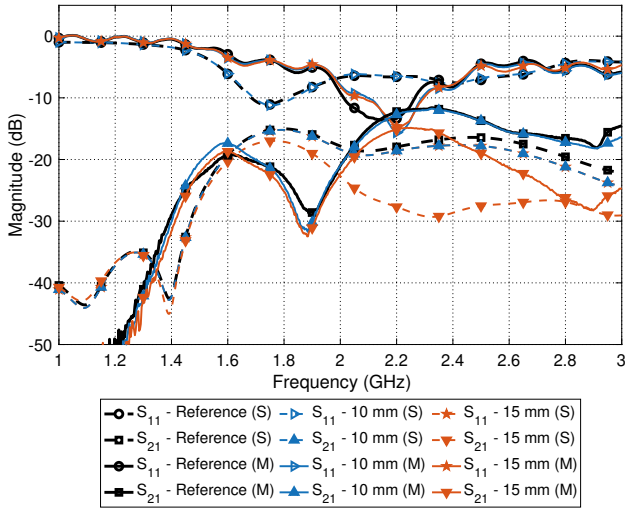

Figure 4.4. *Comparison between measured and simulated work for 10 mm and 15 mm PT sizes at 40 mm PT position.* ***Paper IV****. Reprinted, with permission, from [65]. Copyright ©2017, IEEE.*

4.2 Effect of thickness inhomogeneity in fat tissue on intra-body microwave communication

The effects of inhomogeneity in the fat tissue were investigated when they were used as a channel for intra-body microwave communication at a frequency of 2.45 GHz. The investigation on this aspect of the fat tissue was crucial as the structure/thickness of fat tissue may vary among different individuals. Besides, there is a wide range of fats inside the body, such as visceral abdominal, epicardial, and periadventitial fats among others [66]. A concave and convex model of the three-layered skin-fat-muscle structure was also developed to observe the performance of the Fat-IBC when intra-body communication was involved. This investigation was followed by simulation and experimental setups and the discussion of results in the following subsections.

4.2.1 Numerical modeling representing fat tissue thickness distribution inhomogeneity

The structure used for this study is shown in Figure 4.5. It is based on model from Figure 4.1. The difference between the model and the structure could be seen from the curves in Component 3, which was the channel. Figure 4.5(a) illustrates a concave model, a concave structure positioned inwards from its middle part, while Figure 4.5(b) presents a convex model, positioned outwards from the middle part. For the concave model, the $T_{\mathrm{fat_{min}}}$ value ranged from 5 mm to 25.36 mm by 5 mm step. In the case of the convex model, the $T_{\mathrm{fat_{max}}}$ value ranged from 25.36 mm to 45 mm of fat thickness by 5 mm step. The variation of the thicknesses was based on an elliptical shape from the center of the channel. Overall, the *gap* in both models ranged from 5 mm to 25 mm by 5 mm step from the probes. Similar to previous studies, investigation was made on the $|S_{21}|$ for these structures.

4.2.2 Experimental setup to study the effect of fat tissue thickness variation

In order to validate the results obtained from the simulation, a three-layered tissue-equivalent phantom with two different models was developed in a similar method as the one used in the simulation work. The thickness of the fat tissue for the concave model was set to be 20 mm, while the thickness of the case of the convex model was set to be 35 mm with 10 mm *gap* for both cases. Notably, the primary difference between this study's prototype and the prototype used in Section 4.1 was that the operating frequency of the probe was focused around 2.45 GHz (second probe's prototype). The experimental setup is illustrated in Figure 4.6.

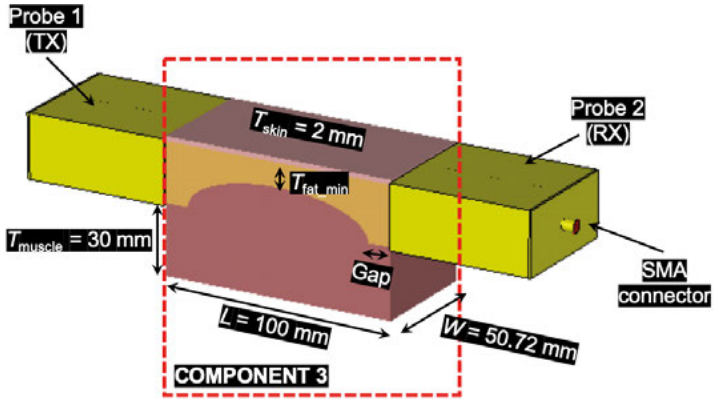

(a) *Concave model.*

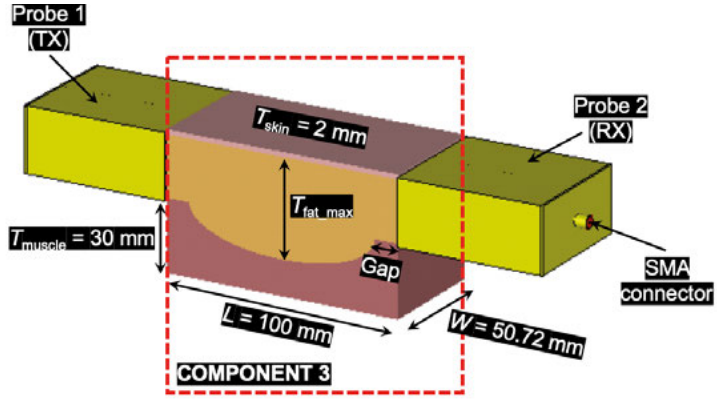

(b) *Convex model.*

Figure 4.5. *The models used for the numerical modeling studies. The simulation was done by varying two parameters, which are the fat thickness, T_{fat_min} or T_{fat_max} and the gap.* ***Paper V****. Reprinted, with permission, from [38]. Copyright ©2018, IEEE.*

4.2.3 Results and discussion to study the effect of fat tissue thickness variation

This subsection investigates on the vulnerability of the quality of the transmitting channel against the fat tissue thickness and the *gap* between the probes for the concave and convex model. The results from the numerical modeling study in section 4.2.1 is shown in Figure 4.7. Notably, to achieve conciseness in the results, only the observations on $|S_{11}|$ were incorporated. Overall, $|S_{11}|$ displayed a good result which was lower –12 dB. However, alterations in the channel's compatibility in terms of the *gap* distance would occur. As for this case, the matching is good; thus, it is not the key parameter to observe the channel propagation behavior. Figure 4.7 shows the $|S_{21}|$'s simulated results for the concave and convex model. It could be seen that $|S_{21}|$ magnitude, specifically the concave model, gradually increased with the increase of fat

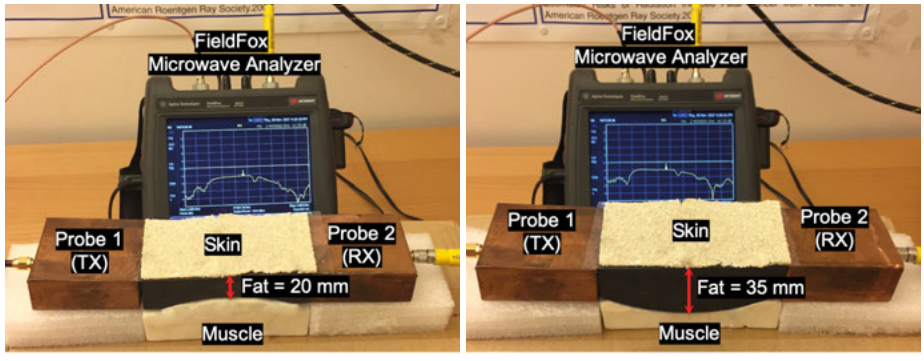

(a) *Concave model.* **(b)** *Convex model.*

Figure 4.6. *Experimental setup based on phantom model for* ***(a)*** *concave* ***(b)*** *convex. The fat thickness for the concave model is 20 mm, and for the convex model is 35 mm. gap for both model is 10 mm.* ***Paper V****. Reprinted, with permission, from [38]. Copyright ©2018, IEEE.*

thickness from 5 mm until its maximum value of 25.4 mm. Nevertheless, the *gap* posed a minor influence on the signal coupling. Moreover, $|S_{21}|$ would be reduced until it reached a plateau for 30 mm of fat thickness and above. Meanwhile, no significant reduction was observed for the case of the convex model.

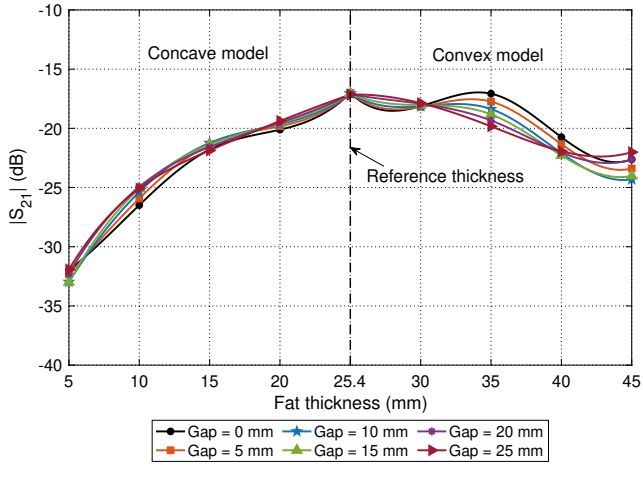

Figure 4.7. *Dependency of the transmission coefficient,* $|S_{21}|$ *with respect to the fat thickness (concave and convex model) and gap parameter at 2.45 GHz.* ***Paper V****. Reprinted, with permission, from [38]. Copyright ©2018, IEEE.*

Figure 4.8 illustrates the comparison between simulation and experimentation results based on phantom model for fat, concave, and convex channel in terms of $|S_{21}|$. It could be seen from this comparison that the variation in the fat thickness influenced the coupling coefficient $|S_{21}|$. It was worthy to note that the simulated and measured results were in an agreement with each other. Overall, the primary findings of this study are: Attenuation is less than 4 dB when the thickness is between 15 mm to 35 mm, *gap* does not affect the transmission properties and last but not the least when fat thickness is less than 15 mm, attenuation in the signal is significant, however, not to the extent to break communication link.

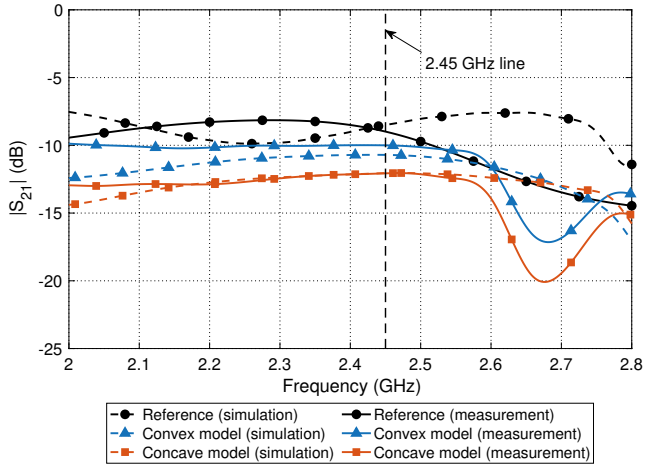

Figure 4.8. *A comparison of $|S_{21}|$ simulated and measured results for the fat channel, concave model and convex model at 2.45 GHz.* ***Paper V*** *Reprinted, with permission, from [38]. Copyright ©2018, IEEE.*

4.3 Impact of blood vessels on intra-body communication at 2.45 GHz

A thorough evaluation of the impact of blood vessel on the signal propagation in fat intra-body communication was conducted in this study. Three entities, namely size, position, and the number of blood vessels were analyzed. Further details and results from this analysis will be discussed in the following sections.

4.3.1 Simulation model for assessment of the impact of blood vessels on intra-body communication

As discussed in Section 4.2, the same probe prototypes were used in this study. Essentially, blood vessels can be classified into five types [67]. However, only three major types of blood vessels were considered in this study, namely arteries, veins, and arterioles, each having an average diameter of 4 mm, 5 mm, and 30 μm respectively. Muscle tissue and copper rods were utilized to imitate the behavior of blood vessels due to the analogy shown by these entities in terms of dielectric and conductivity behavior. The dielectric properties of components used in this experiment and its comparison with the human tissues are shown in Table 4.2.

Table 4.2. *Relative permittivity and conductivity of human tissue and its comparison with the modeled components.*

Tissue	Human tissue	Ex-vivo (measured)	Similarity index (%)
Skin	38 ± 2	40 ± 4	95
Fat	5.3 ± 0.3	5.5 ± 0.5	96.36
Muscle	53 ± 3	51 ± 5	96.22

(a) *Relative permittivity (real part)*

Tissue	Human tissue	Ex-vivo (measured)	Similarity index (%)
Skin	1.5 ± 0.1	1.4 ± 0.1	93.33
Fat	0.1 ± 0.01	0.12 ± 0.01	83.33
Muscle	1.7 ± 0.1	2.2 ± 0.2	77.27

(b) *Conductivity (S/m)*

It could be seen from the similarity index that the chosen materials possessed similar conductivity and permittivity properties. In reality, the incorporation of a blood vessel inside the tissues could be a longitudinal, transverse-vertical, or transverse-horizontal plane. Therefore, these scenarios were emulated and shown in Figure 4.9. The positions and number of blood vessels were varied between the transmitter and the receiver. Vessels were with a step size of 20 mm were relocated for the simulation, with a distance of 10 mm to 90 mm from the transmitter. Following that, they were placed systematically inside the tissues. The position of the blood vessels is indicated through the red dot in Figure 4.10. Figure 4.11 shows the view of the blood vessels from the transmitter side. Images of the aforementioned figures illustrate the position where the number of vessels increased from one to three.

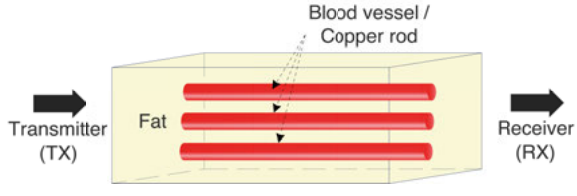

(a) *The longitudinal plane.*

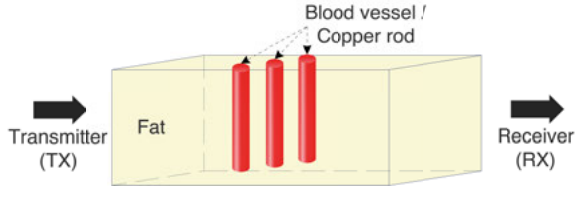

(b) *The transverse-vertical plane.*

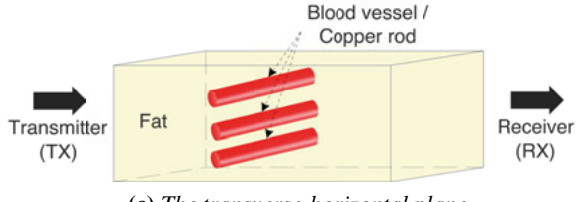

(c) *The transverse-horizontal plane.*

Figure 4.9. *Positioning of blood vessels inside fat tissue.* ***Paper VI****. Reprinted, with permission, from [37]. Copyright ©2019, IEEE.*

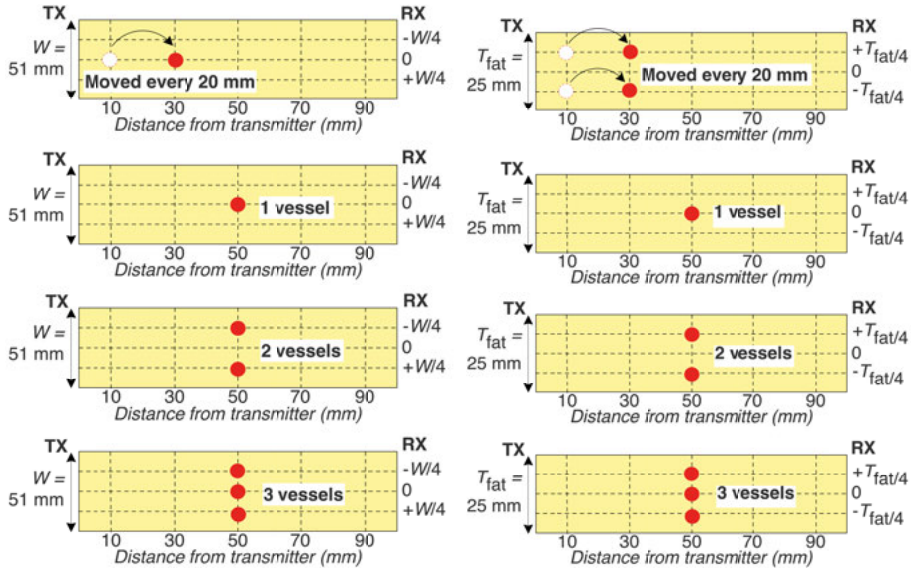

(a) *The transverse-vertical view.* **(b)** *The transverse-horizontal view.*

Figure 4.10. *Blood vessel positioning.* ***Paper VI****. Reprinted, with permission, from [37]. Copyright ©2019, IEEE.*

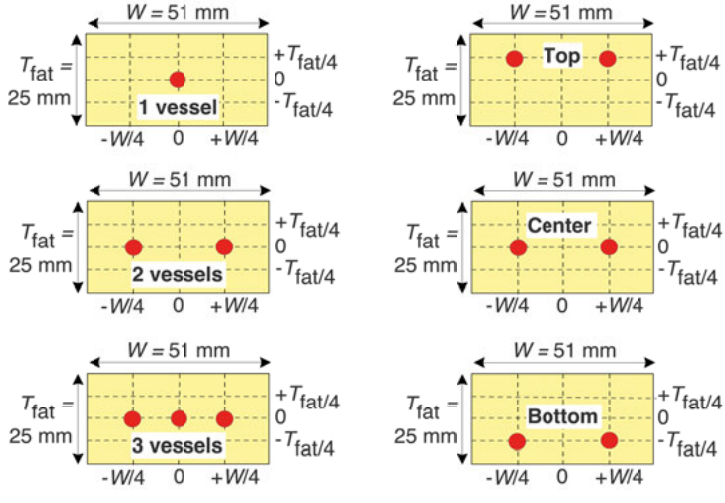

Figure 4.11. *The longitudinal plane. Red dot represents blood vessels.* ***Paper VI****. Reprinted, with permission, from [37]. Copyright ©2019, IEEE.*

4.3.2 Experimental demonstration for assessment of the impact of blood vessels on intra-body communication

A detailed experimental setup was materialized to observe the impact of blood vessels on the fat tissues when fat tissues were used as a channel for intra-body communication.

The fat and muscle for this experiment were extracted from a freshly slaughtered porcine belly. Then, copper rods of various sizes based on the blood vessels were taken. Furthermore, a 3D printer with a dimension of 61 mm $\times$ 230 mm $\times$ 63 mm was used. Cylindrical tubes with a wall thickness of 0.4 mm and diameters of 2 mm, 4 mm, and 6 mm were constructed using the printer. To observe the $|S_{21}|$ parameter at those frequencies at the Fieldfox microwave analyzer, frequencies ranging from 1 to 4 GHz were generated and distributed to the three-layered structure by using the second probe's prototype. All the experiments were conducted under 22° C surrounding temperature. The overall experimental setup is illustrated in Figure 4.12.

4.3.3 Results and discussion on the assessment of the impact of blood vessels as a channel for intra-body communication

This study focused on the effects of various types of blood vessels, which were extracted from copper and porcine belly muscle on the transmission channel. Figure 4.13 illustrates the $|S_{21}|$ parameter results for the simulated and measured setup conducted on the muscle rod, while Figure 4.14 presents the $|S_{21}|$ parameter for the copper rod. This study's system was tested in terms of the three diameters of blood vessels, namely 2 mm, 4 mm, and 6 mm.

It could be seen from Figure 4.13 that the increase in the number of muscle rod was inversely related to the amplitude of $|S_{21}|$. This relation indicated that the signal strength reduced with the increase in the number of muscle rods, which was applied to all diameters. However, a more prominent decrease in the magnitude for $|S_{21}|$ could be seen in a 6 mm diameter muscle, which was from 0.2 to 1.6 dB. Following a similar trend, the results in Figure 4.13 are shown to be completely similar to the results in Figure 4.14, with the use of copper rod as an exception. Based on these figures, a higher signal-coupling effect was observed when the copper rod was placed near the skin compared to its placement on the top of the muscle. This effect was due to the difference between the permittivity of skin, where the skin is thinner with less permittivity, and the muscle's permittivity.

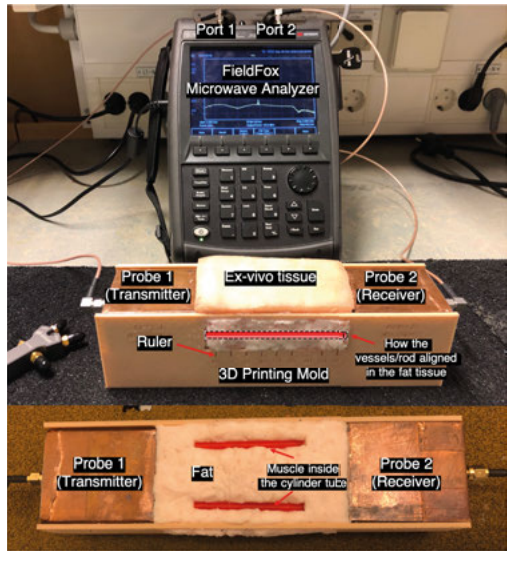

(a) *The longitudinal plane view.*

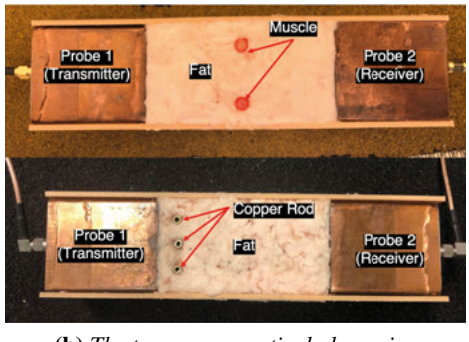

(b) *The transverse-vertical plane view.*

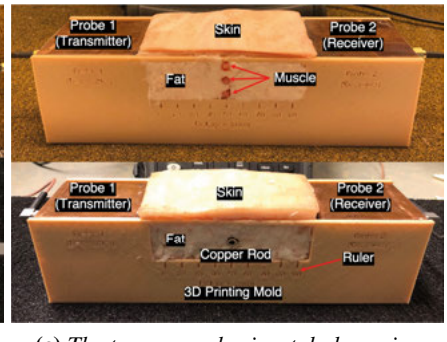

(c) *The transverse-horizontal plane view.*

Figure 4.12. *Experimental setup.* ***Paper VI****. Reprinted, with permission, from [37]. Copyright ©2019, IEEE.*

It is shown in Figure 4.15 that the occurrence of the electric field was due to the blood vessels in longitudinal plane. The simulations for all the cases were conducted where the diameters of the vessels of the muscle and copper rods amounted to 2 mm, 4 mm, and 6 mm. However, only one case of 6 mm muscle and copper rods was present (see Figure 4.15) when the blood vessels were aligned at the top of the muscle and the bottom of the skin.

Similar to the results in Figure 4.13 and Figure 4.14, the results of the transverse-vertical and transverse-horizontal plane were observed. However, to achieve conciseness of results, only the observations were incorporated, where the vessel was placed vertically. It was suggested that $|S_{21}|$ decreased with the increase in the number of rods from 1 to 3. Furthermore, copper rods

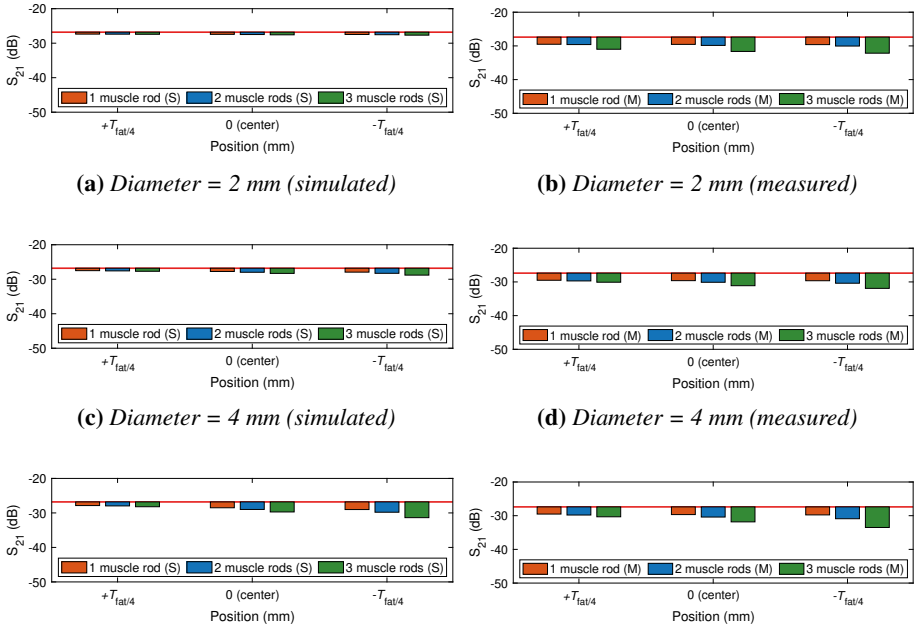

(a) *Diameter = 2 mm (simulated)*

(b) *Diameter = 2 mm (measured)*

(c) *Diameter = 4 mm (simulated)*

(d) *Diameter = 4 mm (measured)*

(e) *Diameter = 6 mm (simulated)*

(f) *Diameter = 6 mm (measured)*

Figure 4.13. *Simulated and experimental results for $|S_{21}|$ parameter for 60 mm long muscle tissue in a longitudinal plane.* ***(a)****,* ***(c)****,* ***(e)*** *is simulated results for 2 mm, 4 mm and 6 mm diameter, respectively and* ***(b)****,* ***(d)*** *and* ***(f)*** *is measured results for 2 mm, 4 mm and 6 mm diameter, respectively.* ***Paper VI****. Reprinted, with permission, from [37]. Copyright ©2019, IEEE.*

led to further degradation compared to muscle rods. The use of the muscle rod with three vessels of 6 mm diameter resulted in 5.13 dB of signal coupling loss in the measured result and 5.11 dB of signal coupling loss in the simulated results. Nevertheless, both results were in an agreement with each other. When the copper rod was tested with three vessels of 6 mm diameter, the signal coupling loss in the experiment amounted to 17.13 dB, while 14.31 dB of signal coupling loss was reported in the simulated case. These significant losses were primarily attributed to the higher reflectivity in copper material. As the rods were placed in the vertical position of the transmitter, orthogonal propagation was observed towards the line of transmission, resulting in prominent reflections. Notably, a stark transverse electric field disruption inside the transmitting media contributed to signal propagation loss, leading to degradation. The dielectric characteristics of blood vessels were comparable to the characteristics of muscles, where less significant propagation degradations took place.

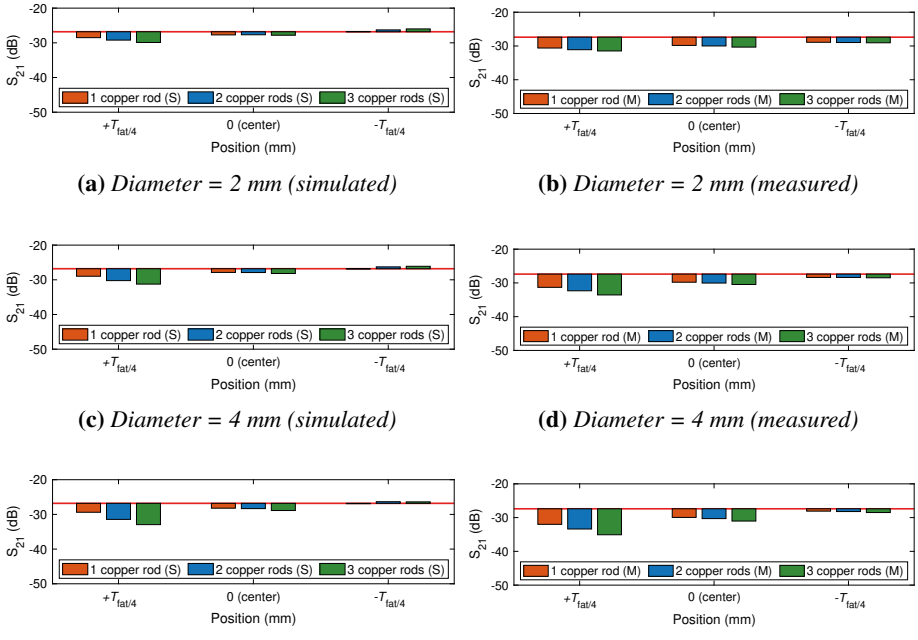

(a) *Diameter = 2 mm (simulated)*

(b) *Diameter = 2 mm (measured)*

(c) *Diameter = 4 mm (simulated)*

(d) *Diameter = 4 mm (measured)*

(e) *Diameter = 6 mm (simulated)*

(f) *Diameter = 6 mm (measured)*

Figure 4.14. *Simulated and experimental results for $|S_{21}|$ parameter for 60 mm long copper rods in a longitudinal plane.* ***(a)****,* ***(c)****,* ***(e)*** *is simulated results for 2 mm, 4 mm and 6 mm diameter, respectively and* ***(b)****,* ***(d)*** *and* ***(f)*** *is measured results for 2 mm, 4 mm and 6 mm diameter, respectively.* ***Paper VI****. Reprinted, with permission, from [37]. Copyright ©2019, IEEE.*

According to a similar method, simulations and measurements for transverse-horizontal plane cases were conducted. It was found that the gradual decrease in the amplitude of $|S_{21}|$ as parallel to the increasing amount of blood vessels. This phenomenon could be justified when the transverse-horizontal placement of blood vessels was considered as a splitter. It was because the re-combiner, which developed the EM wave propagation inside the waveguide, was divided and recombined. The differences were correlated to the misaligned copper rod placement when the measurement was conducted. It could also be observed that the stark error between the values received in the experiment was in contrast to those obtained in the experiment due to the difference between the dielectric properties of the ex-vivo tissue. Throughout the experiment, this finding was comparative to the values obtained from the simulation.

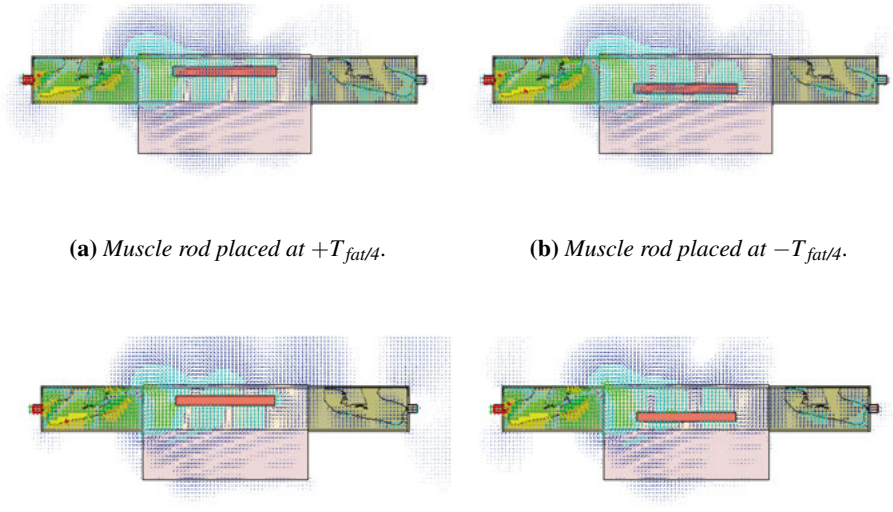

(a) *Muscle rod placed at* $+T_{fat/4}$. **(b)** *Muscle rod placed at* $-T_{fat/4}$.

(c) *Copper rod placed at* $+T_{fat/4}$. **(d)** *Copper rod placed at* $-T_{fat/4}$.

Figure 4.15. *Electric field for the case of three 6 mm diameter blood vessels in longitudinal plane.* ***(a)***, ***(b)*** *muscle rod placed at* $+T_{fat/4}$ *and* $-T_{fat/4}$ *location, respectively* ***(c)*** *and* ***(d)*** *copper rod placed at* $+T_{fat/4}$ *and* $+T_{fat/4}$ *location, respectively.* ***Paper VI****. Reprinted, with permission, from [37]. Copyright ©2019, IEEE.*

It could be summarized that in respect of the longitudinal plane, the placement of muscle rod at $+T_{\text{fat/4}}$ resulted in a more prominent signal coupling effect due to the significant total average loss for both materials. To illustrate this signal was highly attenuated when the copper rod was placed in a transverse-vertical position. Meanwhile, when placed in the transverse-horizontal plane, there was a difference of 3.42 dB and 1.91 dB in muscle and copper rods' readings, which was relative to the reference value of the fat channel. Furthermore, the least prominent effect was posed on the signal coupling due to the presence of the blood vessel(s). Nevertheless, to achieve conciseness of the results, the complete experimental and simulated summary of $|S_{21}|$ results under all situations is illustrated in the tabulated forms, as shown in Table 4.3.

Table 4.3. *Comparison of simulated and measured transmission loss ($|S_{21}|$), average with respect to the fat channel [Average(Reference - $|S_{21}|$)].* ***Paper VI****. Reprinted, with permission, from [37]. Copyright ©2019, IEEE.*

Vessel(s)	No. of Vessel(s)	Average $\|S_{21}\|$ (dB) Measured (Simulated)					
		Longitudinal Plane		Transverse-vertical Plane		Transverse-horizontal Plane	
		Muscle	Copper	Muscle	Copper	Muscle	Copper
2 mm	1	1.17 (0.62)	2.39 (0.86)	0.83 (0.81)	1.51 (2.51)	1.79 (0.57)	1.50 (0.58)
	2	1.44 (0.67)	2.64 (0.91)	0.91 (0.88)	4.53 (3.35)	1.87 (0.65)	1.52 (0.70)
	3	2.47 (0.75)	2.90 (1.09)	1.05 (1.03)	9.12 (7.97)	1.92 (0.69)	1.52 (1.12)
	Average	1.70 (0.68)	2.64 (0.96)	2.12 (2.09)	5.44 (3.20)	1.86 (0.64)	1.51 (0.80)
4 mm	1	1.20 (0.93)	2.44 (1.10)	1.81 (1.79)	7.56 (3.21)	1.90 (0.68)	1.68 (0.67)
	2	1.68 (1.14)	2.86 (1.33)	2.07 (2.04)	9.47 (5.09)	2.15 (0.91)	1.61 (0.88)
	3	2.65 (1.46)	3.45 (1.70)	2.67 (2.66)	15.08 (11.70)	2.31 (1.10)	1.61 (1.74)
	Average	1.84 (1.17)	2.92 (1.37)	2.53 (2.50)	15.08 (11.70)	2.12 (0.90)	1.64 (1.08)
6 mm	1	2.26 (1.66)	2.62 (1.36)	3.71 (3.68)	7.25 (3.87)	2.17 (0.93)	1.38 (0.67)
	2	2.98 (2.11)	3.24 (1.90)	4.59 (4.58)	11.15 (7.13)	2.76 (1.53)	1.56 (1.34)
	3	4.50 (2.96)	4.15 (2.60)	5.13 (5.11)	17.13 (14.31)	3.42 (2.20)	1.91 (3.94)
	Average	3.25 (2.24)	3.33 (1.95)	2.95 (2.93)	13.77 (11.33)	2.79 (1.56)	1.62 (1.99)

4.4 Effect of misalignment in fat tissue on intra-body microwave communication

In this paper, the numerical modeling and experimental validation of the signal path loss at 5.8 GHz are presented within the framework of fat-intrabody communication (Fat-IBC). To propagate information from one implanted device to another, the third probe's prototype was used. The selection of this waveguide probe was due to its capability to direct the radiation through the fat tissue. Notably, this study not only determined the feasibility of implanted devices at 5.8 GHz frequency, it also identified the effects of dynamic body movements.

4.4.1 Simulation and numerical modeling of effect of probe misalignment in fat tissue

To investigate the effects of misalignment between the transmitting and receiving probe, numerical modeling and simulation were conducted. In this phase, two types of experiments were performed. In the first experiment, the transmitting and receiving probes were placed vertically and horizontally. The transmitter was also aligned at four positions, namely up, down, right, and left as shown in Figure 4.16(a). This was followed by the second experiment where a 90° rotation of transmitter was done before both transmitter and receiver were rotated at the same angle. Furthermore, a homogeneous structure of skin, fat, and muscle was developed, where the fat was positioned between skin and muscle. The dimension of the structure was set to be 180 mm $\times$ 80 mm, with 100 mm of distance between the probes. Moreover, a free space medium outside the skin and consider the radiation boundary condition were also taken into account. Figure 4.16(b) illustrates special case when transmitting probe was placed on the top of the muscle, while the receiving probe was placed at the center of the fat.

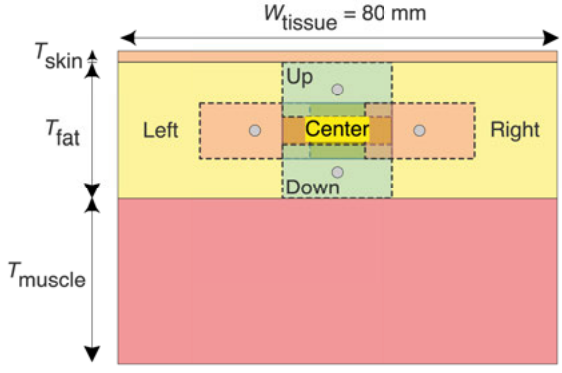

(a) *Cross-view shows misalignment scenarios of the probe.*

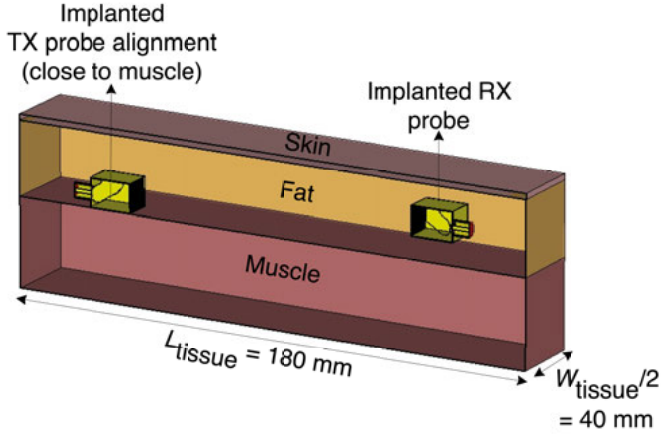

(b) *A specific example of the alignment.*

Figure 4.16. *Numerical modeling setup* ***(a)*** *misalignment scenarios of the probe* ***(b)*** *a specific example.* ***Paper III****. Adapted, from [61].*

4.4.2 Results and discussion on effect of probe misalignment in fat tissue

In this section, the results of two experiments discussed in Section 4.4.1, namely the misalignment and cross-polarization cases, are elaborated. Figure 4.17 displays the simulation results for ex-vivo $|S_{11}|$ and $|S_{21}|$ upon the change of the location of the TX probe in the fat tissue. It also presents the influence of upright displacement of the probes on the signal coupling through the fat-channel. To be specific, Figure 4.17(a) shows that the TX probe skin was dislocated upward or downward to the muscle tissue. However, these dislocations posed negligible effects on $|S_{11}|$ parameter. On the contrary, Figure 4.17(b) illustrates that the TX probe was displaced downwards to the muscle, posing a significant influence on $|S_{11}|$ parameter. It was concluded that the vertical displacement of the probe is formed through a nearly 3 dB and 1 dB increase in the channel insertion loss when the probe is dislocated upwards and downwards, respectively.

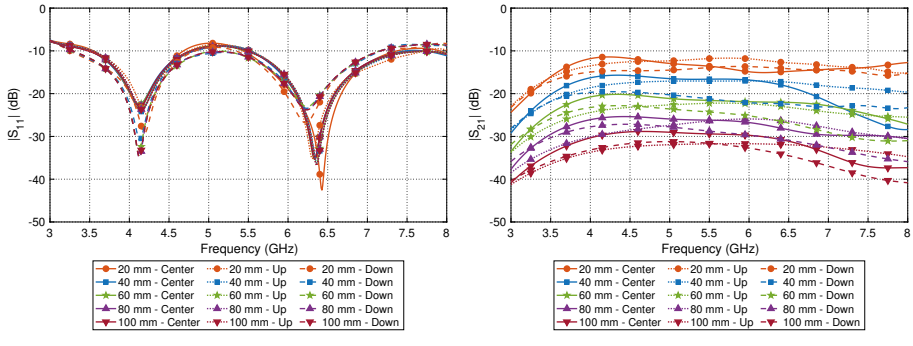

(a) *Reflection coefficient,* $|S_{11}|$. **(b)** *Transmission coefficient,* $|S_{21}|$.

Figure 4.17. *Simulated results of* $|S_{11}|$ *and* $|S_{21}|$ *when TX probe is placed in the center, below the skin, and on top of the muscle. The RX is placed in the center of the fat tissue.* ***Paper III****. Adapted, from [61].*

Figure 4.18a displays the simulated results for ex-vivo of $|S_{11}|$ and $|S_{21}|$ parameter when the location of the TX probe in the fat tissue is changed. Furthermore, it also indicates that the probe's horizontal dislocation affects signal coupling. Figure 4.18(a) demonstrates that the horizontal displacement poses no essential impact on the probe's reflection coefficient. Additionally, the results of the transmission coefficient indicate that, compared to the reference case (see Figure 4.18(b)), 15 mm of horizontal displacement of the insertion loss increases by 2 dB at maximum.

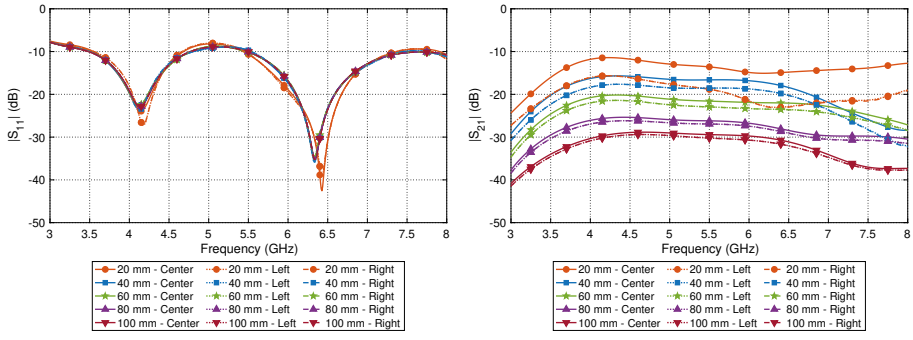

(a) *Reflection coefficient,* $|S_{11}|$. **(b)** *Transmission coefficient,* $|S_{21}|$.

Figure 4.18. *Simulated results of* $|S_{11}|$ *and* $|S_{21}|$ *when TX probe is placed in the center, left side, and on the right side where as RX is centered in the fat tissue.* ***Paper III****. Adapted, from [61].*

The results of the second experiment, which has been discussed in Section 4.4.1, are elaborated in this section. In respect of the 90° rotation of the transmitted probe in the ex-vivo porcine tissue, the results of it are shown in Figure 4.19. It could be seen from this figure that, at 100 mm channel length, the $|S_{21}|$ for the simulation and measurement was reduced by 35 dB and 38.4 dB respectively in terms of its reference (Type D model, as discussed in Chapter 3).

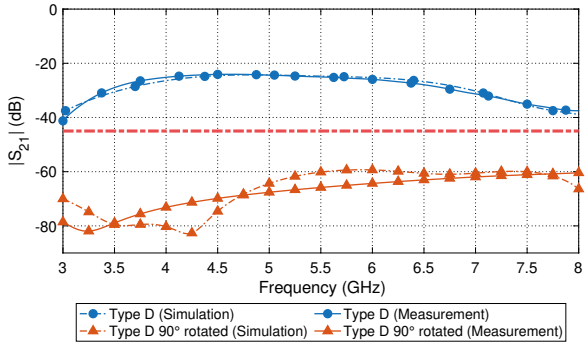

Figure 4.19. *TX probe is 90° rotated for Type D: Transmission coefficient,* $|S_{21}|$ *dB for ex-vivo tissue.* ***Paper III****. Adapted, from [61].*

Similar to the phenomena of parallel plate transmission lines, rotating the transmitting and receiving probe could facilitate the influence of horizontally polarized electric field in the fat channel. Meanwhile, in the case of the rotation of the transmitting and receiving probes at 90° imposing horizontal field in the channel for IBC, the results are illustrated in Figure 4.20. Based on Figure 4.19, it could be seen that the presented scenario had good compati-

bility with the fat channel as the $|S_{11}|$'s value was lower than –15 dB. It was suggested from $|S_{21}|$ parameter at 5.8 GHz that the variation of the results was not significant with the rotation of the probe. Overall, a flat transmission coefficient was found.

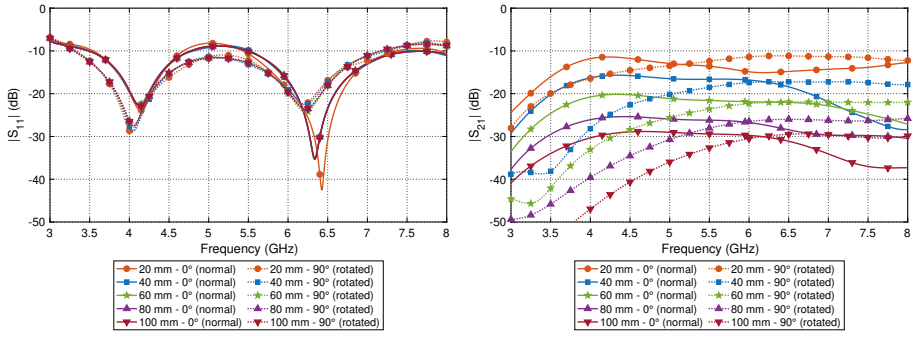

(a) *Reflection coefficient,* $|S_{11}|$. **(b)** *Transmission coefficient,* $|S_{21}|$.

Figure 4.20. *Evaluating* $|S_{11}|$ *and* $|S_{21}|$ *parameters for the case when transmitting and receiving probes are rotated 90°.* ***Paper III****. Adapted, from [61].*

Overall, it could be concluded that the increase in the fat thickness results in lower path loss in channel transmission. The path polarization of the probe posed a negative impact on the signal coupling, leading to the reduction in the received power by approximately –38.4 dB in measurement and –35 dB in simulation. Last but not least, the vertical misalignment between two probes did not pose a significant impact on the signal coupling.

5. Packet transmission and perturbation sensing in the Fat-IBC

The potential factors affecting the reliability of a Fat-IBC channel have been discussed in Chapter 4 as a part of the preliminary study on the feasibility of this approach. Investigations were also conducted to measure the reliability of the channel, the effects of blood vessel orientation, placement, and the communication link. This was followed by experiments on the effects of inhomogeneity fat tissue thickness on communication. In this chapter, we address the issue by sending the data packet transmission through fat tissue supporting wireless connectivity of intra-body devices. Notably, implanted devices, such as cardiac pacemakers, neuro-prosthetics, and cardioverters increased the demand for bandwidth due to the high data rate communication required by the devices [68]. Moreover, fat tissues were used in this study as the medium of microwave communication to transfer and receive a packet. This process involved real data or health information and determined the data packet reception. The numerical modeling, experimental setup, energy consumption, and the results of this part of the study are discussed in the following sections.

- **Section 5.1**: **Paper VII** presents the analysis of Data Packet Reception (PRR), which involved measurement of 2.0 GHz to evaluate the effects of transmission interference on Fat-IBC transmission.
- **Section 5.2**: **Paper IV** presents the investigation on the possibility of the use of a fat-intra-body communication technique for sensing.

To obtain the experimental data in **Paper VII**, the measurement setup was similar to the experimental setup shown in Chapter 2 (Section 3), with changes performed in Component 1 and 2. To be specific, modifications were performed in Component 1, where the TX and RX probes were connected to a USRP B200 SDR for packets measurement setups. To measure the RSS, the RX was connected with the FieldFox Handheld RF and Microwave Analyzer.

5.1 Data packet transmission via fat tissue

An investigation was conducted to prove that the transfer of data packets via fat tissues is possible. Accordingly, R-band frequencies which covered the ISM band of 2.4 GHz were selected [69]. The methods and materials used in this study are presented in the following sections.

5.1.1 Experimental details of data packet transmission via fat tissue

The investigation on low power wireless personal area networks was according to the IEEE 802.15.4 standard. The specifications implemented in this investigation are presented in Table 5.1. As the operation of a standard-compliant IEEE 802.15.4 transceiver was impossible at 2.0 GHz, a software-defined 802.15.4 transceiver was used as an alternative.

Table 5.1. *The used IEEE 802.15.4 standard specifications used.*

Parameter	Value
Frequency	2.0 GHz
No. of channels	16
Channel bandwidth	5 MHz
Modulation scheme	Offset Quadrature Phase Shift Keying
Data rate	250 kbps
Spread spectrum technique	Direct Sequence Spread Spectrum
Data mapping	4 bit mapping to 32 bit pseudo-random sequence
Modulated signal bandwidth	2 MHz

The received signal strength (RSS) setup and packet measurement setup are shown in Figure 5.1. To be specific, a GNU radio-based IEEE 802.15.4 transceiver was used, which also included the use of a USRP B200 software-defined radio (SDR) [70]. Two independent experiments were conducted for the measurement of RSS and data packet reception. As a result, the setup for RSS is presented in Figure 5.1(a), while the setup for data packet reception is illustrated in Figure 5.1(b). This is followed by the overall practical setup in Figure 5.1(c). It could be seen from Figure 5.1(a) that probe 1 was connected to the computer through SDR USRP B200, which transmitted the signal in the fat tissue. The signal then traveled to the receiving probe 2, which was connected to the Fieldfox microwave analyzer used to record the signal strength. Meanwhile, Figure 5.1(b) configuration indicates that both the transmitting and receiving probes were connected to the SDR USRP B200, enabling the acquirement of data packets and the reception rate measurement.

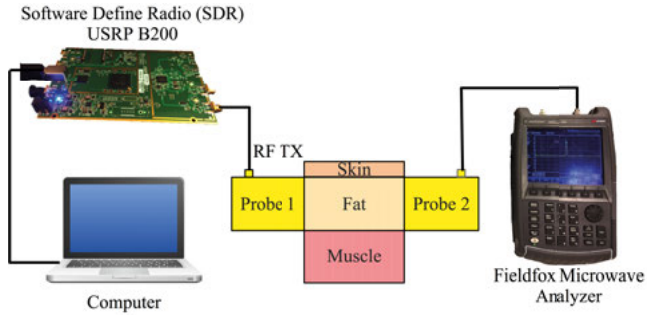

(a) *Illustrative diagram showing the setup to measure the Received Signal Strength (RSS).*

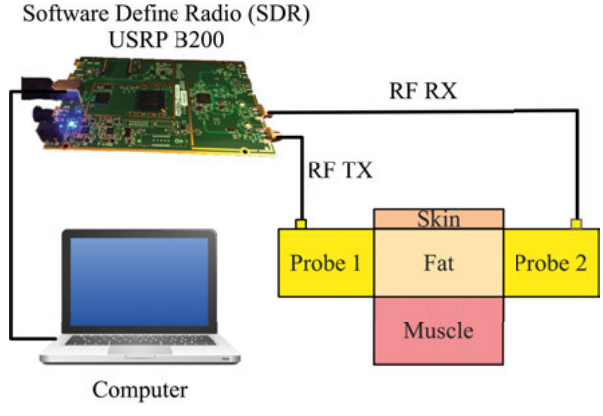

(b) *Illustrative diagram showing the setup to measure the data packet reception.*

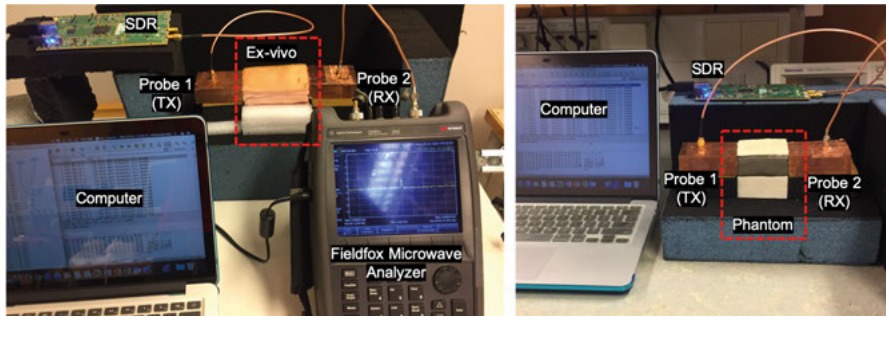

(c) *Ex-vivo and phantom experimental setup.*

Figure 5.1. *Two separate measurement setups to characterize the RSS and data packet reception, and experimentation setup consisting of skin, fat, and muscle layer.* ***Paper VII****. Reprinted, with permission, from [39]. Copyright ©2017, IEEE.*

5.1.2 Results and discussion on the received signal parameter for fat tissue

After identifying the suitability of fat tissue for IBC, further investigations were conducted on the received signal parameter to identify the optimum power for data transmission. In this phase, the system was tested to observe the minimum input power required for reliable signal transmission. Subsequently, the input power required for this transmission ranged from –25 dBm to 0 dBm, including the range of the fat channel length from 10 mm to 100 mm, and a step size of 10 mm. Based on the results shown in Figure 5.2, it could be seen that in respect of the phantom and the ex-vivo, the received power was reduced with the increase in the distance between the transmitter and the receiver and the reduction of coupling. Compared to the phantom where the average RSS as reduced by $\sim$1 dB/cm, the average RSS in the ex-vivo tissue was reduced by $\sim$2 dB/cm.

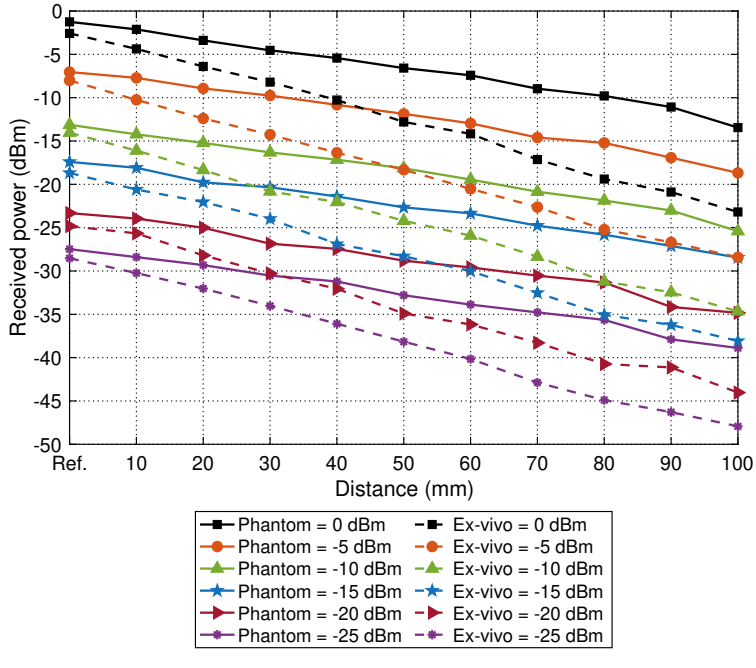

Figure 5.2. *Received signal strength measurement versus channel length for six different input powers for phantom and ex-vivo tissues.* ***Paper VII****. Reprinted, with permission, from [39]. Copyright ©2017, IEEE.*

5.1.3 Packet reception with respect to transmitted power for Fat-IBC

In observing the data packet reception for phantom and ex-vivo tissue, the length of the fat tissue was set to range from 20 mm to 100 mm, with a step size of 20 mm. The transmitted power for Fat-IBC was also set to range from –25 dB to 0 dB. As a result, it could be seen from Figure 5.3 that the approximate percentage of successful packet reception for phantom and ex-vivo tissue was 96 %. It was also suggested that the power could be further reduced from –25 dB to determine the lowest power which was sufficient for good packet reception. –25 dBm was selected as the lower range since it corresponds to the lowest output power of many low-power transceivers. Overall, fat tissue was proven to be a reliable and promising channel for IBC.

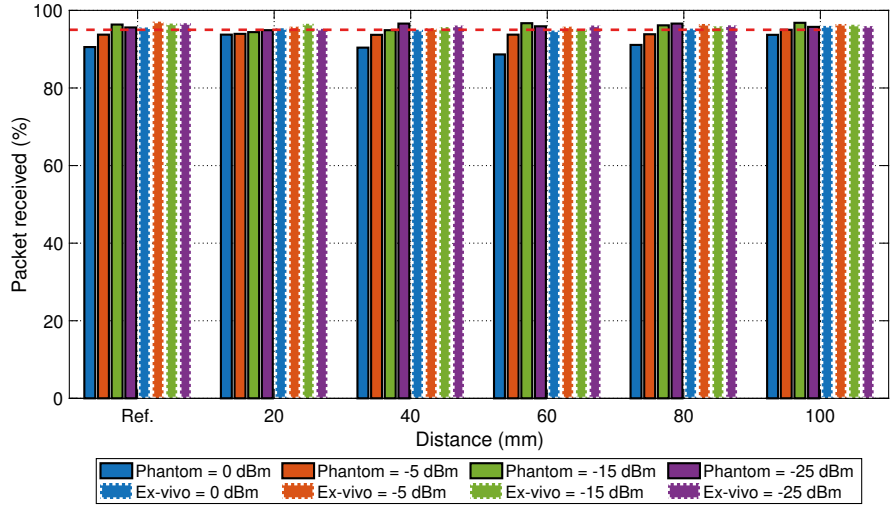

Figure 5.3. *Percentage of packet reception versus channel length for six different input powers for phantom and ex-vivo tissues.* ***Paper VII****. Reprinted, with permission, from [39]. Copyright ©2017, IEEE.*

5.2 Sensing applications of Fat-IBC

In Chapter 4 and Chapter 5, it was indicated through the conducted simulations and experiments that fat tissue is reliable for data rate IBC even at low power consumption. A side-effect of this novel communication technique is its ability to monitor changes in the properties of the communication channel. Such changes could help with early detection of diseases, such as lymphedema or tumour relapse. It could be seen in Section 4.1 that the fat channel could be used for communication even under the presence of a perturbant, for example, a cancerous tissue. This situation was possible if the thickness of perturbant tissue (PT) was lower than 60 % of the thickness of the fat tissue, as shown in Figure 4.3. However, the presence of PT reduced the signal strength in the communication channel between the transmitter and the receiver. This attribute could be used to identify the hindrance occurring due to embedded muscle(s) or tumor(s). It could also be used in tumor detection as the increase in tumor size would result in dramatic changes in communication properties.

The relationship between tumor size and the received signal strength is shown in Figure 5.4. Based on the figure, the blue line indicates the behavior of the received coupling when the PT was present and phantom measurements were conducted. Meanwhile, the orange line indicates the behavior when simulations were conducted on PT with ex-vivo dielectric properties. Overall, a difference of approximately 6 dB from the reference value and PT was 8 mm in radius mainly due to the different materials used to emulate the fat tissue. Nevertheless, similar trend was observed overall. Therefore, it could be concluded that with the increase in tumor size, the signal strength would decrease. This feature could be used for tumor detection.

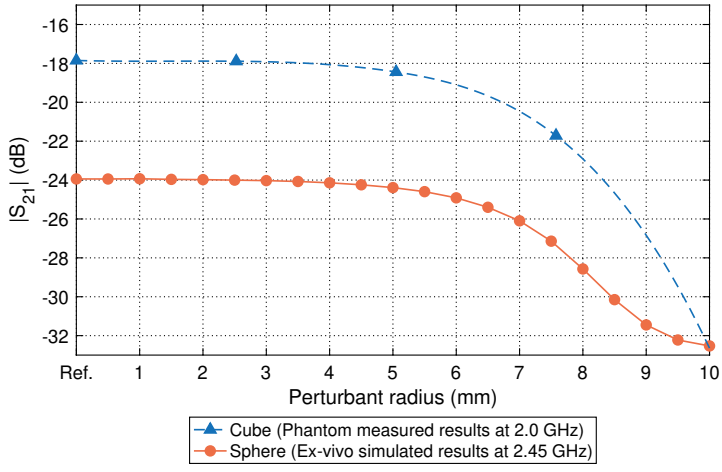

Figure 5.4. *The comparison of perturbant relationship with respect to with the transmission coefficient* S_{21}.

6. Summary of the appended papers

This chapter presents the summary, scientific contribution, key findings, and personal contributions of the papers that are part of the thesis.

6.1 Fat-IBC characterization

This section summarizes three of the papers that deal with the characterization of the Fat-IBC, namely **Papers I–III**.

6.1.1 Paper I – Intra-body microwave communication through adipose tissue

Noor Badariah Asan, Daniel Noreland, Emadeldeen Hassan, Syaiful Redzwan Mohd Shah, Anders Rydberg, Taco J. Blokhuis, Per-Ola Carlsson, Thiemo Voigt, Robin Augustine. 2017. "Intra-body microwave communication through adipose tissue," *Healthcare Technology Letters*, 4(4), pp. 115–121.

Summary

In this paper, we introduce a preliminary study on the impact (or influence) that layers of fat and muscle tissues with different thicknesses will have on the performance of the Fat-IBC channel. We used R-band frequencies since they overlap with the industrial, scientific, and medical (ISM) radio bands. The channel model proposed in the context of human tissues is electromagnetically (EM) simulated and then validated by using the tissue-equivalent phantom and ex-vivo measurements. The measurements are juxtaposed accordingly with numerical modeling. At 2.0 GHz, we obtained a path loss for the phantom of $\sim$1 dB/cm and $\sim$2 dB/cm for ex-vivo, respectively. We estimated the path loss in human tissue to be around 1.5 dB/cm as the dielectric losses in human adipose tissue are almost half of the ex-vivo tissue. This paper is our first step in using the adipose tissue as a transmission medium, and it shows that adipose tissue is feasible for low-loss microwave communication.

Contribution and key findings

- A novel method of using fat tissue as the microwave transmission channel is successfully demonstrated in tissue-equivalent phantom and ex-vivo porcine tissues.

- Fat tissue displays superior performance in comparison to muscle tissue in the context of a low loss communication channel.
- Thicker fat tissue gives lower loss in signal transmission.
- Variation of muscle thickness has minimal impact on signal transmission.
- At 2.0 GHz, losses of $\sim$1 dB/cm and $\sim$2 dB/cm were observed for phantom measurements and ex-vivo measurements, respectively.
- For human fat tissue, an attenuation of approximately $\sim$1.5 dB/cm has been estimated.

Personal contributions
I planned and performed the simulations and experiments, as well as doing the analysis of the data. The probe used was jointly developed. I did major part of writing the manuscript.

6.1.2 Paper II – Characterization of the fat channel for intra-body communication at R-band frequencies

Noor Badariah Asan, Emadeldeen Hassan, Jacob Velander, Syaiful Redzwan Mohd Shah, Daniel Noreland, Taco J. Blokhuis, Eddie Wadbro, Martin Berggren, Thiemo Voigt, and Robin Augustine. 2018. "Characterization of the Fat Channel for Intra-Body Communication at R-Band Frequencies," *Sensors*, 18(9): 2752.

Summary
This paper demonstrates further the characterization of the fat tissue as a medium for communication between implanted devices, specifically in R-band frequencies. We designed the fat channel consisting of the skin, fat, and muscle layers according to the simplified anatomically-tailored model of the human body. We introduced a novel probe that is excellently matched to radiate through the fat tissue at R-band frequencies (i.e., 1.7–2.6 GHz). In order to assess the fat channel path loss, we observe the channel transmission coefficient, S_{21} across the R-band frequencies. An extensive numerical modeling was done and validated via phantom and ex-vivo porcine tissue experimentations. The results of the fat channel characterization display $\sim$0.7 dB/cm and $\sim$1.9 dB/cm propagation path losses for phantom and ex-vivo porcine tissue, respectively. Due to the material used in the development of the probe and also the phantom and ex-vivo tissue, the path loss is slightly different from **Paper I**. We also perform a comparative study between the fat channel and the parallel plate waveguide structure by replacing the skin and muscle layers with copper plates. The result shows that the fat channel behaves as a waveguide structure. The experimentations yield an excellent agreement with the simulations. The results in this paper sufficiently denote the potential and possibility of fat tissue utilization as a mechanism of communication in the purpose of high data rate intra-body networks, explained in **Paper VII** accordingly.

Contribution and key findings

- An evaluation of the capacity of fat tissue as a novel medium for intra-body communication at R-band frequencies (1.7–2.6 GHz).
- Successful development and fabrication of a novel probe equipped with a topology-optimized planar antenna (TOPA), providing an excellent signal match to fat tissue.
- The medium for communication depicts a parallel plate transmission channel consisting of the fat layer with low dielectric permittivity, sandwiched between two layers (skin and muscle) with high dielectric permittivity.
- Skin and muscle tissues function as the conducting layers, whereby their high permittivity and conductivity compared to the fat tissue influence tremendously in affecting the transmission channel via the fat tissue. Such observation is due to the microwave signal being confined in the fat tissue.
- Fat channel characterization yielded $\sim$0.7 dB/cm and $\sim$1.9 dB/cm path losses for phantom and ex-vivo porcine tissues, respectively.

Personal contributions

I planned and performed the simulations and experiments, as well as doing the analysis of the data. I did major part of writing the manuscript.

6.1.3 Paper III – Fat-Intra Body Communication at 5.8 GHz Including Impacts of Dynamic Body Movements

Noor Badariah Asan, Emadeldeen Hassan, Mauricio D. Perez, Laya Joseph, Martin Berggren, Thiemo Voigt, and Robin Augustine. 2019. "Fat-Intra Body Communication at 5.8 GHz Including Impacts of Dynamic Body Movements," *Manuscript*.

Summary

In this paper, numerical modeling and experimental validation of the signal path loss at 5.8 GHz is presented within the framework of fat-intrabody communication (Fat-IBC). In order to propagate information from one implanted device to another, we proposed a topology-optimized waveguide probe which has the capability to direct radiation through the fat tissue. This study not only accesses the feasibility of implanted devices, their performance at 5.8 GHz frequency but also includes the effect of dynamic body movements. Our results show that by changing the channel length from 20 mm to 100 mm and observed that an average path loss of as low as 1.4 dB/cm at 5.8 GHz. In order to study the impact of misalignment, we first assumed that the probe is surrounded by the fat tissue and is placed at the center (taken as a reference). We moved the probe up (towards the skin) and then we moved the probe down (towards the muscle). Our results suggest that the movement of the probe toward the skin contributes to less losses as compared to the probe movement

towards the muscle. However, the horizontal displacement has essentially no impact on the probe's reflection coefficient. When the transmitting probe is 90° rotated from the reference point, S_{21} is dropped by 35 dB. Furthermore, the misalignment between two probes vertically does not strongly affect the signal coupling, which is as low as 1 dB and 2 dB for both cases.

Contribution and key findings

- The path loss is depended on the surrounding fat environment. In ex-vivo, Type A (same L, W, and T_{fat} according to the dimension of the probes) and Type B (width of the channel is extended) have double losses in the path loss compared to the Type C (fat thickness is extended) and D (both the thickness and width of the fat-channel is extended) because of differences in their fat thickness. The increase in the fat thickness produced lower path loss in the channel transmission.
- The polarization mismatch of the probe is having a negative impact on the signal coupling, reducing the received power around –38.4 dB (measurement) and –35 dB (simulation).
- The misalignment between two probes vertically does not strongly affect the signal coupling, which is as low as 1 dB and 2 dB for both cases.

Personal contributions

I planned and performed the simulations and experiments, as well as doing the analysis of the data. I developed and fabricated the topology-optimized waveguide probe, as well as prepared the ex-vivo porcine tissue and 3D printed the mold to support the probes. I did major part of writing the manuscript.

6.2 Factors affecting performance of the Fat-IBC

Three of the papers deal with the factors affecting performance of the Fat-IBC, namely **Papers IV–VI**.

6.2.1 Paper IV – Reliability of the fat tissue channel for intra-body microwave communication

Noor Badariah Asan, Jacob Velander, Syaiful Redzwan Mohd Shah, Emadeldeen Hassan, Daniel Noreland, Taco J. Blokhuis, Thiemo Voigt, and Robin Augustine. "Reliability of the Fat Tissue Channel for Intra-body Microwave Communication," *in 2017 IEEE Conference on Antenna Measurements & Applications (CAMA)*, Tsukuba, Japan. 2017, pp. 310–313.

Summary

This paper presents our work to assess the manner in which disturbances in the channel are capable of impeding reliable microwave propagation through the fat tissue. We incorporate various sizes of perturbants, with the resulting simulation and experimental outcomes depicting positive results. Our results indicate the transmission channel remains non-impacted by perturbants measuring less than 15 mm^3. This information allows us to estimate the performance of the fat channel communication against perturbants such as embedded muscle layers, and blood vessels.

Contribution and key findings

- Besides being a communication channel, the Fat-IBC potentially functions as a sensing system. An example of such an application is tumor presence detection in breast tissue.
- The results show extensive resilience of up to 60 % channel height by the the fat channel in the the context of disturbances such as the embedded muscle layer.

Personal contributions

I planned and performed the simulations and experiments, as well as doing the analysis of the data. I did major part of writing the manuscript.

6.2.2 Paper V – Effect of thickness inhomogeneity in fat tissue on in-body microwave propagation

Noor Badariah Asan, Jacob Velander, Syaiful Redzwan Mohd Shah, Mauricio D. Perez, Emadeldeen Hassan, Taco J. Blokhuis, Thiemo Voigt, and Robin Augustine. "Effect of Thickness Inhomogeneity in Fat Tissue on In-Body Microwave Propagation," *in 2018 IEEE International Microwave Biomedical Conference (IMBioC)*, Philadelphia, PA, USA. 2018, pp. 136–138.

Summary

In this paper, we present our work to evaluate the influence of inhomogeneous fat tissue thicknesses for in-body microwave communication at 2.45 GHz by incorporating the tissue-equivalent phantom models. The method incorporates the models of concave and convex geometrical fat distributions to represent such inhomogeneous thicknesses from 5–45 mm across 100 mm channel length. We vary the distance (*gap*) which incorporates the interval between the transmitter/receiver and the onset and termination of concavity/convexity between 0–25 mm. The present work utilizes phantoms of concave and convex geometries validating the numerical studies. We observe that the signal transmission improves up to 30 mm fat thicknesses where a plateau is reached and the transmission does not improve for larger thicknesses. Our results demonstrate the convex model yields a higher signal coupling in contrast to the concave model. The signal coupling decreases by 2.2 dB and 1.5 dB for the convex model, and by 3.6 dB and 3.5 dB for the concave model (via simulation and measurement, respectively) with respect to the fat channel. Our work successfully assesses the feasibility of a stable and reliable intra-body communication channel in the inhomogeneous fat tissue.

Contribution and key findings

- The convex model does not show a significant reduction of the signal coupling compared to the concave model.
- The fat thickness plays a role in determining the signal coupling in the transmission channel.
- The signal blockage by the muscle tissue decreases the signal coupling in the concave model.
- The distance (*gap*) between the transmitter/receiver and the onset and termination of the concavity/convexity does not affect the transmission.

Personal contributions

I planned and performed the simulations and experiments, as well as doing the analysis of the data. I did major part of writing the manuscript.

6.2.3 Paper VI – Assessment of blood vessel effect on fat-intrabody communication using numerical and ex-vivo models at 2.45 GHz

Noor Badariah Asan, Emadeldeen Hassan, Mauricio D. Perez, Syaiful Redzwan Mohd Shah, Jacob Velander, Taco J. Blokhuis, Thiemo Voigt, and Robin Augustine. 2019. "Assessment of Blood Vessel Effect on Fat-Intrabody Communication using Numerical and Ex-vivo Models at 2.45 GHz," *IEEE Accesss* vol. 7, pp. 89886–89900.

Summary

This paper investigates, in the context of Fat-IBC, the signal transmission in the presence of blood vessels in the fat tissue. We design the models of the blood vessel system in numerical modeling and implement the ex-vivo porcine tissue and phantom experimentations by varying three parameters; the orientations, sizes, and positions. We classify the orientations of the blood vessels into three types, that are orthogonally different, namely longitudinal plane, transverse-horizontal plane, and transverse-vertical plane. For the experimentation, we used copper rods and ex-vivo muscle tissues to emulate the blood vessel models and chose different sizes of blood vessels and varied their location. We use an ex-vivo muscle tissue due to its similarity in dielectric properties to that of blood vessels, and we use copper rods due to their higher conductivity compared to blood vessels. The experimental results are comparable to those of the numerical modeling and supported by the electric field (E-field) visualization. The outcome of this paper represents an extreme case of a realistic scenario and clarifies their predominant impact on signal transmission. The overall results show the signal transmission is lower and more affected by having larger blood vessels.

Contribution and key findings

- The difference in the signal transmission performance between three configurations is caused by the blood vessels position.
- The transverse-vertical plane has high reflection due to a mirror-based behavior. The loss increases with the number of blood vessels and diameter sizes.
- The transverse-horizontal plane functions as a splitter and combiner, and have the least losses.
- The longitudinal plane functions as a splitter, whereby there is no electric field recombination due to mismatches in signal propagation.
- The transverse-vertical plane has the most impact towards the signal coupling, followed by the longitudinal plane. The transverse-horizontal plane displays the least influence on the signal coupling by the presence of the blood vessel.

Personal contributions
I planned and performed the simulations and experiments, as well as doing the analysis of the data. I was responsible for the 3D printed mold for the blood vessel models and prepared the copper rods for the experiment, as well as prepared the ex-vivo porcine tissue. I did major part of writing the manuscript.

6.3 Data transmission in the Fat-IBC

6.3.1 Paper VII - Data packet transmission through fat tissue for wireless intrabody networks

Noor Badariah Asan, Carlos P. Penichet, Syaiful Redzwan Mohd Shah, Daniel Noreland, Emadeldeen Hassan, Anders Rydberg, Taco J. Blokhuis, Thiemo Voigt, and Robin Augustine. 2017. "Data Packet Transmission through Fat Tissue for Wireless IntraBody Networks," *in IEEE Journal of Electromagnetics, RF and Microwaves in Medicine and Biology*, 1(2), pp. 43–51.

Summary
This paper describes the process to evaluate high data rate microwave communication through the fat tissue. Here, we envisioned the wide bandwidth as a requirements for intra-body area networks (i-BANs). We conduct experimentations in the context of data packet reception in connection with tissue length (varies from 20 mm to 100 mm) and power transmission (varies from –25 dBm to 0 dBm). In this paper, the performance of the experimentations require an IEEE 802.15.4-based WBAN real testbed to measure the performance of the fat tissue channel. We demonstrate a data rate communication channel via fat tissue by using tissue-equivalent phantom and ex-vivo environments. Our result yields approximately 96 % data packet reception in both environments, as well as decrements of the received signal strength by $\sim$1 dB/cm and $\sim$2 dB/cm in phantom and ex-vivo environments, respectively. Both experimentations validate the proposed approach to achieve high data rate communication via fat tissue for intra-body network applications. The outcome of this paper opens up new opportunities for high bandwidth wireless intra-body networks, explicitly Fat-IBC, in supporting high data rate in devices that are to be implanted, ingested, or injected, accordingly.

Contribution and key findings
- The work yields data reception as high as 96 % for tissue-equivalent phantom and ex-vivo communications.
- The results reveal signal strength decrements by $\sim$1 dB/cm and $\sim$2 dB/cm in tissue-equivalent phantom and ex-vivo environment, respectively.
- The average path losses are 1 dB/cm and 2 dB/cm in the three-layer phantom and ex-vivo tissues, respectively.

- The results indicate that the transmission loss (dB) observed in the muscle layer is two-folds higher than in the fat layer.

Personal contributions

I planned and performed the simulations and experiments, as well as doing the analysis of the data. I did major part of writing the manuscript.

7. Concluding remarks and future perspectives

In this chapter, the essence of this research, which was mainly focused on Fat-IBC, is presented. Provided that Fat-IBC is a new area of research, there was an emergence of challenges that needed to be addressed they were all set for commercialization. Therefore, recommendations are presented in this chapter for future work to address the present challenges faced by Fat-IBC.

7.1 Conclusions

Due to the growth of human population and aging, functional and efficient health care will be even more crucial for society in the future. New methods for health monitoring and diagnosis are therefore needed.

In this thesis, the design and implementation of intrabody communication for medical applications were discussed. Intra-body communication indicates the placement of sensors inside the body and their communication with each other. Furthermore, when the sensors are placed within certain distances, the presence of certain media is essential for the establishment of wireless communication. The scope of work in the thesis is based on the simplified three-layered (i.e., skin-fat-muscle) tissue model. The media available for intra-body communication are the muscle and fat tissues. This study aims to determine the medium which was more feasible for IBC. Therefore, extensive simulations and experimentation were conducted by transmitting at a wide range of frequencies (R-band and F-band) in muscle tissues and fat tissues. It was suggested from the results that fat displayed a more superior performance compared to muscle tissue. It also offered lesser amount of loss for microwave IBC, i.e., thick fat tissue offers about $\sim$1 dB and $\sim$2 dB/cm losses for phantom and ex-vivo, respectively. Notably, the thickness of fat tissue was inversely related to the losses, which could be seen from how the thick fat tissue offered low losses, and how the losses were independent of the thickness of the muscle tissue.

Further investigations were conducted on the factors of Fat-IBC. Firstly, the effects of the blood vessel on IBC were determined. As a result, it was suggested that when blood vessels were placed in the transverse-vertical plane inside the fat tissue, higher losses were obtained compared to the other two orientations due to presence of higher reflections. The transverse-horizontal plane inflicted the least influence on the signal coupling due to the presence of blood vessels. Moreover, the increase in the diameter of the blood vessel(s)

increases led to further loss. Overall, the simulated and practical results were in an agreement with each other.

The observation was conducted on the inhomogeneity in the fat tissues when they were used as a channel for intra-body microwave communication at a frequency of 2.45 GHz. This is an important aspect to be investigated as the structure/thickness of an individual's fat may vary from one another. In this study, the concave and convex models of the three-layered structure were developed to observe the performance of the fat tissues when used for IBC. As a result, no significant reduction in the signal coupling was found from the convex model, in comparison to the concave model. The signal blockage by the muscle tissue reduced the signal coupling in the concave model. Moreover, the distance between the transmitter/receiver and the distance between the onset and termination of the concavity/convexity did not impact the transmission. Overall, it was indicated that fat thickness plays a role in determining the signal coupling in the transmission channel.

In another experiment, the reliability of fat tissue as a source of communication channel for IBC was investigated. Accordingly, the S_{21} parameter was observed under the presence and absence of the perturbant tissue. As a result, it was found that the fat tissue could function as a reliable medium for intra-body communication even under the presence of blockage of small size, in comparison to the homogeneous thickness of the fat tissue. However, with a PT size which was larger than the width of the fat tissue by 60 % or higher, a significant decrease in the magnitude of S_{21} occurred. Moreover, PT reduced the signal strength in the communication channel between the transmitter and the receiver. This characteristic could be used in identifying or sensing the hindrance caused by embedded muscle(s) or tumor(s).

With the materialization of implanted devices, such as cardiac pacemakers, neuro-prosthetics, and cardioverters, the demand for bandwidth increases as these devices require high data rate communication. To determine whether Fat-IBC supported higher data rates, the data packet reception and the path loss at a frequency of 2.0 GHz were observed, with a data rate of 250 kbps. The results of this study were in an agreement with the previous experiments conclusion that fat tissue is a superior medium for IBC. In respect of the data reception, a high percentage of 96 % was reported for tissue-equivalent phantom and ex-vivo communications. Meanwhile, in the case of the received signal strength, the average path losses of 1 dB/cm and 2 dB/cm were reported in the three-layered phantom and ex-vivo tissues respectively. The general finding of implants was that power consumption by the sensor was required to be as low as possible to enhance the sensor's lifetime. Overall, it was indicated from the results that the power level transmission could be reduced until –25 dBm to achieve effective communication at a distance of 100 mm with approximately 96 % of successful data packet reception.

7.2 Future recommendations

Intra-body communication is a multi-disciplinary research area, which is relatively new in the research community. There are various aspects of this matter, including efficient antenna design and the achievement of higher and reliable throughput over a longer distance and robust networking. The first design constraint in this study was frequency selection. To be specific, although low frequencies were ideal in terms of losses, the heating effect could occur in the tissues and antennas with compromised sizes. The communication at higher frequencies, especially in the microwave range, are well established and can be scaled and restructured cost-effectively in the intra-body communication scenario. However, the bio-compatibility requirement has to be met. Therefore, thorough investigation of this trade-off was crucial in order to determine the appropriate frequency-supporting mass networking, economics, and human safety. Notably, IEEE/ITU plays a role in ensuring human safety by issuing several standards or recommendations about the specific absorption rate (SAR) and maximum allowable power for IBC.

In the case of the antenna design prospects, miniature antennas need to be developed with a design that has a proper fit inside the human body to ensure unobtrusiveness. This characteristic is essential for practical realization of intra-body communication. In contrast, the miniature designing, using conventional three-layered human body modelling approach, would not be effective. Therefore, new human body models should be developed to incorporate the miniature antenna. Notably, the installation of multiple sensors inside the human body is an aspect that has not been investigated. They may operate at higher frequencies and have to resolved for interferences.

It was suggested in the results from Chapter 5 that the communication link was effective even at the lowest level when the reliability of packets was tested under different power levels. Therefore, the extent of power reduction is worthy to be investigated to establish a reliable communication link through different hardware. According to the convention in the field of biomedical engineering and medicine, the system in this study was first tested on animals before it was tested on humans. The sample of this study was from the freshly slaughtered porcine belly. As human samples have not been involved in studies, future experiments which use human tissue samples from humans of different body parts, gender, and race are recommended. It is also important to determine the effects of long-term use in the human body by taking the anthropometric characteristics and the subject's movement into account.

Bionic arms can utilize the Fat-IBC to receive actuation signals based on electric pulses generated in muscle or even brain. Inherent confinement of signals in Fat-IBC facilitates data privacy. With the advancement in encryption methods it is also possible to offer security in Fat-IBC against external threats. The capability of Fat-IBC in the security and privacy perspective is recommended for future analysis.

Svensk sammanfattning

I detta kapitel presenteras de viktigaste resultaten från forskningen om fettintrakroppslig kommunikation (engelska: Fat-Intra Body Communication, Fat-IBC). Eftersom Fat-IBC är ett nytt forskningsområde finns det många utmaningar som måste lösas innan applikationerna kan kommersialiseras. Här presenteras även rekommendationer för framtida arbete som kan ta itu med utmaningarna som Fat-IBC står inför.

Slutsatser

Världens befolkning ökar i snabb takt. År 2019 uppskattas världens befolkning till 7,7 miljarder och förväntas öka till ungefär 8,5 miljarder år 2030 och till ungefär 9,7 miljarder 2050 [71]. Utöver en ej tidigare skådad befolkningstillväxt förväntas befolkningen i alla länder att åldras. På grund av den ökande och samtidigt åldrande befolkning finns det ett stort behov att utveckla hälsovården. Lyckligtvis har det gjorts stora framsteg inom elektronik och informationssystem som har lett fram till helt nya metoder för att behandla patienter och för att övervaka deras tillstånd. Utöver konventionella metoder för patientövervakning och diagnostik måste nya metoder utvecklas som använder de senast vetenskapliga verktygen.

I denna avhandling har vi undersökt utvecklingen och tillämpningen av intrakroppslig kommunikation (IBC) för medicinska tillämpningar. Med IBC menas att sensorerna implanteras i kroppen och att de kommunicerar med varandra. När sensorer placeras på ett visst avstånd från varandra måste det finnas ett medium mellan dem som vågorna kan utbreda sig genom. I avhandlingen behandlas en förenklad trelagersmodell bestående av hud, fett och muskler. Två av de medier som står till buds för IBC är muskelvävnad och fettvävnad. Först undersöktes vilket av dessa media som var mest lämpligt för IBC. Noggranna simuleringar och mätningar genomfördes genom att utsätta muskel- och fett vävnad för signaler av ett brett frekvensområde (R-band och F-band). Resultaten visar att fettvävnad är överlägsen muskelvävnad med bland annat lägre förluster och lämpar sig bättre för IBC vid mikrovågsfrekvenser. Tjockleken hos fettvävnaden står i omvänd proportion till förlusterna, eller med andra ord, tjock fettvävnad har små förluster, ungefär 1 dB/cm för fantomer och 2 dB/cm för ex-vivo, och förlusterna är oberoende av muskelvävnadens tjocklek.

Vidare genomfördes fördjupande undersökningar av de faktorer som påverkar Fat-IBC. Först undersöktes hur blodkärl påverkar IBC. Detta gjordes

genom numerisk simulering samt genom ex-vivo modellering. Blodkärlen placerades på olika avstånd mellan sändaren och mottagaren och sedan ändrades blodkärlens orientering och mätningar gjordes i transversella vertikalplanet, transversella horisontalplanet och longitudplanet. Dessutom varierades antalet blodkärl från ett till tre. Resultaten visar att när blodkärlen placeras i transversella vertikalplanet i fettvävnaden ökar reflektionerna och förlusterna blir större jämfört med de andra två orienteringarna. Med ökande diameter på blodkärlen ökar också förlusterna. Med blodkärlen orienterade i transversella horisontalplanet erhålls minst påverkan på signalen. I samtliga fall överensstämde simuleringarna med mätningarna.

Därefter studerades effekterna av inhomogeniteter i fettvävnaden då denna användes som en kanal för mikrovågs IBC vid 2.4 GHz. Detta är en viktig aspekt att studera då strukturen och tjockleken på olika personers fettvävnad kan skilja sig åt. En konkav- och en konvex fettmodell med trelagerstruktur utvecklades för att studera effekterna på IBC. Från experimentet kunde ett antal slutsatser dras. Den konvexa modellen uppvisar ingen tydlig reduktion av signalkopplingen jämfört med den konkava. Tjockleken på fettlagret påverkar signalkopplingen i utbredningskanalen. För den konkava modellen blockerar muskelvävnaden signalen och minskar signalkopplingen. Avståndet mellan sändare och mottagare samt början och avslutningen på konkaviteten/konvexiteten påverkar inte överföringen.

I ett annat experiment studerades tillförlitligheten hos fettvävnad som kommunikationskanal för IBC. S_{21} uppmättes med och utan inhomogeniteter inuti fettvävnaden. Storleken på inhomogeniteterna varierades från 5 mm till 20 mm och de placerades på olika avstånd mellan sändare och mottagare. Resultaten visar att fettvävnaden, också då denna innehåller blockerande strukturer som är små jämfört med dess tjocklek, kan användas som ett tillförlitligt medium för IBC. Då inhomogeniteten är 60 % eller mer av tjockleken på fettvävnaden sjunker beloppet på S_{21} markant. Närvaron av inhomogeniteter reducerar signalstyrkan i kommunikationskanalen mellan sändare och motagare. Denna egenskap kan användas för att detektera störningar orsakade av inbakade muskler eller tumörer.

Genom nya implantat som kräver höga dataöverföringshastigheter, såsom pacemakers, neuro-proteser och elkonverterare, har bandbreddsbehovet ökat. För att undersöka om Fat-IBC kan understödja höga datahastigheter uppmättes mottagningen av datapaket och signaldämpningen vid en frekvens på 2.0 GHz och en datahastighet på 250 kbps. Resultaten av experimenten stöder den tidigare slutsatsen att fettvävnad fungerar utmärkt för IBC. Mottagandet av datapaket var så hög som 96 % både för vävnadsliknande fantom och ex-vivo vävnad. Signaldämpningen uppmättes i medeltal till 1 dB/cm i en fantom bestående av tre lager och till 2 dB/cm för ex-vivo vävnad. För att ett implantat ska ha en lång livslängd bör det förbruka så låg energi som möjligt. Våra resultat tyder på att det räcker med en effekt på –25 dBm för att kommunicera över ett avstånd på 100 mm med ungefär 96 % korrekt överförda datapaket.

Rekommendationer för framtiden

IBC är ett tvärvetenskapligt forskningsområde som är relativt nytt. Inom området finns stora utvecklingsmöjligheter från effektiv antennkonstruktion, till erhållande av större och pålitligare överföring över längre sträckor, samt robusta nätverk. Det första designkriteriet är valet av frekvens. Låga frekvenser ger låga förluster men kan orsaka uppvärmning av vävnader och innebär också att antennerna måste göras större. Högre frekvenser ger mindre och mer hanterliga antenner men också större utbredningsförluster och dyrare nätverkslösningar. Därför finns det ett behov att undersöka denna kompromiss och hitta en fördelaktig frekvens för storskaliga nätverk, ekonomi och personsäkerhet. På personsäkerhetsområdet kan IEEE/ITU utöva inflytande genom att specificera standarder eller rekommendationer för SAR-värdet (Special Absorption Rate) och maximalt tillåten effekt för IBC.

Miniatyriserade antenner behöver konstrueras så att de lämpar sig som implantat och inte påverkar patienten. Detta steg är helt nödvändigt för att möjliggöra IBC. Däremot är kroppsmodellen med tre olika typer av vävnad otillräcklig för att fullt ut beskriva människokroppen. Nya kroppsmodeller som är anpassade till miniatyriserade antenner måste utvecklas. En annan aspekt som ännu inte studerats är inoperering av ett flertal sensorer i människokroppen. Sensorerna skulle använda högre frekvenser och kunna störa varandra. Därför är det viktigt att undersöka hur de kopplar till varandra och modellera utbredningen av vågorna samt analysera överföringskapaciteten.

I den aktuella undersökningen användes USRP B200 Software Defined Radio (SDR) som har sådana effektkrav att det kanske inte fungerar bra för effekter under –25 dBm. Resultaten (i Kapitel 5) visar att kommunikationslänkens överföring av datapaket fungerade bra också vid de lägsta undersökta effektnivåerna. Däremot kunde effekter under –25 dBm inte undersökas på grund av restriktioner hos USRP B200 SDR systemet. Därför är det värt att undersöka andra hårdvarualternativ för att utröna hur låga effektnivåer som kan användas och ändå upprätthålla en väl fungerande kommunikationskanal. Som följer av konventionen inom biomedicinsk forskning och medicin skall tester först utföras på djur och sedan på människor. I studien användes sidfläsk från en nyslaktad gris. Så vitt vi vet har inga försök hittills gjorts på mänskliga prov. Därför är det viktigt att försök görs på mänskliga vävnader tagna från olika kroppsdelar och från personer av olika kön och ras. Dessutom är det också viktigt att studera långtidseffekter av användningen inuti människor genom att ta hänsyn till antropometriska egenskaper och försökspersonernas rörelser.

Avslutningsvis kan sägas att mycket återstår att göra inom området för medicinska implantat. När IBC transceivrar på miniatyriserad skala konstrueras för att etablera nätverk och registrera mänskliga data är det väldigt viktigt att dataintegriteten och integriteten kan bevaras. Det finns ett behov av säkra och pålitliga miniatyriserade elektriska och mekaniska komponenter för att möjliggöra denna typ av kommunikation i större skala.

Acknowledgement

Since the past few years, I have met various individuals who have inspired, encouraged, and supported throughout the development of this thesis. It has been a long journey, and I am truly thankful for all the encounters I had with them.

First and foremost, I would like to express my sincere gratitude to my dedicated supervisor, **Assoc. Prof. Robin Augustine**, for his patience, motivation, immense knowledge, and the continuous support for my Ph.D. study and the works of research related to it. Thank you for listening to my opinions and for providing me with guidance, inspiration, and encouragement throughout my study. You were constantly available at your office whenever I was faced with troubles or questions about my research or writing. I could not have imagined having a better advisor and mentor for my Ph.D. study.

I have great pleasure in acknowledging my gratitude to my co-supervisor, **Prof. Thiemo Voigt**, for his constant help, invaluable support, and encouragement. Besides the assistance and reassurance he gave, he also guided me in the right direction in my study whenever I needed it.

My most sincere appreciation is also addressed to **Prof. Anders Rydberg** for his supervision, advice and guidance from the very early stage of this research. I would also like to extend my deepest gratitude to **Prof. Jörgen Olsson** for his unwavering support, genuine concern, invaluable scientific assistance and extraordinary human qualities. He always gave me constant encouragement and providing advice many times during my study, despite his busy agenda.

I am grateful for the funding provided for my Ph.D. from the **Ministry of Higher Education Malaysia (MOHE)** and **Universiti Teknikal Malaysia Melaka (UTeM)**. A token of appreciation goes to **Anna Maria Lundin's scholarship foundation** as well for enabling me to attend an international conference. A special gratitude also goes out to all down at **research project grants**, H2020 RIA – SINTEC, Soft Intelligent Epidermal Communication (ID: 824984) (2019–2022), Vinnova – Smart electronics 2018, "Anslut min kropp: från in-body kommunikation till hälsovårdssystemet" (ID: 2018-01532) (2018–2020), and Foundation for Strategic Research, SSF, Sweden, "LifeSec: Don't Hack My Body" (ID: RIT-17-0020) (2018–2022), for the research funding.

Thank you, **Ingrid Ringård**, **Karin Ringefors Finn**, **Maria Skoglund**, and **Ida Näslund** for taking care of administrative issues. I am thankful to **Jonatan Bagge** for the continuous support regarding all matters related to computer and software. Not to forget is **Ramy Salameh** for always entertain my "oink" purchased ☺.

My special thanks are dedicated to **Mauricio Perez** and **Roger Karlsson** for delivering constructive comments and suggestions throughout the experimental and thesis works, which have significantly contributed to the success of this research. He had often pointed out the incompleteness of my works and helped me to improve my understandings on each problem. I gratefully acknowledge the help of **Roger Karlsson** for the Swedish translation. Without you, there will be no Svensk sammanfattning section in this thesis.

I highly appreciate the support received throughout the collaborative work undertaken during the first phase of my work until now. Specifically, my sincere gratitude goes to **Emadeldeen Hassan** from Umeå University for sparing valuable time whenever I approached and showing me the way ahead. I am also very grateful for his scientific advice and knowledge and many insightful discussions and suggestions. To **Daniel Noreland**, thank you for making the first few months of experimentation and data collection meaningful to me.

*No matter what happens, some memories can never be replaced.. **FRIENDS**...*

I also would like to thank my fellow lab mates and friends, **Syaiful Redzwan** and **Jacob Velander**, for sharing the happy and painful moments with me as Ph.D. students in those four years of being in a group. In fact, our journey started from zero to hero, and from nothing to everything. I am deeply thankful for all the precious memories.

I would like to express my gratitude to my neighbors, **Imran Aziz** and **Viktor Mattsson**. Thank you for being good neighbors and for always lending a helping hand to me in any way. You have been generous and gracious always. All the best for your Ph.D. study!!

A appreciation also goes to my friends from Microwave group, **Dragos Dancila** and **Long**. Thank you for being a good teammates. To my friends under Microwaves in Medical Engineering Group (MMG) from the past to the present, **George**, **Jasmin**, **Laya**, **Javad**, **Pramod**, **Bappaditya**, **Eric**, **Rocco**, and **Marwa**, thank you for adding the sweets and spices throughout my Ph.D. journey.

The same goes for my friends from the Department of Information Technology, especially **Carlos P. Penichet**, for your assistance and generosity in sharing knowledge with me. To **Wenqing Yan** and **Sam Hylamia**, thank you for being a part of my Ph.D. life! Keep going to secure the fat-IBC.

Not only that, to all my **friends in the Division of Solid State Electronics**, thank you for the friendships and memories.

To **Dr. Duen** & **Dr. Mona**, thank you for helping me and sharing tips to begin a new life as a Ph.D. student in Uppsala with my daughter. I am proud to say that I have successfully survived this journey.

Furthermore, I am indebted to all my Malaysian friends and family in Uppsala who welcomed me to their homes during times when I was overcome with stress. They were always helpful in numerous ways. My special thanks go to my former and current friends, **Fadli** & **Maisarah**, **Kak Dalina**, **Muzafar Affa**, **Nasir** & **Azhan An**, **Khadijah KD**, and **Akma**.

My acknowledgement would be incomplete without thanking the biggest source of my strength, my family... To my parents, and brothers and sisters for the spiritual support given throughout my journey in this thesis development and my life in general. Your prayer for me is what has been sustaining me until now.
Istimewa: Terima kasih yang tak terhingga kepada; mak – **Minah Sidek** *dan ayah* – **Asan Abdullah** *yang tak putus mendoakan kejayaan ida; dan abang* **Faaz A. Fitri** *kerana sentiasa support ida sekaligus merangkap graphic designer bagi menjayakan tesis ini.* ☺

Last but not least, my heartfelt thanks go to my loving, supportive, encouraging, and patient husband, **Zulkifli Shariff**, who provides me with unending support and inspiration. His continuous love and support have always been the sources of my strength. His patience and sacrifice will remain as the inspirations throughout my life. Thank you, "sayang" for everything. My appreciation also goes to my beloved daughter **Nur Alia Safiyya**. I would like to express her infinite thanks for always being a good daughter and for cheering me up throughout Ph.D. journey. Kakak Yaya is a strong girl, therefore, I knows that you will be a good sister to baby **Alexander Dzulqarnayn**.

♥♥ Ida.Asan ♥♥
Uppsala, Sweden
2015–2019

References

[1] J. Galgani and E. Ravussin, "Energy metabolism, fuel selection and body weight regulation," *International journal of obesity (2005)*, 32 Suppl 7(Suppl 7), S109–S119, 2008. doi:10.1038/ijo.2008.246

[2] A. S. Jackson, P. R. Stanforth, J. Gagnon, T. Rankinen, A. S. Leon, D. C. Rao, J. S. Skinner, C. Bouchard, and J. H. Wilmore, "The effect of sex, age and race on estimating percentage body fat from body mass index: The Heritage Family Study," *International journal of obesity*, vol. 26, no. 6, p. 789, 2002. doi: https://doi.org/10.1038/sj.ijo.0802006

[3] "National Health and Nutrition Examination Survey, 1999–2004". Available at http://www.cdc.gov/nchs/nhanes.htm.

[4] F. F. Anhê, T. V. Varin, M. Le Barz, Y. Desjardins, E. Levy, D. Roy, and A. Marette, "Gut microbiota dysbiosis in obesity-linked metabolic diseases and prebiotic potential of polyphenol-rich extracts," *Current obesity reports*, vol. 4, no. 4, pp.389–400, 2015.

[5] H. K. Park, M. K. Kwak, H. J. Kim, and R. S. Ahima, "Linking resistin, inflammation, and cardiometabolic diseases," *The Korean journal of internal medicine*, vol. 32, no. 2, pp. 239, 2017.

[6] K. Sharma, "Obesity and diabetic kidney disease: role of oxidant stress and redox balance," *Antioxidants & redox signaling*, vol. 25, no. 4, pp. 208–216, 2016.

[7] E. Börgeson, A. M. Johnson, Y. S. Lee, A. Till, G. H. Syed, S. T. Ali-Shah, P. J. Guiry, J. Dalli, R. A. Colas, C. N. Serhan, K. Sharma, and C. Godson, "Lipoxin A4 attenuates obesity-induced adipose inflammation and associated liver and kidney disease," *Cell metabolism*, vol. 22, no. 1, pp. 125–137, 2015.

[8] J. M. Larsen, "The immune response to Prevotella bacteria in chronic inflammatory disease," *Immunology*, vol. 151, no. 4, pp. 363–374, 2017. doi: 10.1111/imm.12760

[9] Z. Jie et al., "The gut microbiome in atherosclerotic cardiovascular disease," *Nature communications*, vol. 8, no. 845, 2017. doi:10.1038/s41467-017-00900-1

[10] World Health Organization Factsheets. Retrieved on September 7, 2019 from https://www.who.int/news-room/fact-sheets/detail/cardiovascular-diseases-(cvds)

[11] D. Elleri, D. B. Dunger, and R. Hovorka, "Closed-loop insulin delivery for treatment of type 1 diabetes," *BMC Medicine*, vol. 9, no. 120, 2011. doi:10.1186/1741-7015-9-120

[12] World Health Organization, "Ageing and health," Retrieved on September 25, 2019, URL: https://www.who.int/news-room/fact-sheets/detail/ageing-and-health

[13] L. Stephen, “In developing world, pollution kills more than Disease,” *IPS News*, Accessed 25/09/2019, URL: http://www.ipsnews.net/2014/06/in-developing-world-pollution-kills-more-than-disease/
[14] Y. H. Joung, “Development of implantable medical devices: from an engineering perspective,” *International neurourology journal*, vol. 17 no. 3, pp. 98–106, 2013. doi:10.5213/inj.2013.17.3.98
[15] K. Bazaka and M. V. Jacob, “Implantable devices: Issues and challenges,” *Electronics*, vol. 2, no. 1, pp. 1–34, 2013. doi:10.3390/electronics2010001
[16] C. Camara, P. Peris-Lopez, and J. E. Tapiador, “Security and privacy issues in implantable medical devices: A comprehensive survey,” *Journal of biomedical informatics*, vol. 55, pp. 272–289, 2015. doi: https://doi.org/10.1016/j.jbi.2015.04.007
[17] M. S. Wegmüller, “Intra-body communication for biomedical sensor networks,” *Doctoral dissertation*, ETH Zurich, 2007.
[18] T. G. Zimmerman, “Personal area networks: near-field intrabody communication,” *IBM systems Journal*, vol. 35, no. 3.4, pp.609–617, 1996.
[19] M. Seyedi, B. Kibret, D. T. H. Lai, and M. Faulkner, “A survey on intrabody communications for body area network applications,” *in IEEE Transactions on Biomedical Engineering*, vol. 60, no. 8, pp. 2067–2079, Aug. 2013. doi: 10.1109/TBME.2013.2254714
[20] D. P. Chandima, K. D. U. I. Dayarathna, H. G. D. A. Jayasinghe, W. K. K. R. Dharmasiri, and H. M. Weerasinghe, “Inductive power transmission, charging and communication for implantable devices,” *2017 IEEE International Conference on Industrial and Information Systems (ICIIS)*, Peradeniya, 2017, pp. 1–6. doi: 10.1109/ICIINFS.2017.8300356
[21] M. D. Pereira, G. A. Alvarez-Botero, and F. Rangel de Sousa, “Characterization and modeling of the capacitive HBC channel,” *in IEEE Transactions on Instrumentation and Measurement*, vol. 64, no. 10, pp. 2626–2635, Oct. 2015. doi: 10.1109/TIM.2015.2420391
[22] C. K. Ho, J. H. Cheong, J. Lee, V. Kulkarni, P. Li, X. Liu, and M. Je, “High bandwidth efficiency and low power consumption Walsh code implementation methods for body channel communication,” *in IEEE Transactions on Microwave Theory and Techniques*, vol. 62, no. 9, pp. 1867–1878, 2014.
[23] M. A. Callejón, J. Reina-Tosina, D. Naranjo-Hernández, and L. M. Roa, “Measurement issues in galvanic intrabody communication: influence of experimental setup,” *in IEEE Transactions on Biomedical Engineering*, vol. 62, no. 11, pp. 2724–2732, 2015. doi: 10.1109/TBME.2015.2444916
[24] M. Swaminathan, U. Muncuk, and K. R. Chowdhury, “Tissue safety analysis and duty cycle planning for galvanic coupled intra-body communication,” *in 2016 IEEE International Conference on Communications (ICC)*, Kuala Lumpur, 2016, pp. 1–6. doi: 10.1109/ICC.2016.7511387
[25] W. Li, “Wireless considerations in ocular implants based on microsystems,” *in Handbook of Mems for Wireless and Mobile Applications*, Woodhead Publishing, pp. 424–462, 2013.
[26] B.P. Brockway, P.A. Mills, and L.M. Zwiers, “Transoma Medical Inc, “Implantable sensor with wireless communication,” *U.S. Patent*, 6,409,674, 2002.

[27] A. Kerselaers and L. Gomme, NXP BV, "Apparatus and method for wireless body communication," *U.S. Patent*, 9,819,395, 2017.
[28] M. A. Hannan, S. Mutashar, S. A. Samad, and A. Hussain, "Energy-harvesting for the implantable biomedical devices: issues and challenges," *Biomed. Eng. Online*, vol. 13, 2014.
[29] S. Ullah, H. Higgin, M. A. Siddiqui, and K. S. Kwak (2008) "A study of implanted and wearable body sensor networks," *in: Nguyen N.T., Jo G.S., Howlett R.J., Jain L.C. (eds) Agent and Multi-Agent Systems: Technologies and Applications. KES-AMSTA 2008*, Lecture Notes in Computer Science, vol 4953. Springer, Berlin, Heidelberg.
[30] W. J. Tomlinson, S. Banou, C. Yu, M. Stojanovic, and K. R. Chowdhury, "Comprehensive survey of galvanic coupling and alternative intra-body communication technologies," *in IEEE Communications Surveys & Tutorials*, vol. 21, no. 2, pp. 1145–1164, 2019. doi: 10.1109/COMST.2018.2879643
[31] N. B. Asan, R. Augustine, and T. Voigt, 2019. "In-body internet of things networks using adipose tissue," *IEEE Internet of Things Newsletter*, Retrieved from https://iot.ieee.org/newsletter/may-2019/in-body-internet-of-things-networks-using-adipose-tissue.
[32] M. Vallejo, J. Recas, P. G. Del Valle, and J. L. Ayala, "Accurate human tissue characterization for energy-efficient wireless on-body communications," *Sensors (Basel, Switzerland)*, vol. 13, no. 6, pp. 7546–7569, 2013. doi:10.3390/s130607546
[33] R. Augustine, "Electromagnetic modelling of human tissues and its application on the interaction between antenna and human Body in the BAN context," *Ph.D. Thesis*, Université Paris-Est; Paris, France, 2009.
[34] C. A. Da Graça-Lopes, "Characterisation of the radio channel in on-Body communications," *Ph.D. Thesis*, Universidade Técnica de Lisboa, Lisboa, Portugal, Nov, 2010.
[35] N. B. Asan, E. Hassan, J. Shah, D. Noreland, T. Blokhuis, E. Wadbro, M. Berggren, T. Voigt, and R. Augustine, "Characterization of the fat channel for intra-body communication at R-band frequencies," *Sensors*, vol. 18, no. 9, p. 2752, 2018.
[36] N. B. Asan, D. Noreland, E. Hassan, S. R. Mohd Shah, A. Rydberg, T. J. Blokhuis, P. O. Carlsson, T. Voigt, and R. Augustine, "Intra-body microwave communication through adipose tissue," *Healthcare technology letters*, vol. 4 no. 4, pp. 115–121, 2017. doi: 10.1049/htl.2016.0104
[37] N. B. Asan, E. Hassan, M. D. Perez, S. R. Mohd Shah, J. Velander, T. J. Blokhuis, T. Voigt, and R. Augustine, "Assessment of blood vessel effect on fat-intrabody communication using numerical and ex-vivo models at 2.45 GHz," *in IEEE Access*, vol. 7, pp. 89886–89900, 2019. doi: 10.1109/ACCESS.2019.2926646
[38] N. B. Asan, J. Velander, S. R. Mohd Shah, M. Perez, E. Hassan, T. J. Blokhuis, T. Voigt, and R. Augustine, "Effect of thickness inhomogeneity in fat tissue on in-body microwave propagation," *2018 IEEE International Microwave Biomedical Conference (IMBioC)*, Philadelphia, PA, 2018, pp. 136–138. doi: 10.1109/IMBIOC.2018.8428872
[39] N. B. Asan, C. P. Penichet, S. R. Mohd Shah, D. Noreland, E. Hassan, A.

Rydberg, T. J. Blokhuis, T. Voigt, and R. Augustine, "Data packet transmission through fat tissue for wireless intrabody networks," *in IEEE Journal of Electromagnetics, RF and Microwaves in Medicine and Biology*, vol. 1, no. 2, pp. 43–51, Dec. 2017. doi: 10.1109/JERM.2017.2766561

[40] C. Edman and D. Drinan, "A review of the management of implanted medical devices for diabetes: trends and directions", *Journal of diabetes science and technology*, vol. 2, no. 6, pp. 995–1002, 2008. doi:10.1177/193229680800200609

[41] Y. Chen, R. Pan, and A. Pfeifer, "Fat tissues, the brite and the dark sides," *Pflügers Archiv-European Journal of Physiology*, 468(11–12), pp. 1803–1807, 2016. doi:10.1007/s00424-016-1884-8

[42] R. E. Smith, and B. A. Horwitz, "Brown fat and thermogenesis," *Physiological Reviews*, vol. 49 no. 2, pp. 330–425, 1969.

[43] J. Nedergaard, T. Bengtsson, and B. Cannon, "Unexpected evidence for active brown adipose tissue in adult humans," *American Journal of Physiology-Endocrinology and Metabolism*, vol. 293 no. 2, pp E444–E452, 2007.

[44] L. S. Hoffmann, C. J. Larson, and A. Pfeifer, "cGMP and brown adipose tissue," *in Metabolic Control*, Springer, Cham, pp. 283–299, 2015.

[45] C. Gabriel, S. Gabriel, and Y. E. Corthout, "The dielectric properties of biological tissues: I. Literature survey," *Physics in medicine & biology*, vol. 41, no. 11, p. 2231, 1996.

[46] M. A. Stuchly and S. S. Stuchly, "Dielectric properties of biological substances-tabulated," *Journal of Microwave Power*, 15(1), pp. 19–25, 1980.

[47] J. Garrett and E. Fear, "Stable and flexible materials to mimic the dielectric properties of human soft tissues," *in IEEE Antennas and Wireless Propagation Letters*, vol. 13, pp. 599–602, 2014. doi: 10.1109/LAWP.2014.2312925

[48] J. Corominas, Y. Ramayo-Caldas, A. Puig-Oliveras, J. Estellé, A. Castelló, E. Alves, R. N. Pena, M. Ballester, and J. M. Folch, "Analysis of porcine adipose tissue transcriptome reveals differences in de novo fatty acid synthesis in pigs with divergent muscle fatty acid composition," *BMC genomics*, vol. 14 no. 843, 2013. doi:10.1186/1471-2164-14-843

[49] T. Karacolak, R. Cooper, E. S. Unlu, and E. Topsakal, "Dielectric properties of porcine skin tissue and in vivo testing of implantable antennas using pigs as model animals," *in IEEE Antennas and Wireless Propagation Letters*, vol. 11, pp. 1686–1689, 2012. doi: 10.1109/LAWP.2013.2241722

[50] D. Werber, A. Schwentner, and E. M. Biebl, "Investigation of RF transmission properties of human tissues," *Advances in Radio Science*, 4(Kleinheuba), pp.357–360, 2006.

[51] O. Akkus, A. Oguz, M. Uzunlulu, and M. Kizilgul, "Evaluation of skin and subcutaneous adipose tissue thickness for optimal insulin injection" *Journal of Diabetes Metabolism* col. 3, no. 8, pp. 1–5, 2012.

[52] M. A. Gibney, C. H. Arce, K. J. Byron, and L. J. Hirsch, "Skin and subcutaneous adipose layer thickness in adults with diabetes at sites used for insulin injections: Implications for needle length recommendations," Current Med. Res. Opinion, vol. 26, no. 6, pp. 1519–1530, 2010. doi: 10.1185/03007995.2010.481203.

[53] M. Swaminathan, F. S. Cabrera, J. S. Pujol, U. Muncuk, G. Schirner, and K. R. Chowdhury, "Multi-path model and sensitivity analysis for galvanic coupled intra-body communication through layered tissue," *IEEE Trans. Biomed. Circuits Syst.*, vol. 10, no. 2, pp. 339–351, Apr. 2016.

[54] T. S. P. See, X. Qing, Z. N. Chen, C. K. Goh, and T. M. Chiam, "RF transmission in/through the human body at 915 MHz," *2010 IEEE Antennas and Propagation Society International Symposium*, Toronto, ON, pp. 1–4, 2010. doi: 10.1109/APS.2010.5561947

[55] A. Venara, A. Gaudin, J. Lebigot, G. Airagnes,J. F. Hamel, N. Jousset, C. Ridereau-Zins, D. Mauillon, and C. Rouge-Maillart, "Tomodensitometric survey of the distance between thoracic and abdominal vital organs and the wall according to BMI, abdominal diameter and gender: Proposition of an indicative chart for the forensic activities," *Forensic Science International*, vol. 229, no. 1–3, pp. 167.e1–167.e6, 2013. doi: https://doi.org/10.1016/j.forsciint.2013.03.039

[56] M. D. Pozar, *Microwave Engineering*, 4th ed.; Hoboken, NJ: Wiley, 2012, pp. 102–110.

[57] "6 techniques for measuring dielectric properties, " *in Microwave and Radio-Frequency Technologies in Agriculture*. Boston, USA: Sciendo Migration. 2006. doi: https://doi.org/10.1515/9783110455403-007

[58] S. Gabriel, R. W. Lau, and C. Gabriel, "The dielectric properties of biological tissues: II. Measurements in the frequency range 10 Hz to 20 GHz," *Phys. Med. Biol.* 1996, 41, pp. 2251–2269.

[59] S. Gabriel, R. W. Lau, and C. Gabriel, "The dielectric properties of biological tissues: III. Parametric models for the dielectric spectrum of tissues," *Phys. Med. Biol.* 1996, 41, pp. 2271–2293.

[60] D. Andreuccetti, R. Fossi, and C. Petrucci, "An internet resource for the calculation of the dielectric properties of body tissues in the frequency range 10 Hz–100 GHz". IFAC-CNR, Florence (Italy), 1997. Based on data published by C.Gabriel *et al.* in 1996. [Online]. Available: http://niremf.ifac.cnr.it/tissprop/

[61] T. S. Rappaport, "Wireless communications: principles and practice," vol. 2. *New Jersey: Prentice hall PTR*, 1996.

[62] L. Roelens, S. Van den Bulcke, W. Joseph, G. Vermeeren, and L. Martens, "Path loss model for wireless narrowband communication above flat phantom," *Electronics Letters*, vol. 42, no. 1, pp. 10–11, 2006.

[63] C. Yeh and F. I. Shimabukuro, "The essence of dielectric waveguides", Springer: Los Angeles, CA, USA, 2008, ISBN 978-0-387-30929-3.

[64] N. B. Asan, E. Hassan, M. D. Perez, L. Joseph, M. Berggren, T. Voigt, and R. Augustine, "Fat-Intra body communication at 5.8 GHz including impacts of dynamic body movements", 2019 (manuscript).

[65] N. B. Asan, J. Velander, S. R. Mohd Shah, E. Hassan, D. Noreland, T. Voigt, T. J. Blokhuis, and R. Augustine, "Reliability of the fat tissue channel for intra-body microwave communication," *2017 IEEE Conference on Antenna Measurements & Applications (CAMA)*, Tsukuba, 2017, pp. 310–313.

[66] H. S. Sacks and J. N. Fain, "Human epicardial adipose tissue: a review," *American heart journal*, vol. 153 no. 6, pp. 907–917, 2007.

[67] B. Koeppen and B. Stanton. Berne and Levy Physiology. 6th edition. *Elsevier,*

Inc, 2008.
[68] F. V.Y. Tjong, T. F. Brouwer, K. M. Kooiman, L. Smeding, B. Koop, B. Soltis, A. Shuros, A. A. M. Wilde, M. Burke, and R. E. Knops, "Communicating antitachycardia pacing-enabled leadless pacemaker and subcutaneous implantable defibrillator," *Journal of the American College of Cardiology*, vol. 67, no. 15, pp. 1865–1866, 2016. doi: 10.1016/j.jacc.2016.02.039
[69] T. G. Zimmerman, "Wireless networked digital devices: A new paradigm for computing and communication," *IBM Systems Journal*, vol. 38, no. 4, pp. 566–574, 1999.
[70] K. VonEhr, W. Neuson, and B. E. Dunne, 2016, "Software Defined Radio: Choosing the right system for your communications course," *in Proceedings of the 123rd ASEE Annual Conference and Exposition*, New Orleans, LA.
[71] United Nations, "World population prospects 2019," Retrieved on September 12, 2019 from https://population.un.org/wpp/Publications/Files/WPP2019_Highlights.pdf

Acta Universitatis Upsaliensis

Digital Comprehensive Summaries of Uppsala Dissertations from the Faculty of Science and Technology 1863

Editor: The Dean of the Faculty of Science and Technology

A doctoral dissertation from the Faculty of Science and Technology, Uppsala University, is usually a summary of a number of papers. A few copies of the complete dissertation are kept at major Swedish research libraries, while the summary alone is distributed internationally through the series Digital Comprehensive Summaries of Uppsala Dissertations from the Faculty of Science and Technology. (Prior to January, 2005, the series was published under the title "Comprehensive Summaries of Uppsala Dissertations from the Faculty of Science and Technology".)

Distribution: publications.uu.se
urn:nbn:se:uu:diva-393444

ACTA
UNIVERSITATIS
UPSALIENSIS
UPPSALA
2019